THE MEASUREMENT OF ELECTRIC QUADRUPOLE MOMENTS OF GAS MOLECULES BY INDUCED BIREFRINGENCE

BY

DAVID ALEXANDER IMRIE BSc(Hons)(NATAL)

Submitted in partial fulfilment of
the requirements for the degree of
Doctor of Philosophy
in the
Department of Physics,
University of Natal

Pietermaritzburg
December, 1993

Abstract

Determining the electric quadrupole moments of gas molecules from measurements of birefringence induced in the gas by an applied electric field gradient is widely recognised as being the most direct experimental technique for this purpose. This thesis presents a new molecular theory of the experiment, and also describes the apparatus used in the measurement of the quadrupole moments of a number of gases and the revisions made to the manner in which the experiment was performed.

A recent eigenvalue theory of light propagation in matter has been used to derive an expression relating the induced birefringence to the electric quadrupole moment of the molecule, whether this be dipolar or not. This expression is different from that which has previously been applied to dipolar molecules. It is shown that the new expression is independent of molecular origin only if it is cast in terms of the primitive quadrupole moment, as opposed to the traceless moment.

Previous work using the same set of apparatus yielded results for carbon dioxide which were significantly lower than those reported by other workers. By using the Jones calculus to re-examine the cascade of optical components used in the experiment, it was found that the previous method of performing the experiment did not completely eliminate the effects of an imperfect retardance in the quarter-wave plate used, nor of strain-induced birefringence in the windows of the the cell containing the gas. These effects could cause results to be underestimated by as much as 8%. It is shown that a better method of performing the experiment is to amplify the optical signal by deliberately offsetting the analysing prism, rather than the quarter-wave plate as was previously done.

The results of measurements made using this technique are reported for carbon dioxide, carbon monoxide, nitrogen, ethene, chlorine, and boron trifluoride. The measured quadrupole moment of carbon dioxide is in good agreement with the most recent values found by other workers using a similar experiment, and with the latest theoretical value of this quantity.

Preface

The work reported in this thesis was carried out in the Department of Physics, University of Natal, Pietermaritzburg, under the supervision of Professor R E Raab and Dr C Graham between December 1989 and May 1993.

I declare this work to be the result of my own research. Where results due to other authors have been used, this is indicated by explicit citations in the text. This thesis has not been submitted in any form for any degree or examination to any other University.

Signed ..... on this ..... day

of ..... , 1993.

Contents

List of Tables

List of Figures

Acknowledgements

To my supervisors, Professor R E Raab and Dr C Graham, I extend my most heartfelt appreciation for the interest which they have shown in this project, for the guidance and encouragement which they have given me, and for the knowledge which they have patiently imparted.

I am also indebted to Dr J Pierrus for initially instructing me in the use of the apparatus and for offering helpful advice during the course of the work.

The technical support which I received for the duration of the project was excellent. In this regard, I am especially grateful to Mr A J Wilsenach for the expeditious and cheerful manner in which he undertook the machining of new parts and the modification of existing ones. My thanks go to Messrs R H Barker, N A Cullis, G M Dewar, A C Hill, and J H P Woodley for their contributions towards the construction of the original apparatus and for their invaluable assistance in servicing it, and to Mr R S Sewrathan for his help on the numerous occasions on which the apparatus had to be reassembled.

Professor P Jackson and the remaining staff of the Pietermaritzburg Physics Department are thanked for cheerfully accommodating and assisting me in untold ways.

The manuscript was typed by the author using the $\mathcal{AMS}$-LaTeX typsetting package. Mr G Maltby is sincerely thanked for his support in furnishing and configuring the necessary software, and for the rendering of expert advice on its use.

My warmest thanks go to my wife, Nola, for her unfailing support and encouragement in this venture, and for patiently lending an ear to more on the subject of quadrupole moments than she ever really cared to hear.

I am grateful to the Foundation for Research and Development and to the University of Natal for furnishing me with generous grants for the duration of my postgraduate work, and to the CSIR for awarding me an undergraduate bursary and for deferring my assumption of duty to enable me to undertake this postgraduate study.

Chapter 1

INTRODUCTION AND REVIEW

1.1 The Multipole Expansion

The interaction between two molecules, as the simplest intermolecular process, is in reality a many-body problem if one were to consider the effects of all the charges on each other. To reduce this to a tractable description, simplifying assumptions are made. In particular, the internal motion of the electrons in a molecule is often ignored, as is the motion of the molecule as a whole, so that electrostatic theory may be employed. The justification for this is that magnetic effects due to charges moving at non-relativistic speeds are negligible when compared with the electrostatic interaction. Furthermore, it is often sufficient to assume that the molecules are well-separated, in which case the electrostatic field of the molecule need be determined only at distances in excess of the molecular dimensions. The usual approach then is to expand the electrostatic potential of a molecule about an arbitrary origin close to the charges, giving rise to a series of moments of charge which may then be measured and used to characterize the molecule.

Consider a distribution of charges q_i in a vacuum with displacements $\mathbf{r}_i$ from an arbitrary origin O, which is within, or close to, the distribution. The electrostatic potential to which the charge distribution gives rise at a point P having displacement $\mathbf{R}$ from O is given by

$$\phi(\mathbf{R}) = \frac{1}{4\pi\varepsilon_0} \sum_i \frac{q_i}{|\mathbf{R} - \mathbf{r}_i|}.$$

If the distance from the field point P is much greater than the dimensions of the charge distribution then we may use the binomial theorem to expand the denominator in the summation, giving

$$\phi(\mathbf{R}) = \frac{1}{4\pi\varepsilon_0} \left[\frac{1}{R} \sum_i q_i + \frac{R_\alpha}{R^3} \sum_i q_i r_{i\alpha} + \frac{3R_\alpha R_\beta - R^2\delta_{\alpha\beta}}{2R^5} \sum_i q_i r_{i\alpha} r_{i\beta} + \cdots \right]. \quad (1.1)$$

In this expression, and throughout this work, Greek subscripts are used to denote Cartesian components, a repeated Greek subscript implies a summation over x, y, and z, and $\delta_{\alpha\beta}$ is the Kronecker delta tensor.

From (1.1) we may extract and name the various moments of charge of the distribution. These are:

1. The total charge
$$q = \sum_i q_i;$$

2. The electric dipole moment
$$\mu_\alpha = \sum_i q_i r_{i\alpha}; \tag{1.2}$$

3. The electric quadrupole moment
$$q_{\alpha\beta} = \sum_i q_i r_{i\alpha} r_{i\beta}. \tag{1.3}$$

Higher-order moments are named octopole, hexadecapole etc., but, because they make successively smaller contributions to the electrostatic potential of molecules possessing an electric quadrupole moment, we will not consider them here. It is worth remarking at this point that the definition of the electric quadrupole moment given above is one of two in current use; indeed, it would be true to say that it has hitherto been the less favoured of the two. This matter is discussed at length in §1.2.

Written in terms of the moments of charge, the electrostatic potential of the charge distribution becomes

$$\phi(\mathbf{R}) = \frac{1}{R}q + \frac{R_\alpha}{R^3}\mu_\alpha + \frac{3R_\alpha R_\beta - R^2\delta_{\alpha\beta}}{2R^5}q_{\alpha\beta} + \cdots . \tag{1.4}$$

From this expression it is evident that terms involving successively higher multipole moments make contributions to the electrostatic potential which are successively smaller by a factor of order $\frac{1}{R}$. So the usefulness of the multipole expansion is that the leading non-vanishing moment describes the expanded property to a good approximation at large R. Each multipole moment is regarded as being located at the origin O, because its contribution to the expanded property depends only on the displacement $\mathbf{R}$ of the field point P from O.

An electrostatic field $\mathbf{E}$ applied to the distribution will cause it to experience a net force $\mathbf{F}$, given by

$$\begin{aligned} F_\alpha &= \sum_i q_i E_{i\alpha} \\ &= q(E_\alpha)_o + \mu_\beta(\nabla_\beta E_\alpha)_o + \tfrac{1}{2}q_{\beta\gamma}(\nabla_\beta\nabla_\gamma E_\alpha)_o + \cdots , \end{aligned} \tag{1.5}$$

in which the bracketed field derivatives are evaluated at the origin O about which the field has been Taylor-expanded. This expression may be used to show that a quadrupolar distribution will experience a torque in a region of uniform field gradient.

It may also be used to find the potential energy of the charge distribution in the field, given by

$$U = -\int_{r_1(\mathbf{E}=\mathbf{0})}^{r_2(\mathbf{E}=\mathbf{E})} F_\alpha \, dr_\alpha$$
$$= q\phi - \int_0^{\mathbf{E}} \mu_\alpha \, dE_\alpha - \tfrac{1}{2}\int_0^{\mathbf{E}} q_{\alpha\beta} \, d(\nabla_\beta E_\alpha) - \cdots . \tag{1.6}$$

If the distribution is rigid then only permanent moments contribute to (1.6), which then becomes

$$U = q\phi - \mu_\alpha^{(0)} E_\alpha - \tfrac{1}{2} q_{\alpha\beta}^{(0)} \nabla_\alpha E_\beta - \cdots . \tag{1.7}$$

The superscripted $^{(0)}$ on a multipole moment is used throughout this work to denote a permanent moment of charge.

1.2 Definitions of Quadrupole Moments

Many authors [1, 2] prefer not to use the definition of quadrupole moment given in (1.3), and which we shall henceforth refer to as the *primitive quadrupole moment*, but choose an alternative definition of a *traceless quadrupole moment*

$$\theta_{\alpha\beta} = \tfrac{1}{2}(3q_{\alpha\beta} - q_{\gamma\gamma}\delta_{\alpha\beta}) = \tfrac{1}{2}\sum_i q_i(3r_{i\alpha}r_{i\beta} - r_i^2\delta_{\alpha\beta}), \tag{1.8}$$

so named because $\theta_{\alpha\alpha} = 0$. This definition is now almost universally accepted[1], particularly by experimentalists, and is represented in the literature by either $\theta_{\alpha\beta}$ or $Q_{\alpha\beta}$. In this work $\theta_{\alpha\beta}$ and $\Theta_{\alpha\beta}$ denote, respectively, the traceless quadrupole moment of a single molecule and the macroscopic traceless quadrupole moment density; and $q_{\alpha\beta}$ and $Q_{\alpha\beta}$ are used to represent the corresponding quantities for the primitive quadrupole moment.

Through suitable choice of a system of principal axes for a charge distribution, the off-diagonal components of $\theta_{\alpha\beta}$ and $q_{\alpha\beta}$ may be made to vanish. Inspection of (1.8) shows that the two definitions of quadrupole moment will share the same set of principal axes for a given charge distribution. Referred to such axes, only the three diagonal elements remain. These are independent in the case of $q_{\alpha\beta}$, but related by $\theta_{\alpha\alpha} = 0$ in the case of the traceless tensor. This means that only two independent components are, in general, needed to specify $\theta_{\alpha\beta}$. For a molecule having an axis of 3-fold or higher rotational symmetry, taken to be the z-axis, only one independent component, θ_{zz}, exists. It is this single component of the traceless quadrupole moment which authors often denote by θ or Q, and which is referred to simply as the quadrupole moment of a linear molecule.

[1]The factor $\frac{1}{2}$ is occasionally omitted by some authors.

Since it generally requires one less number to specify a traceless quadrupole moment than it does to specify a primitive one, it appears advantageous to adopt the traceless definition. In this case one should consistently use traceless definitions for higher multipole moments, in the sense of these being traceless in any two of their tensor subscripts. Raab [3] has shown that traceless moments of higher order than the quadrupole are unable to specify the interaction Hamiltonian describing the interaction between an electromagnetic field and a system of charged particles; nor are they able to describe the radiation field of such a system. Furthermore, the necessarily fewer independent components needed to specify traceless moments are sometimes inadequate when describing a dynamic process. For instance, a molecule having $C_{\infty v}$ symmetry has only one independent component of its traceless octopole moment, but this single number is insufficient to describe its interaction with a plane light wave. The primitive octopole moment, on the other hand, has two independent components which together are able to account completely for octopole interactions in general.

Buckingham [1] motivates the use of the traceless quadrupole definition by pointing out that it gives a measure of the departure from spherical symmetry of a charge distribution. The primitive quadrupole moment $q_{\alpha\beta}$ is not, in general, zero for a sphere. Nuclear physicists define the nuclear quadrupole moment to be traceless for much the same reason.

It is shown in (1.7) that the primitive quadrupole moment contributes to the energy of a rigid charge distribution in a vacuum in an externally applied field through the term $-\frac{1}{2}q^{(0)}_{\alpha\beta}\nabla_\alpha E_\beta$. From (1.8) we may solve for the primitive quadrupole moment,

$$q_{\alpha\beta} = \tfrac{2}{3}\theta_{\alpha\beta} + \tfrac{1}{3}q_{\gamma\gamma}\delta_{\alpha\beta}, \tag{1.9}$$

and then rewrite the quadrupolar energy contribution as

$$-\tfrac{1}{3}\theta^{(0)}_{\alpha\beta}\nabla_\alpha E_\beta - \tfrac{1}{6}q^{(0)}_{\gamma\gamma}\nabla_\alpha E_\alpha = -\tfrac{1}{3}\theta^{(0)}_{\alpha\beta}\nabla_\alpha E_\beta,$$

since, from Laplace's equation $\nabla_\alpha E_\alpha = 0$, the trace term vanishes. Thus, when describing the energy of a system of charges in an applied field, it is sufficient to replace $\frac{1}{2}q^{(0)}_{\alpha\beta}$ with $\frac{1}{3}\theta^{(0)}_{\alpha\beta}$, despite the fact that these are not identical. To see that we have gained nothing by doing so, we may expand the tensor contraction of the energy contribution from the primitive quadrupole moment, referred to principal axes, and rearrange it to give

$$\begin{aligned} -\tfrac{1}{2}q^{(0)}_{\alpha\beta}\nabla_\alpha E_\beta &= -\tfrac{1}{2}[q^{(0)}_{xx}\nabla_x E_x + q^{(0)}_{yy}\nabla_y E_y + q^{(0)}_{zz}\nabla_z E_z] \\ &= -\tfrac{1}{2}[(q^{(0)}_{yy} - q^{(0)}_{xx})\nabla_y E_y + (q^{(0)}_{zz} - q^{(0)}_{xx})\nabla_z E_z], \end{aligned}$$

in which Laplace's equation has been used to express one component of the field-gradient tensor in terms of the other two. From this it may be seen that the interaction energy requires the specification of only two quadrupole parameters; these being the *differences* between any two primitive quadrupole components and the third. Conversely, any experiment, such as the birefringence experiment described in this work,

in which the observable is a manifestation of the effects due to the energy of interaction between a molecule and an applied field, can at most measure these two parameters. Redefining these quantities as a new tensor may lead to erroneous results if, on replacing the primitive quadrupole moment with the traceless form, exact equivalence between the two definitions is violated.

An example of this concerns the form of the quadrupolar contribution to the **D**-vector in Maxwell's equations, when expressed in terms of the traceless quadrupole moment. This expression may be shown to have the form [4, 5]

$$D_\alpha = \varepsilon_0 E_\alpha + P_\alpha - \tfrac{1}{2}\nabla_\beta Q_{\alpha\beta} + \cdots , \tag{1.10}$$

in which P_α is the macroscopic electric dipole moment density. As with the energy, we may substitute into this the macroscopic equivalent of the identity in (1.9) to obtain

$$D_\alpha = \varepsilon_0 E_\alpha + P_\alpha - \tfrac{1}{3}\nabla_\beta \Theta_{\alpha\beta} - \tfrac{1}{6}\nabla_\alpha Q_{\gamma\gamma} + \cdots . \tag{1.11}$$

However, the form used by some workers [6, 2] in the past has been

$$D_\alpha = \varepsilon_0 E_\alpha + P_\alpha - \tfrac{1}{3}\nabla_\beta \Theta_{\alpha\beta} + \cdots , \tag{1.12}$$

despite the fact that $Q_{\gamma\gamma}$ is not necessarily uniform everywhere.

Logan [7] has used (1.12) in considering the non-linear dielectric response of an ideal gas to an externally applied non-uniform electrostatic field, and has found that the dielectric vector so obtained is dependent on the arbitrary origin to which the molecular moments are referred. This is physically untenable since the interpretation of experiments in which measurements are made of bulk physical observables of matter in order to obtain estimates of multipole moments cannot depend on an arbitrary choice of origin in a charge distribution.

Graham *et al.* [5] have taken this further and have shown that this form for D_α leads to a set of Maxwell equations which are themselves origin-dependent. This is not the case if the trace term in (1.11) is retained. In their analysis of the birefringence experiment based on the use of Maxwell's equations, Imrie and Raab [8] have also found that the use of (1.12) leads to an expression for an observable which is not origin-independent.

For the above reasons, the primitive quadrupole moment will be used in this work, except in certain cases where reference is made to the work of authors who have adopted the traceless definition.

1.3 Experimental Determination of Electric Quadrupole Moments

1.3.1 The importance of measuring quadrupole moments

A number of methods are available for measuring electric dipole moments with good accuracy, whereas the electric quadrupole moment is somewhat more difficult to establish. Judging from the number and diversity of experimental methods which have

been used to measure electric quadrupole moments, it is apparent that endeavouring to obtain these experimental values is considered a worthwhile pursuit. Justification for the experimental determination of electric quadrupole moments is well-documented, since seemingly few authors appear willing to begin a paper on the subject without including at least a few lines vindicating their work. Reasons given usually fall into one of two broad groupings.

The first group includes all the interaction effects which are greatly illuminated by the inclusion of the quadrupole term in expressions for the intermolecular forces and energies. This is of greatest importance in those molecules for which the leading contribution in the interaction is quadrupolar. In an early review Buckingham [1] showed that a number of effects and properties arise as a consequence of significant contributions being made by the electric fields of quadrupole moments to the orientation-dependent part of intermolecular forces . Knowing the form of the intermolecular potential for two similar molecules may yield valuable information regarding the condensed phase of a substance. In the case of nitrogen, the properties of the solid and liquid phase are primarily dependent on the intermolecular potential energy, which Böhm [9] has shown to be quite sensitive to the quadrupole moment. The possibility of predicting the structure of van der Waals molecules using theoretical models based on electric moments of the monomers has also highlighted the need for accurate values for these quantities [10].

In the second class of reasons are those which require an accurate experimental quadrupole moment to test a theoretical prediction. The importance of this becomes apparent when one considers that molecular quadrupole moments are sensitive to the distribution of charge in the outer regions of the molecule, in contrast to the energy which is largely determined by the electron density closer to the nuclei. This makes quadrupole moments a very good test of the correctness of the wave functions used to predict them. Once quadrupole moments are able to be calculated with accuracy, greater confidence will be placed in theoretical values of higher multipole moments which do not lend themselves to accurate experimental determination.

1.3.2 The method of induced birefringence

Although (1.7) suggests that the quadrupole moment of a molecule might be measured through the change in energy when a known field gradient is applied to it, this approach is impracticable owing to the difficulty of producing a sufficiently large field gradient over molecular dimensions.

An experiment first proposed by Buckingham [11] in 1958 provides an elegant variation on this idea. Gas molecules with permanent quadrupole moments are contained in a cell having on its axis a region of uniform high field gradient which, through the torque it exerts on a quadrupole, partially orientates the molecules, causing the gas to become anisotropic and to exhibit birefringence. Within certain approximations the induced birefringence may be shown to be proportional to the product of a component of the field gradient tensor and the expression $3q^{(0)}_{\alpha\beta}\alpha_{\alpha\beta} - q^{(0)}_{\alpha\alpha}\alpha_{\beta\beta}$, in which $\alpha_{\alpha\beta}$

is the high frequency polarizability tensor of the molecule. It is easily shown that, for a molecule having 3–fold or higher axial symmetry about the z-axis, this molecular factor becomes $(q_{zz}^{(0)} - q_{xx}^{(0)})(\alpha_{zz} - \alpha_{xx})$. The difference $\alpha_{zz} - \alpha_{xx}$ may be found from light-scattering experiments, thereby allowing the induced birefringence experiment to yield a value for $q_{zz}^{(0)} - q_{xx}^{(0)}$ for linear molecules. Whilst there is no doubt that this is the most direct way of measuring this difference, it is certainly a drawback that the components of the quadrupole tensor cannot be separated using this experiment. An example of the analysis of birefringence measurements performed on non-linear gas molecules is given in §5.3.6 which deals with the results of measurements performed on ethene.

Since it is only the leading moment of charge which is independent of origin [1], it follows that the quadrupole moment of a dipolar molecule must necessarily be dependent on the origin to which it is referred. Just where this origin is located in polar molecules was a matter first investigated by Buckingham and Longuet-Higgins [12] and later by Imrie and Raab [8]. Although the results from these calculations do not coincide, they do establish that the origin of the quantity $q_{zz}^{(0)} - q_{xx}^{(0)}$ measured in the birefringence experiment is a point within the charge distribution at which a certain linear combination of molecular tensor components vanishes. This point is usually referred to as the *effective quadrupole centre* [12] and is certainly not the centre of mass of the molecule, which is the point usually taken as the origin when quadrupole moments are calculated theoretically, or when other experiments to determine this quantity are performed. In the case of linear molecules, for which both these points lie on the molecular axis of rotational symmetry (taken as the z-axis), quadrupole moments referred to these two different origins are easily shown to be related through the equation

$$\Theta_{zz}^{(0)}(\text{c.m.}) - \Theta_{zz}^{(0)}(\text{e.q.c.}) = 2R\mu_z^{(0)}, \tag{1.13}$$

in the case of the traceless quadrupole moment, or

$$q_{xx}^{(0)}(\text{c.m.}) - q_{xx}^{(0)}(\text{e.q.c.}) = 0 \tag{1.14}$$

and

$$q_{zz}^{(0)}(\text{c.m.}) - q_{zz}^{(0)}(\text{e.q.c.}) = 2R\mu_z^{(0)}, \tag{1.15}$$

in the case of the primitive quadrupole moment. In these equations $\mu_z^{(0)} = |\boldsymbol{\mu}^{(0)}|$ is the electric dipole moment and R is the distance from the inertial centre to the effective quadrupole centre of the molecule. From this it may be argued that molecules having relatively small dipole moments, as is the case with carbon monoxide (CO) ($\mu_z^{(0)} = 0.366 \times 10^{-30}\,\text{Cm}$), will possess quadrupole moments which should show very little dependence on which of these two origins is used, whereas the specification of the origin is very important in highly polar molecules, such as carbon sulphide (CS) ($\mu_z^{(0)} = 6.54 \times 10^{-30}\,\text{Cm}$) [13]. Furthermore, if the quadrupole moment is measured by two different experiments which refer it to these two different origins, then the above relationships may be used, together with the dipole moment of the molecule,

to determine the displacement of the effective quadrupole centre from the centre of mass [13]. However, if this displacement is not known from some other method, then it is not possible to compare meaningfully the quadrupole moments of strongly polar molecules as measured by the optical birefringence method with those found from other experiments or from theoretical calculations.

1.3.3 The second virial coefficient method

Deviations from ideal behaviour in a gas are entirely due to the effects of interactions between the gas molecules. One may expand the deviation from the ideal gas law in inverse powers of the molar volume V_m, thereby obtaining

$$\left(\frac{PV_m}{RT} - 1\right) = \frac{B_p}{V_m} + \frac{C_p}{V_m^2} + \frac{D_p}{V_m^3} + \cdots ,$$

where B_p, C_p, and D_p are, respectively, the second, third, and fourth pressure virial coefficients, and are, in general, functions of the temperature of the gas. Other symbols in this equation have their usual meanings. An explicit expansion for B_p in terms of the interaction potential for non-polar molecules has as its leading unknown parameter, the electric quadrupole moment [14]. Since the second virial coefficient of a gas may be experimentally determined with good accuracy, such data may then be used to provide an estimate of the electric quadrupole moment. The results are, however, dependent on the choice of model used to describe the interaction potential. Spurling and Mason [15] have obtained estimates of molecular quadrupole moments from pressure virial coefficient data, as well as from viscosity measurements, but agreement with results obtained from more accurate experiments, such as the optical birefringence technique, is, in most cases, poor.

Whilst the second pressure virial coefficient no longer finds favour as a means of determining electric quadrupole moments, Bose *et al.* [16, 17, 18, 19, 20] have, for more than two decades, been publishing work relating to the determination of quadrupole moments from the second dielectric virial coefficient . In this approach it is the Clausius-Mosotti function $\frac{\varepsilon_r - 1}{\varepsilon_r + 2} V_m$ which is expressed in inverse powers of the molar volume:

$$\frac{\varepsilon_r - 1}{\varepsilon_r + 2} V_m = A_\varepsilon + \frac{B_\varepsilon}{V_m} + \frac{C_\varepsilon}{V_m^2} + \cdots ,$$

where ε_r is the static dielectric constant, and $A_\varepsilon, B_\varepsilon$, and C_ε are, respectively, the first, second, and third dielectric virial coefficients, accounting for contributions from single molecules, pairs, and three-body interactions. In the case of a non-polar gas, such as nitrogen, the first dielectric virial coefficient is given by

$$A_\varepsilon = \frac{N_0 \alpha}{3\varepsilon_0},$$

where N_0 is Avogadro's Number and α is the polarizability of the molecule. From the classical statistical theory of Buckingham and Pople [21], the second dielectric virial

coefficient may be expressed as the sum of two terms:

$$B_\varepsilon = B_{\mathrm{IND}} + B_{\mathrm{OR}},$$

in which B_{IND} accounts for the effect of interactions between the external field and the dipole moment induced in a pair of molecules, whilst B_{OR} is due to the moments induced in one molecule of the pair by the multipole field of the other. It is B_{OR} which, for a non-polar molecule, may be expressed in terms of the electric quadrupole moment [22], and so it is necessary to eliminate B_{IND} from the the above expression for B_ε. This may be accomplished by considering another virial coefficient expansion; this time it is the optical frequency analogue of the Clausius-Mosotti equation, the Lorenz-Lorentz equation

$$\frac{n^2-1}{n^2+1}V_m = A_R + \frac{B_R}{V_m} + \frac{C_R}{V_m^2} + \cdots,$$

in which n is the refractive index, and A_R, B_R, and C_R are the first, second, and third refractivity virial coefficients, respectively. At optical frequencies $B_R = B_{\mathrm{IND}}$ [22], and hence measurements of the second dielectric and refractivity virial coefficients will yield a value for B_{OR}, from which the electric quadrupole moment may be obtained. As in the case with the second pressure virial coefficient method, the result is dependent on the model chosen for the interaction potential. A recent result reported by Bose and Huot [22] in which they used this approach with a Lennard-Jones pair potential to determine the quadrupole moment of molecular nitrogen, is in very good agreement with results obtained from induced birefringence measurements.

1.3.4 The anisotropic magnetic susceptibility method

By the end of the 1960s microwave spectroscopy had been established as an effective technique for measuring the molecular Zeeman effect in diamagnetic molecules. Until about this time measurements in the microwave region were restricted to the measuring of effects linear in the applied magnetic field, yielding values for the diagonal components of the molecular g-tensor. However, it now became possible to separate out effects which are quadratic in the field, and from such experiments to obtain values for the g-tensor and the anisotropy in the magnetic susceptibility of a linear molecule.

These two pieces of information may be used in the determination of molecular quadrupole moments, since Hüttner *et al* [23] have shown that, in the system of cgs units, for linear molecules,

$$\Theta_{zz}^{(0)} = q_{xx}^{(0)} - q_{zz}^{(0)} = \frac{\hbar|e|g_{xx}}{4\pi M_p B} - \frac{4mc^2}{|e|}(\chi_{zz} - \chi_{xx}),$$

in which e is the electronic charge, M_p and m are the proton and electron masses, B is the rotational constant, c the speed of light, and χ the magnetic susceptibility.

The measurement of molecular g-tensors and susceptibilities is an important undertaking in its own right; the determination of electric quadrupole moments is just one

of several important molecular properties which may be deduced from these results. Another is the direction of the electric dipole moment, which may be determined for molecules having at least two different isotopic species. Flygare *et al.* [24] have reported the construction of a very large magnet capable of producing fields in excess of 30 kG over a length of 1.8 m which they have used to perform measurements of high precision on various molecules [25, 26, 27] . Despite the precision of these measurements the quadrupole moments obtained are not always of great accuracy, because the two terms in the above expression for the quadrupole moment are often large in comparison with their difference. This is, for example, the case with carbon monoxide [13].

A useful feature of this method, which is not shared by the optical birefringence technique, concerns the number of components of the quadrupole moment that may be determined. In general, the measurement of the magnetic effects allows one to measure the sign and magnitude of the diagonal components of the quadrupole moment tensor along the principal inertial axes of the molecule. In the case of symmetric tops or asymmetric top molecules with a two-fold symmetry axis, the principle axes of the quadrupole and inertial tensors coincide, and so for these molecules the entire quadrupole moment tensor may be measured [28].

1.3.5 Other methods

Probably the most popular quadrupole measuring technique not yet discussed is that which uses measurements of collision-induced line broadening in the infrared and microwave spectra of molecules. As with all indirect approaches, results from this technique are dependent on the model adopted to describe the interaction potential. Some workers have succeeded in obtaining results which are in reasonable agreement with those obtained from birefringence measurements [29, 30], but the precision of reported values is seldom better than 10%, whereas the birefringence technique is now capable of far greater accuracy than this.

An entirely different approach, to which only a single reference was found, entails calculating molecular quadrupole moments using data obtained from ion-molecule scattering experiments [31]. Low-energy ions were scattered off various simple molecules, and the molecular cross-sections calculated. Scattering of low energy particles is essentially determined by the long-range potential which, for the molecules chosen, is quadrupolar in nature. Results reported for nitrogen and carbon dioxide are in excellent agreement with the best birefringence results available at that time, but again the precision is to only two significant figures.

The last experimental method worth mentioning is that which relates the quadrupole moment to the nuclear spin relaxation times for gas molecules. Bloom *et al.* [32] have reported a series of such experiments on elementary gas molecules . Despite several approximations in the theory, the quadrupole moments thus found are in surprisingly good agreement with birefringence results.

There is no doubt that the induced optical birefringence experiment, being the only direct technique, is currently the most accurate experiment for determining the

electric quadrupole moments of gas molecules. Other methods, however, should not be summarily dismissed, since they are very often capable of producing results in cases where the optical birefringence technique is inapplicable due to the smallness of the effect. Furthermore, they may also be able to render additional information about the quadrupole moment tensor, as is the case with the anisotropic susceptibility method.

Chapter 2

THEORY

2.1 Outline of the Experiment

The method of determining electric quadrupole moments of gas molecules by measuring birefringence induced in the gas was first described by Buckingham in 1959 [11]. Containing the gas is a cell made from a hollow conducting cylinder, down the length of which are strung two thin wires, separated by a small distance[1]. By earthing the cylinder and holding the wires at a high potential, a region of high electric field gradient and zero electric field is created on the axis of the cylinder. Choosing Cartesian axes such that the wires lie in the yz-plane and the z-axis coincides with that of the cylinder, it may be shown (see Appendix A) that the electric field-gradient tensor in the region between the wires has the form

$$\nabla_\alpha E_\beta = E'_{\alpha\beta} = \begin{bmatrix} E'_{xx} & 0 & 0 \\ 0 & -E'_{xx} & 0 \\ 0 & 0 & 0 \end{bmatrix}. \tag{2.1}$$

On, or near, the axis of the cell, a molecule possessing a permanent electric quadrupole moment will experience an orientating torque analogous to that experienced by dipoles in a region of uniform field; the molecule will attempt to orient itself in such a way as reduce its potential energy by an amount $-\frac{1}{2}q^{(0)}_{\alpha\beta}E'_{\alpha\beta}$. The partial alignment of molecules results in the gas in this region becoming anisotropic and exhibiting birefringence. This effect, though small, may be measured through the use of techniques described in Chapter 3. The problem discussed in this chapter is that of relating the measured birefringence to the permanent electric quadrupole moment of a single gas molecule.

[1] Buckingham originally proposed generating the field gradient by using a quadrupolar arrangement of four wires, but this was rejected in favour of the two-wire configuration because of the smaller likelihood of arcing occurring at high voltages.

2.2 The Special Case of Non-Polar Molecules

Historically, the problem under discussion was first solved by Buckingham [11] in 1959 for the special case of non-polar molecules. Because this theory has since been superseded by the more general theories of Buckingham and Longuet-Higgins (1968) [12] and Imrie and Raab (1991) [8], only the main result is presented here. Many of the techniques employed in obtaining this result, such as expressing the molecular moments in terms of polarizability tensors and the field and field gradient, and the principle of orientational averaging, are common to all three theories and will be discussed in §2.4.

There is an important check for the theories that followed the earlier work: the expressions from these theories should reduce to that from the original theory for the special case $\mu_\alpha = 0$. The result from the original theory is this: The optical birefringence induced in a dilute gas by the electric field gradient is

$$n_x - n_y = \frac{1}{4\pi\varepsilon_0}\frac{4\pi N_0 E'_{xx}}{15V_m}\left[B_{\alpha\beta\alpha\beta} + \frac{1}{kT}\theta^{(0)}_{\alpha\beta}\alpha_{\alpha\beta}\right] \tag{2.2}$$

in terms of the traceless quadrupole moment, and

$$n_x - n_y = \frac{1}{4\pi\varepsilon_0}\frac{4\pi N_0 E'_{xx}}{15V_m}\left[\tfrac{1}{2}(3b_{\alpha\beta\alpha\beta} - b_{\alpha\alpha\beta\beta}) + \frac{1}{2kT}(3q^{(0)}_{\alpha\beta}\alpha_{\alpha\beta} - q^{(0)}_{\alpha\alpha}\alpha_{\beta\beta})\right] \tag{2.3}$$

in terms of the primitive quadrupole moment. The symbols appearing in these equations have the following meanings: n_x and n_y are the indices of refraction for monochromatic light passing along the axis of the cell and polarized in the x- and y-directions, respectively; ε_0 is the permittivity of free space; N_0 is Avogadro's number; V_m is the molar volume of the gas; E'_{xx} is the single independent component of the electric field-gradient tensor; k is Boltzmann's constant; T is the absolute temperature of the gas; and $\alpha_{\alpha\beta}$ is the polarizability at the frequency of the light wave. The tensor $B_{\alpha\beta\gamma\delta}$ describes the traceless quadrupole moment induced in a molecule by a uniform electric field, whilst $b_{\alpha\beta\gamma\delta}$ is the corresponding tensor for the primitive quadrupole moment.

The existence of a non-zero electric field off the axis of the cell means that there will exist additional birefringence in the region traversed by the light beam due to the Kerr effect, and proportional to the square of the electric field. By modulating the field at a frequency f and using phase-sensitive detection techniques, we may eliminate Kerr effect contributions since these may be resolved into a static component and a component of frequency $2f$. Hence it is unnecessary to include expressions for the Kerr effect in (2.2) and (2.3).

2.3 The Buckingham and Longuet-Higgins Theory—A Forward-Scattering Approach

Birefringence measurements may equally well be performed on polar molecules as on non-polar molecules and then (2.3) may be used to find their 'quadrupole moments'.

But the quadrupole moment of a polar molecule depends on the origin to which it is referred, so the question arises as to just where the origin is located if the quadrupole moment is evaluated in this way. Buckingham and Longuet-Higgins [12] tackled this problem by using a radiation or 'forward-scattering' approach. Their result disagrees with that found by Imrie and Raab [8] whose eigenvector approach based on Maxwell's equations is described in §2.4. In order to be able to compare these two theories and the expressions which they yield, an account of Buckingham and Longuet-Higgins' forward-scattering theory is presented here, reworked in terms of the primitive quadrupole moment.

We begin by rotating the axes chosen in §2.1 by $-\frac{\pi}{4}$ about the z-axis. If we consider only field points $\mathbf{r} = (x, y, z)$ lying close to the z-axis, then the forms of the field and field gradient are

$$\mathbf{E}(\mathbf{r}) = (\eta y, \eta x, 0) \tag{2.4}$$

and

$$E'_{\alpha\beta} = \begin{bmatrix} 0 & \eta & 0 \\ \eta & 0 & 0 \\ 0 & 0 & 0 \end{bmatrix}, \tag{2.5}$$

in which η is a constant of proportionality which depends on the geometry of the cell and the wire voltage.

Consider a molecule whose origin, assumed to lie close to the molecule, is arbitrarily taken to be at the point $S = (x, y, 0)$. From (1.7) the orientational energy of interaction of the molecule with the field to terms which are of first order in the field and field gradient is given by

$$\begin{aligned} U =& -\mu^{(0)}_\alpha E_\alpha - \tfrac{1}{2} q^{(0)}_{\alpha\beta} E'_{\alpha\beta} - \cdots \\ =& -\eta[\mu^{(0)}_x y + \mu^{(0)}_y x + q^{(0)}_{xy} + \cdots]. \end{aligned} \tag{2.6}$$

The number of molecules in a volume element dv is given by $N dv$, where N is the number density of molecules in a field-free region and is assumed to be unaffected by small fields. For infinitesimal dv, $N dv$ represents the probability of finding a molecule in this volume element. The assumption of small fields also allows us to assume that the rotational energy levels of the molecule are continuously distributed, having a Boltzmann distribution factor $e^{-U(\tau)/kT}$, where τ is an orientational element. Hence the probability of finding a molecule in the volume element dv at S(x,y,0) and in the orientational element $d\tau$ at τ is

$$\begin{aligned} P(x, y, 0, \tau) dv\, d\tau =& \frac{N}{\int d\tau} e^{-U(\tau)/kT} dv\, d\tau \\ \approx& \frac{N}{\int d\tau} \left(1 + \frac{\eta}{kT}[\mu^{(0)}_x y + \mu^{(0)}_y x + q^{(0)}_{xy} + \cdots]\right) dv\, d\tau. \end{aligned} \tag{2.7}$$

This expression will be used later as a weighting factor when integrating over the beam aperture.

An electromagnetic plane wave polarized in the x-direction and propagating in the z-direction with velocity c is incident on on the molecule at $(x, y, 0)$. Then the radiation field at this point is

$$\mathscr{E}_x = \mathscr{E}_{0x} e^{i\omega t},$$

where ω is its angular frequency . Buckingham and Longuet-Higgins [12] make the following observation:

> A weak out-of-phase and perpendicular plane wave $i\mathscr{E}_y^{(0)} \exp(i\omega(t - z/c)$ is generated in front of the detector at the point $D = (0, 0, z)$ by a wave plate or a Kerr cell. The observable is the intensity at the detector D which varies linearly with η and is polarized in the y-direction.

Understanding this statement requires some knowledge of how the experiment is performed. This is discussed in the next chapter, but it suffices to say here that the quadrupole cell is located between two crossed polarizers, so that for an incident beam polarized in the x-direction, only emergent light with y-polarization is 'seen' by the detector. Furthermore, a wave-plate (or Kerr cell) is located between the quadrupole cell and the analyser for the purpose of converting elliptically-polarized light emerging from the quadrupole cell back into a state of linear polarization. Even in the absence of birefringence within the cell, this wave-plate will, because its fast and slow axes do not coincide exactly with the x- and y-axes, give rise to a component of emergent light that will pass through the analyser.

The electromagnetic wave induces in the molecule at $S(x, y, 0)$ oscillating electric and magnetic moments

$$\begin{aligned} \mu_\alpha(t) &= \mu_{0\alpha} e^{i\omega t}, \\ q_{\alpha\beta}(t) &= q_{0\alpha\beta} e^{i\omega t}, \\ m_\alpha(t) &= m_{0\alpha} e^{i\omega t}, \end{aligned} \tag{2.8}$$

where the magnetic dipole is given by

$$m_\alpha = \sum_i \frac{q_i}{2m_i} (\mathbf{r}_i \times \mathbf{p}_i)_\alpha, \tag{2.9}$$

in which q_i, m_i, and $\mathbf{p}_i$ are, respectively, the charge, mass, and linear momentum of the ith particle; and $\mathbf{r}_i$ is its displacement from the origin. Since effects due to electric quadrupole moments are comparable to those due to magnetic dipole moments, we shall consistently retain terms which are of similar order in the electric quadrupole/magnetic dipole approximation.

The oscillating moments give rise to a vector and scalar potential at D which may be used to find the radiation electric field. The general expression for the field in

vacuum is given by Raab [3]; to terms linear in the electric quadrupole and magnetic dipole it is

$$\mathscr{E}_\alpha(\mathbf{R},t) = \frac{1}{4\pi\varepsilon_0}[\{(R_\alpha R_\beta - R^2\delta_{\alpha\beta})/c^2R^3\}\{\ddot{\mu}_\beta(t') + (R_\gamma/2cR)\dddot{q}_{\beta\gamma}(t') + \cdots\}$$
$$+ \varepsilon_{\alpha\lambda\beta}(R_\lambda/c^3R^2)\ddot{m}_\beta(t') + \cdots], \tag{2.10}$$

in which $t' = t - R/c$ is the retarded time, $\mathbf{R}$ is the vector from $S(x,y,0)$ to $D(0,0,z)$, and $\varepsilon_{\alpha\lambda\beta}$ is the alternating tensor. When applying (2.10) to the geometry considered here, we must, therefore, set $R_x = -x$, $R_y = -y$, and $R_z = z$. Time derivatives of the moments of charge are evaluated from (2.8) and then substituted in the expression for the y-component of (2.10), since it is this component that reaches the detector. The total electric field at D with y-polarization is then given by

$$\mathscr{E}_y = \left[i\mathscr{E}_y^{(0)} + \frac{1}{4\pi\varepsilon_0}\frac{\omega^2 e^{-i\omega(R-z)/c}}{zc^2}\left\{\left(\mu_y + \frac{y}{z}\mu_z\right) - \frac{1}{c}\left(m_x + \frac{x}{z}m_z\right)\right.\right.$$
$$\left.\left. + \frac{i\omega}{2c}\left(q_{yz} + \frac{y}{z}(q_{zz} - q_{yy}) - \frac{x}{z}q_{yx}\right) + \cdots\right\}\right]e^{i\omega(t-z/c)}, \tag{2.11}$$

in which it has been recognised that $R_x, R_y \ll R_z$ and $R_z \approx z$ for molecules on or near the axis of the cell. As expected, the orthogonal component of the $\mathscr{H}$-field of the light wave is given by

$$\mathscr{H}_x = -\mathscr{E}_y,$$

so that the intensity recorded at $D(0,0,z)$, given by the time-averaged Poynting vector, is

$$I_y = -\frac{c}{16\pi}\overline{\mathscr{E}_y\mathscr{H}_x^* + \mathscr{E}_y^*\mathscr{H}_x} = \frac{c}{8\pi}\overline{\mathscr{E}_y\mathscr{E}_y^*}, \tag{2.12}$$

where the bar denotes a statistical average over all molecular positions and orientations with the weighting of (2.7), and the superscripted * denotes a complex conjugate.

If the beam diameter $2r_0$ is much smaller than the distance to the detector z then we may replace $R - z$ with $(x^2 + y^2)/2z$. This approximation is good to within 0.25% for $z \geq 10r_0$. Replacing R with z in places other than in the exponential to obtain (2.11) introduces an error of less than 0.5% if $z \geq 10r_0$. Integrating the expression for $\mathscr{E}_y\mathscr{E}_y^*$ over the aperture of the beam introduces three kinds of integrals:

1.
$$\int_{-r_0}^{r_0}\int_{-r_0}^{r_0} e^{\pm i\omega(x^2+y^2)/2zc}dx\,dy;$$

2.
$$\int_{-r_0}^{r_0}\int_{-r_0}^{r_0} xe^{\pm i\omega(x^2+y^2)/2zc}dx\,dy;$$

3.

$$\int_{-r_0}^{r_0}\int_{-r_0}^{r_0} x^2 e^{\pm i\omega(x^2+y^2)/2zc} dx\, dy.$$

Buckingham and Longuet-Higgins replace these integrals with the limiting case $r_0 \to \infty$. We consider here the validity of doing so.

The integrand in the second case is an odd function of x so this integral is always zero. The third case is reducible to integrals of the first and second case through the technique of integrating by parts. Thus we need only consider the first integral, which may be rewritten in the following way:

$$\begin{aligned}\int_{-r_0}^{r_0}\int_{-r_0}^{r_0} e^{\pm i\omega(x^2+y^2)/2zc} dx\, dy &= 4\left[\int_0^{r_0}\cos\left(\frac{\omega x^2}{2zc}\right)dx \pm i\int_0^{r_0}\sin\left(\frac{\omega x^2}{2zc}\right)dx\right]^2 \\ &= \frac{4\pi zc}{\omega}\left[\int_0^{r_0\sqrt{\frac{\omega}{\pi zc}}}\cos\left(\frac{\pi}{2}t^2\right)dt \pm i\int_0^{r_0\sqrt{\frac{\omega}{\pi zc}}}\sin\left(\frac{\pi}{2}t^2\right)dt\right]^2 \\ &= \frac{4\pi zc}{\omega}\left[C\left(r_0\sqrt{\frac{\omega}{\pi zc}}\right) \pm iS\left(r_0\sqrt{\frac{\omega}{\pi zc}}\right)\right]^2,\end{aligned} \tag{2.13}$$

where $C(x)$ and $S(x)$ are Fresnel integrals defined by [33]

$$\begin{aligned}C(x) &= \int_0^x \cos\left(\frac{\pi}{2}t^2\right)dt, \\ S(x) &= \int_0^x \sin\left(\frac{\pi}{2}t^2\right)dt.\end{aligned}$$

The limiting cases of these integrals are

$$\lim_{x\to\infty} C(x) = \lim_{x\to\infty} S(x) = \tfrac{1}{2}.$$

Convergence to these limits is relatively slow; the expressions given on page 300 of [33] which generate approximate values for Fresnel integrals for $x > 5$ may be used to show that $C(x)$ and $S(x)$ are bounded within 1% of their limits only when $x > 60$. Thus, if we are to replace the Fresnel integrals in (2.13) with their limiting values, we must ensure that

$$r_0\sqrt{\frac{\omega}{\pi zc}} = r_0\sqrt{\frac{2}{z\lambda}} > 60.$$

If we use a He-Ne laser wavelength of 638 nm and consider the case of $z = 10r_0$, then this leads to the restriction $r_0 > 11$ mm. Typical laser beam diameters are of the order of 1 mm, whilst z may be as much as 2 m. This raises questions about the validity of using the limiting case $r_0 \to \infty$. Furthermore, it is clear that the range of ratios of z to r_0 that make all the above approximations valid is bounded above and below. If the pathlength of the beam through the gas is much greater than the

diameter of the beam then some of these restrictions must necessarily be experimentally violated. Notwithstanding these reservations concerning the cogency of this step, we shall present the remainder of the forward-scattering theory on the assumption that all these approximations are valid.

If distortion of the molecule by the field and field gradient is ignored then (2.11) and (2.12) yield

$$\begin{aligned}\frac{8\pi}{c}I_y = (\mathscr{E}_y^{(0)})^2 - \frac{1}{4\pi\varepsilon_0}\frac{2\pi N\omega\mathscr{E}_y^{(0)}Z_0}{c}\Big\langle \frac{\eta}{kT}q_{xy}^{(0)}\Big\{(\mu_y+\mu_y^*) - \frac{1}{c}(m_x+m_x^*) \\ + \frac{i\omega}{2c}(q_{yz}-q_{yz}^*)\Big\} \\ - \frac{ic\eta}{\omega kT}\mu_x^{(0)}\Big\{\mu_z - \mu_z^* - \frac{i\omega}{2c}(q_{yy}+q_{yy}^*-q_{zz}-q_{zz}^*)\Big\} \\ + \frac{ic\eta}{\omega kT}\mu_y^{(0)}\Big\{\frac{1}{c}(m_z-m_z^*) + \frac{i\omega}{2c}(q_{yx}+q_{yx}^*)\Big\} + \cdots\Big\rangle.\end{aligned} \tag{2.14}$$

Expressions for the induced moments and quantum-mechanical expressions for the polarizability tensors should properly be introduced and justified here. However, in order that the discussion of the alternative theory to be presented in §2.4.1 might be self-contained, we shall not do so here and instead use the results given in (2.16), (2.17), (2.18) and (2.24). These express the oscillating moments as:

$$\begin{aligned}\mu_\alpha &= \alpha_{\alpha\beta}\mathscr{E}_\beta + \tfrac{1}{2}a_{\alpha\beta\gamma}\nabla_\gamma\mathscr{E}_\beta + \omega^{-1}G'_{\alpha\beta}\dot{\mathscr{B}}_\beta + \cdots, \\ q_{\alpha\beta} &= a_{\gamma\alpha\beta}\mathscr{E}_\gamma + \cdots, \\ m_\alpha &= -\omega^{-1}G'_{\beta\alpha}\dot{\mathscr{E}}_\beta + \cdots.\end{aligned}$$

Since the only non-zero component of $\mathscr{E}_\alpha$ is

$$\mathscr{E}_x = \mathscr{E}_{0x}e^{i\omega(t-z/c)},$$

the amplitudes of these moments become

$$\begin{aligned}\mu_{0\alpha} &= \Big(\alpha_{\alpha x} - \frac{i\omega}{2c}a_{\alpha zx} + \frac{i}{c}G'_{\alpha y}\Big)\mathscr{E}_x^{(0)}, \\ q_{0\alpha\beta} &= a_{x\alpha\beta}\mathscr{E}_x^{(0)}, \\ m_{0\alpha} &= -iG'_{x\alpha}\mathscr{E}_x^{(0)}.\end{aligned}$$

Substituting these into (2.14), making use of the fact that the polarizability tensors are real (see (2.22) – (2.26)), and using the isotropic averages given in (2.37) to perform the averaging, yield the final expression for the intensity at the detector:

$$\begin{aligned}\frac{8\pi}{c}I_y = (\mathscr{E}_y^{(0)})^2 - \frac{1}{4\pi\varepsilon_0}\frac{\pi N\omega\mathscr{E}_x^{(0)}\mathscr{E}_y^{(0)}Z_0\eta}{15ckT}\Big[6q_{\alpha\beta}^{(0)}\alpha_{\alpha\beta} - 2q_{\alpha\alpha}^{(0)}\alpha_{\beta\beta} \\ - \mu_\alpha^{(0)}\Big(6a_{\beta\beta\alpha} - 2a_{\alpha\beta\beta} + \frac{20}{\omega}\varepsilon_{\alpha\beta\gamma}G'_{\beta\gamma}\Big)\Big].\end{aligned} \tag{2.15}$$

Buckingham and Longuet-Higgins have also investigated the distorting effect of the applied field and field gradient on the polarizability tensors. We shall include this effect in the presentation of the new theory, but do not consider it here since it provides no further insight into the principles of the forward-scattering approach. Discussion and interpretation of (2.15) are deferred until §2.5 where comparison with the analogous result from §2.4 will be made.

2.4 Theory of Induced Birefringence Based on Maxwell's Equations

The molecular theory of the induced birefringence experiment presented in this section was developed as an alternative approach to the radiation treatment outlined in §2.3. Its presentation here closely mirrors the manner in which it has been reported [8].

2.4.1 Molecular multipole moments induced by a light wave

In the treatment that follows we shall consider a dilute gas of neutral diamagnetic molecules.

We begin by considering the effects due to a plane monochromatic light wave of angular frequency ω impinging on an isolated gas molecule. The multipole moments induced by the oscillating electric and magnetic fields, $\mathscr{E}$ and $\mathscr{B}$, and the space and time derivatives of these fields are given by

$$\mu_\alpha = \alpha_{\alpha\beta}\mathscr{E}_\beta + \tfrac{1}{2}a_{\alpha\beta\gamma}\nabla_\gamma\mathscr{E}_\beta + \omega^{-1}G'_{\alpha\beta}\dot{\mathscr{B}}_\beta + \cdots , \tag{2.16}$$

$$q_{\alpha\beta} = a_{\alpha\beta\gamma}\mathscr{E}_\gamma + \cdots , \tag{2.17}$$

$$m_\alpha = \omega^{-1}\mathscr{G}'_{\alpha\beta}\dot{\mathscr{E}}_\beta + \cdots . \tag{2.18}$$

Buckingham [34] has discussed the expression of induced moments in terms of polarizability tensors and applied electromagnetic and electrostatic fields. Moments may be induced by these fields, their space derivatives, and the first time derivative of the electromagnetic fields. There are two reasons why not all such terms are included in (2.16)–(2.18). Firstly, in terms of Neumann's principle a diamagnetic molecule may not possess any time-antisymmetric properties; thus we do not include polarizability tensors that are time-antisymmetric. Secondly, only terms which are of comparable magnitude to within the electric quadrupole/magnetic dipole approximation are retained. The relative magnitudes of the polarizability tensors can be gauged by inspection of their quantum-mechanical expressions.

The applied electrostatic field E_α and field gradient $\nabla_\beta E_\alpha$ may also perturb the internal electronic and vibrational states of a molecule, and we account for this by

extending the equations describing the induced moments to

$$\mu_\alpha = \alpha_{\alpha\beta}\mathscr{E}_\beta + \beta_{\alpha\beta\gamma}\mathscr{E}_\beta E_\gamma + \tfrac{1}{2}b_{\alpha\beta\gamma\delta}\mathscr{E}_\beta\nabla_\delta E_\gamma + \tfrac{1}{2}a_{\alpha\beta\gamma}\nabla_\gamma\mathscr{E}_\beta + \tfrac{1}{2}\mathscr{b}_{\alpha\beta\gamma\delta}\nabla_\gamma\mathscr{E}_\beta E_\delta + \omega^{-1}G'_{\alpha\beta}\dot{\mathscr{B}}_\beta + \omega^{-1}J'_{\alpha\beta\gamma}\dot{\mathscr{B}}_\beta E_\gamma + \cdots, \tag{2.19}$$

$$q_{\alpha\beta} = a_{\alpha\beta\gamma}\mathscr{E}_\gamma + d_{\alpha\beta\gamma\delta}\mathscr{E}_\gamma E_\delta + \cdots, \tag{2.20}$$

$$m_\alpha = \omega^{-1}\mathscr{G}'_{\alpha\beta}\dot{\mathscr{E}}_\beta + \omega^{-1}\mathscr{J}'_{\alpha\beta\gamma}\dot{\mathscr{E}}_\beta E_\gamma + \cdots. \tag{2.21}$$

For a low-intensity light wave it is sufficient to include in (2.19)–(2.21) only terms which are linear in the fields of the light wave. The new tensors which have been introduced really describe the distortion of the polarizability tensors in (2.16)–(2.18) by the static field and its gradient, and are referred to as *hyperpolarizability* tensors.

2.4.2 Quantum-mechanical expressions for the polarizability tensors

We require quantum-mechanical expressions for the tensors appearing in (2.16)–(2.18) in order that any relationships which exist between them may be established, together with any symmetry in the tensor subscripts. Furthermore, it will be necessary to check the origin dependence of tensor expressions for observables, and hence we will need to know the effects of a shift in origin on the individual tensors. These may be determined only from the quantum-mechanical expressions for the tensors.

To obtain these expressions, use is made of first-order time-dependent perturbation theory. Details of these calculations may be found in Appendix B; only the results are presented here, which, for quantum state n, are

$$\alpha_{\alpha\beta} = 2\hbar^{-1}\sum_j Z_{jn}\omega_{jn}\,\mathrm{Re}\{\langle n|\mu_\alpha|j\rangle\langle j|\mu_\beta|n\rangle\} = \alpha_{\beta\alpha}, \tag{2.22}$$

$$a_{\alpha\beta\gamma} = 2\hbar^{-1}\sum_j Z_{jn}\omega_{jn}\,\mathrm{Re}\{\langle n|\mu_\alpha|j\rangle\langle j|q_{\beta\gamma}|n\rangle\} = a_{\alpha\gamma\beta}, \tag{2.23}$$

$$a_{\alpha\beta\gamma} = 2\hbar^{-1}\sum_j Z_{jn}\omega_{jn}\,\mathrm{Re}\{\langle n|q_{\alpha\beta}|j\rangle\langle j|\mu_\gamma|n\rangle\} = a_{\gamma\alpha\beta}, \tag{2.24}$$

$$G'_{\alpha\beta} = -2\hbar^{-1}\sum_j Z_{jn}\omega\,\mathrm{Im}\{\langle n|\mu_\alpha|j\rangle\langle j|m_\beta|n\rangle\}, \tag{2.25}$$

$$\mathscr{G}'_{\alpha\beta} = -2\hbar^{-1}\sum_j Z_{jn}\omega\,\mathrm{Im}\{\langle n|m_\alpha|j\rangle\langle j|\mu_\beta|n\rangle\} = -G'_{\beta\alpha}. \tag{2.26}$$

In these expressions, $\mu_\alpha, q_{\alpha\beta}$, and m_α are operators based on the corresponding classical quantities defined in (1.2), (1.3), and (2.9), whilst

$$\omega_{jn} = \hbar^{-1}(E_j - E_n), \tag{2.27}$$

and, for energies far from a transition,

$$Z_{jn} = (\omega_{jn}^2 - \omega^2)^{-1}.$$

It is also shown in Appendix B how expressions for the hyperpolarizability tensors introduced in (2.19)–(2.21) are found by perturbing the state vectors $|n\rangle$ and $|j\rangle$ in (2.22)–(2.26) and the transition frequency in (2.27) with the applied electrostatic field and its gradient. Comparison of the results obtained from first-order time-independent perturbation theory with the explicit expressions for the distortion of the polarizability tensors by the electrostatic field and field gradient yields

$$\begin{aligned}\beta_{\alpha\beta\gamma} = \beta_{\beta\alpha\gamma} = 2\hbar^{-2}\mathrm{Re}\Bigg\{&\sum_j Z_{jn}^2(\omega_{jn}^2+\omega^2)[\langle j|\mu_\gamma|j\rangle - \langle n|\mu_\gamma|n\rangle]\langle n|\mu_\alpha|j\rangle\langle j|\mu_\beta|n\rangle \\ &+ \sum_{j,k\neq n} Z_{jn}\omega_{kn}^{-1}\omega_{jn}[\langle n|\mu_\gamma|k\rangle\langle k|\mu_\alpha|j\rangle\langle j|\mu_\beta|n\rangle + \langle n|\mu_\alpha|j\rangle\langle j|\mu_\beta|k\rangle\langle k|\mu_\gamma|n\rangle] \\ &+ \sum_{j,k\neq j} Z_{jn}\omega_{kj}^{-1}\omega_{jn}[\langle n|\mu_\alpha|k\rangle\langle k|\mu_\gamma|j\rangle\langle j|\mu_\beta|n\rangle + \langle n|\mu_\alpha|j\rangle\langle j|\mu_\gamma|k\rangle\langle k|\mu_\beta|n\rangle]\Bigg\},\end{aligned} \tag{2.28}$$

$$\begin{aligned}b_{\alpha\beta\gamma\delta} = b_{\beta\alpha\gamma\delta} = b_{\alpha\beta\delta\gamma} = 2\hbar^{-2}\mathrm{Re}\Bigg\{&\sum_j Z_{jn}^2(\omega_{jn}^2+\omega^2)[\langle j|q_{\gamma\delta}|j\rangle - \langle n|q_{\gamma\delta}|n\rangle] \\ &\times \langle n|\mu_\alpha|j\rangle\langle j|\mu_\beta|n\rangle + \sum_{j,k\neq n} Z_{jn}\omega_{kn}^{-1}\omega_{jn}[\langle n|q_{\gamma\delta}|k\rangle\langle k|\mu_\alpha|j\rangle\langle j|\mu_\beta|n\rangle \\ &+ \langle n|\mu_\alpha|j\rangle\langle j|\mu_\beta|k\rangle\langle k|q_{\gamma\delta}|n\rangle] \\ &+ \sum_{j,k\neq j} Z_{jn}\omega_{kj}^{-1}\omega_{jn}[\langle n|\mu_\alpha|k\rangle\langle k|q_{\gamma\delta}|j\rangle\langle j|\mu_\beta|n\rangle \\ &+ \langle n|\mu_\alpha|j\rangle\langle j|q_{\gamma\delta}|k\rangle\langle k|\mu_\beta|n\rangle]\Bigg\},\end{aligned} \tag{2.29}$$

$$\begin{aligned}\wp_{\alpha\beta\gamma\delta} = \wp_{\alpha\gamma\beta\delta} = 2\hbar^{-2}\mathrm{Re}\Bigg\{&\sum_j Z_{jn}^2(\omega_{jn}^2+\omega^2)[\langle j|\mu_\delta|j\rangle - \langle n|\mu_\delta|n\rangle] \\ &\times \langle n|\mu_\alpha|j\rangle\langle j|q_{\beta\gamma}|n\rangle + \sum_{j,k\neq n} Z_{jn}\omega_{kn}^{-1}\omega_{jn}[\langle n|\mu_\delta|k\rangle\langle k|\mu_\alpha|j\rangle\langle j|q_{\beta\gamma}|n\rangle \\ &+ \langle n|\mu_\alpha|j\rangle\langle j|q_{\beta\gamma}|k\rangle\langle k|\mu_\delta|n\rangle] \\ &+ \sum_{j,k\neq j} Z_{jn}\omega_{kj}^{-1}\omega_{jn}[\langle n|\mu_\alpha|k\rangle\langle k|\mu_\delta|j\rangle\langle j|q_{\beta\gamma}|n\rangle \\ &+ \langle n|\mu_\alpha|j\rangle\langle j|\mu_\delta|k\rangle\langle k|q_{\beta\gamma}|n\rangle]\Bigg\},\end{aligned} \tag{2.30}$$

$$J'_{\alpha\beta\gamma} = 2\hbar^{-2}\mathrm{Im}\left\{\sum_j 2Z^2_{jn}\omega\omega_{jn}[\langle j|\mu_\gamma|j\rangle - \langle n|\mu_\gamma|n\rangle]\langle n|\mu_\alpha|j\rangle\langle j|m_\beta|n\rangle \right.$$
$$+ \sum_{j,k\neq n} Z_{jn}\omega^{-1}_{kn}\omega[\langle n|\mu_\gamma|k\rangle\langle k|\mu_\alpha|j\rangle\langle j|m_\beta|n\rangle + \langle n|\mu_\alpha|j\rangle\langle j|m_\beta|k\rangle\langle k|\mu_\gamma|n\rangle]$$
$$\left. + \sum_{j,k\neq j} Z_{jn}\omega^{-1}_{kj}\omega[\langle n|\mu_\alpha|k\rangle\langle k|\mu_\gamma|j\rangle\langle j|m_\beta|n\rangle + \langle n|\mu_\alpha|j\rangle\langle j|\mu_\gamma|k\rangle\langle k|m_\beta|n\rangle]\right\}, \tag{2.31}$$

$$d_{\alpha\beta\gamma\delta} = \ell_{\gamma\alpha\beta\delta}, \quad \mathscr{J}'_{\alpha\beta\gamma} = -J'_{\beta\alpha\gamma}.$$

From the results of this section, (2.20) and (2.21) become

$$q_{\alpha\beta} = a_{\gamma\alpha\beta}\mathscr{E}_\gamma + \ell_{\gamma\alpha\beta\delta}\mathscr{E}_\gamma E_\delta + \cdots, \tag{2.32}$$
$$m_\alpha = -\omega^{-1}G'_{\beta\alpha}\dot{\mathscr{E}}_\beta - \omega^{-1}J'_{\beta\alpha\gamma}\dot{\mathscr{E}}_\beta E_\gamma + \cdots. \tag{2.33}$$

2.4.3 Orientational averaging

The induced multipole moments in (2.19), (2.32), and (2.33) are those for a given orientation of the molecule relative to laboratory-fixed axes. In practice, the orientation of any given molecule changes rapidly with time, and so we must find expressions for the time-averaged values of the induced moments as seen by an observer who is stationary in the laboratory. When we write μ_α we are taking a component of the induced electric dipole moment relative to the laboratory axes. Clearly, this is a function of the orientation of the molecule relative to these axes, which in turn depends on the rotational energy state of the molecule. In the absence of external fields, it is apparent that all orientations are equally probable, and the time-averaging is achieved by performing an isotropic average. However, in the presence of an applied electric field $\mathbf{E}$ and field gradient $\nabla\mathbf{E}$, the distribution of the rotational energy states of the molecule is no longer flat, but takes on a Boltzmann distribution. If we assume that the distribution is unaffected by weak light wave fields, then the probability that the molecule lies within an orientational element $d\tau$ at an orientation τ is

$$\frac{\exp(-U(\mathbf{E},\nabla\mathbf{E},\tau)/kT)d\tau}{\int \exp(-U(\mathbf{E},\nabla\mathbf{E},\tau)/kT)d\tau},$$

in which the energy $U(\mathbf{E},\nabla\mathbf{E},\tau)$ is given by

$$U(\mathbf{E},\nabla\mathbf{E},\tau) = U^{(0)} - \mu^{(0)}_\alpha(\tau)E_\alpha - \tfrac{1}{2}q^{(0)}_{\alpha\beta}(\tau)\nabla_\beta E_\alpha - \cdots. \tag{2.34}$$

In this $\mu^{(0)}_\alpha$ and $q^{(0)}_{\alpha\beta}$ are the permanent electric dipole and quadrupole moments, respectively.

At room temperature the rotational energy levels of most molecules lie close enough together for their orientation to be regarded as continuous, and the average of a molecular quantity X in the presence of $\mathbf{E}$ and $\nabla\mathbf{E}$ is then found by integrating over all

orientations, namely

$$\overline{X(\mathbf{E},\nabla\mathbf{E})} = \frac{\int X(\mathbf{E},\nabla\mathbf{E},\tau)\exp(-U(\tau)/kT)d\tau}{\int \exp(-U(\tau)/kT)d\tau}. \tag{2.35}$$

In the cases of molecules in which the rotational energy states are too widely spaced to assume continuity, a discrete summation must be performed over the energy levels. This is discussed further in §2.6.

By Taylor-expanding X in powers of the independent quantities E_α and $\nabla_\beta E_\alpha$ about $E_\alpha = 0$ and $\nabla_\beta E_\alpha = 0$ we obtain from (2.35)

$$\begin{aligned}\overline{X(\mathbf{E},\nabla\mathbf{E})} = \langle X\rangle &+ E_\alpha\left\{\left\langle\frac{\partial X}{\partial E_\alpha}\right\rangle - \frac{1}{kT}\left[\left\langle X\frac{\partial U}{\partial E_\alpha}\right\rangle - \langle X\rangle\left\langle\frac{\partial U}{\partial E_\alpha}\right\rangle\right]\right\}\\ &+ \nabla_\beta E_\alpha\left\{\left\langle\frac{\partial X}{\partial \nabla_\beta E_\alpha}\right\rangle - \frac{1}{kT}\left[\left\langle X\frac{\partial U}{\partial \nabla_\beta E_\alpha}\right\rangle - \langle X\rangle\left\langle\frac{\partial U}{\partial \nabla_\beta E_\alpha}\right\rangle\right]\right\} + \cdots,\end{aligned} \tag{2.36}$$

where $\langle\cdots\rangle$ denotes an isotropic average for zero field and field gradient. Non-vanishing isotropic averages are well documented [35], and those used in this work are

$$\begin{aligned}\langle i_\alpha i_\beta\rangle = \langle j_\alpha j_\beta\rangle = \langle k_\alpha k_\beta\rangle &= \tfrac{1}{3}\delta_{\alpha\beta},\\ \langle i_\alpha j_\beta k_\gamma\rangle &= \tfrac{1}{6}\varepsilon_{\alpha\beta\gamma},\\ \langle i_\alpha i_\beta i_\gamma i_\delta\rangle = \langle j_\alpha j_\beta j_\gamma j_\delta\rangle = \langle k_\alpha k_\beta k_\gamma k_\delta\rangle &= \tfrac{1}{15}(\delta_{\alpha\beta}\delta_{\gamma\delta} + \delta_{\alpha\gamma}\delta_{\beta\delta} + \delta_{\alpha\delta}\delta_{\beta\gamma}),\\ \langle i_\alpha i_\beta j_\gamma j_\delta\rangle = \langle j_\alpha j_\beta k_\gamma k_\delta\rangle = \langle k_\alpha k_\beta i_\gamma i_\delta\rangle &= \tfrac{1}{30}(4\delta_{\alpha\beta}\delta_{\gamma\delta} - \delta_{\alpha\gamma}\delta_{\beta\delta} - \delta_{\alpha\delta}\delta_{\beta\gamma}),\end{aligned} \tag{2.37}$$

where $\mathbf{i},\mathbf{j},\mathbf{k}$ are unit vectors along the x, y, z axes, respectively, of a Cartesian system fixed in space. All other averages up to 4th rank are zero. It follows from the antisymmetric property of $\varepsilon_{\alpha\beta\gamma}$ that the average of any third-rank tensor with permutation symmetry in two of its subscripts will be zero.

By applying (2.36) and (2.34) to (2.19), (2.32), and (2.33) one obtains

$$\begin{aligned}\bar{\mu}_\alpha = \langle\alpha_{\alpha\beta}\rangle\mathscr{E}_\beta &+ \omega^{-1}\langle G'_{\alpha\beta}\rangle\dot{\mathscr{B}}_\beta + E_\delta\{\tfrac{1}{2}\langle\mathscr{b}_{\alpha\beta\gamma\delta}\rangle\nabla_\gamma\mathscr{E}_\beta + \omega^{-1}\langle J'_{\alpha\beta\gamma}\rangle\dot{\mathscr{B}}_\beta\\ &+ (kT)^{-1}(\tfrac{1}{2}\langle\mu^{(0)}_\delta a_{\alpha\beta\gamma}\rangle\nabla_\gamma\mathscr{E}_\beta + \omega^{-1}\langle\mu^{(0)}_\delta G'_{\alpha\beta}\rangle\dot{\mathscr{B}}_\beta)\} + \tfrac{1}{2}\nabla_\delta E_\gamma\{\langle b_{\alpha\beta\gamma\delta}\rangle\\ &+ (kT)^{-1}(\langle q^{(0)}_{\gamma\delta}\alpha_{\alpha\beta}\rangle - \langle q^{(0)}_{\gamma\delta}\rangle\langle\alpha_{\alpha\beta}\rangle)\}\mathscr{E}_\beta + \cdots,\end{aligned} \tag{2.38}$$

$$\bar{q}_{\alpha\beta} = E_\delta\{\langle\mathscr{b}_{\gamma\alpha\beta\delta}\rangle + (kT)^{-1}\langle\mu^{(0)}_\delta a_{\gamma\alpha\beta}\rangle\}\mathscr{E}_\gamma + \cdots, \tag{2.39}$$

$$\overline{m}_\alpha = -\omega^{-1}\{\langle G'_{\beta\alpha}\rangle + E_\gamma[\langle J'_{\beta\alpha\gamma}\rangle + (kT)^{-1}\langle\mu^{(0)}_\gamma G'_{\beta\alpha}\rangle]\}\dot{\mathscr{E}}_\beta + \cdots. \tag{2.40}$$

In these equations only terms with magnitude greater than that of $q^{(0)}_{\alpha\beta}a_{\gamma\delta\varepsilon}$ have been retained.

2.4.4 Electromagnetic theory

The electric field of the light wave in the gas is represented by

$$\mathscr{E} = \mathscr{E}^{(0)} \exp\{-i\omega(t - n\mathbf{r} \cdot \boldsymbol{\sigma}/c)\}, \tag{2.41}$$

where $\boldsymbol{\sigma}$ is the unit vector in the direction of propagation and n is the refractive index of the gas for the polarization state of the wave described by the complex amplitude $\mathscr{E}^{(0)}$. From (2.41) and the Maxwell equation

$$\nabla \times \mathscr{E} = -\dot{\mathscr{B}}$$

it follows that

$$\nabla_\beta \mathscr{E}_\alpha = i\omega n c^{-1} \sigma_\beta \mathscr{E}_\alpha, \tag{2.42}$$

$$\mathscr{B}_\alpha = n c^{-1} \varepsilon_{\alpha\beta\gamma} \sigma_\beta \mathscr{E}_\gamma. \tag{2.43}$$

Use of (2.41)–(2.43) in (2.38)–(2.40) yields

$$\begin{aligned} \bar{\mu}_\alpha &= R_{\alpha\beta} \mathscr{E}_\beta, \\ \bar{q}_{\alpha\beta} &= S_{\alpha\beta\gamma} \mathscr{E}_\gamma, \\ \overline{m}_\alpha &= T_{\alpha\beta} \mathscr{E}_\beta, \end{aligned} \tag{2.44}$$

in which

$$\begin{aligned} R_{\alpha\beta} = {} & \langle \alpha_{\alpha\beta} \rangle + inc^{-1} \varepsilon_{\beta\gamma\delta} \sigma_\gamma \langle G'_{\alpha\delta} \rangle + i\omega n c^{-1} \sigma_\gamma E_\varepsilon \{ \tfrac{1}{2} \langle \mathscr{b}_{\alpha\beta\gamma\varepsilon} \rangle \\ & + \omega^{-1} \varepsilon_{\beta\gamma\delta} \langle J'_{\alpha\delta\varepsilon} \rangle + (kT)^{-1} (\tfrac{1}{2} \langle \mu_\varepsilon^{(0)} a_{\alpha\beta\gamma} \rangle + \omega^{-1} \varepsilon_{\beta\gamma\delta} \langle \mu_\varepsilon^{(0)} G'_{\alpha\delta} \rangle) \} \\ & + \tfrac{1}{2} \nabla_\delta E_\gamma \{ \langle b_{\alpha\beta\gamma\delta} \rangle + (kT)^{-1} (\langle q_{\gamma\delta}^{(0)} \alpha_{\alpha\beta} \rangle - \langle q_{\gamma\delta}^{(0)} \rangle \langle \alpha_{\alpha\beta} \rangle) \} + \cdots, \end{aligned} \tag{2.45}$$

$$S_{\alpha\beta\gamma} = E_\delta \{ \langle \mathscr{b}_{\gamma\alpha\beta\delta} \rangle + (kT)^{-1} \langle \mu_\delta^{(0)} a_{\gamma\alpha\beta} \rangle \} + \cdots, \tag{2.46}$$

$$T_{\alpha\beta} = i \{ \langle G'_{\beta\alpha} \rangle + E_\gamma [\langle J'_{\beta\alpha\gamma} \rangle + (kT)^{-1} \langle \mu_\gamma^{(0)} G'_{\beta\alpha} \rangle] \} + \cdots. \tag{2.47}$$

The macroscopic multipole moment densities for electric dipole, electric quadrupole, and magnetic dipole are given by [36]

$$P_\alpha = N \bar{\mu}_\alpha, \quad Q_{\alpha\beta} = N \bar{q}_{\alpha\beta}, \quad M_\alpha = N \overline{m}_\alpha, \tag{2.48}$$

where N is the number density of molecules.

These macroscopic quantities are substituted in the Maxwell equation for a source-free medium

$$\nabla \times \mathbf{H} = \dot{\mathbf{D}}, \tag{2.49}$$

giving

$$D_\alpha = \varepsilon_0 E_\alpha + P_\alpha - \tfrac{1}{2} \nabla_\beta Q_{\alpha\beta} + \cdots, \tag{2.50}$$

$$H_\alpha = \mu_0^{-1} B_\alpha - M_\alpha + \cdots. \tag{2.51}$$

Combining (2.48)–(2.51) and (2.44) yields

$$\varepsilon_{\alpha\beta\gamma}\nabla_\beta\{n(\mu_0 c)^{-1}\varepsilon_{\gamma\delta\varepsilon}\sigma_\varepsilon + NT_{\gamma\delta}\}\mathscr{E}_\delta = i\omega\{\varepsilon_0\mathscr{E}_\alpha + NR_{\alpha\beta}\mathscr{E}_\beta - \tfrac{1}{2}N\nabla_\beta S_{\alpha\beta\gamma}\mathscr{E}_\gamma\}, \tag{2.52}$$

in which ∇ differentiates $\mathscr{E}$ and also $\mathbf{E}$ in $T_{\gamma\delta}$ and $S_{\alpha\beta\gamma}$ in (2.46) and (2.47). When the experiment is performed, the applied field is modulated to facilitate the use of phase-sensitive detection techniques. Despite this, the time-derivative expressed in (2.49) is not extended to the applied field $\mathbf{E}$ and its gradient, which enter (2.50) and (2.51) through (2.45)–(2.47), since this would give rise to terms containing the modulation frequency as a factor, and which would therefore be several orders of magnitude smaller than the corresponding terms which arise as a consequence of taking the time-derivative of $\mathscr{E}$. After the differentiation in (2.52) we set $\mathbf{E} = \mathbf{0}$, since the light beam in the quadrupole experiment travels along, or close to, the axis of the cell, where the field gradient is uniform and the electric field is zero. In fact, it is not correct to set $\mathbf{E} = \mathbf{0}$ for this reason, since there are off-axis regions which the beam traverses and where the electric field very clearly is not zero. However, we have already discussed how this is accounted for experimentally in §2.2. One finally obtains

$$\begin{aligned} n^2c^{-2}(\sigma_\alpha\sigma_\beta - \delta_{\alpha\beta})\mathscr{E}_\beta^{(0)} + \mu_0\varepsilon_0\mathscr{E}_\alpha^{(0)} + \mu_0 N\{\langle\alpha_{\alpha\delta}\rangle - inc^{-1}\sigma_\gamma(\varepsilon_{\gamma\delta\varepsilon}\langle G'_{\alpha\varepsilon}\rangle + \varepsilon_{\alpha\gamma\varepsilon}\langle G'_{\delta\varepsilon}\rangle)\}\mathscr{E}_\delta^{(0)} \\ + \mu_0 N\nabla_\delta E_\gamma\{\tfrac{1}{2}\langle b_{\alpha\beta\gamma\delta}\rangle - \tfrac{1}{2}\langle\ell_{\beta\alpha\delta\gamma}\rangle - \omega^{-1}\varepsilon_{\alpha\delta\varepsilon}\langle J'_{\beta\varepsilon\gamma}\rangle - (kT)^{-1}(\tfrac{1}{2}\langle\mu_\gamma^{(0)}a_{\beta\alpha\delta}\rangle \\ + \omega^{-1}\varepsilon_{\alpha\delta\varepsilon}\langle\mu_\gamma^{(0)}G'_{\beta\varepsilon}\rangle + \tfrac{1}{2}\langle q_{\gamma\delta}^{(0)}\rangle\langle\alpha_{\alpha\beta}\rangle - \tfrac{1}{2}\langle q_{\gamma\delta}^{(0)}\alpha_{\alpha\beta}\rangle)\}\mathscr{E}_\beta^{(0)} = 0. \end{aligned} \tag{2.53}$$

In this the phase factor in (2.41) has been suppressed since (2.53) applies for all t and $\mathbf{r}$. Within the electric quadrupole/magnetic dipole approximation this is the basic equation for describing light propagation in a dilute gas in a region of zero field and uniform field gradient.

2.4.5 Expression for the induced birefringence

We have already established that the applied electric field may be taken to be zero whilst, by choosing Cartesian axes such that the wires lie in the zy-plane with the z-axis coinciding with the axis of the cell, the electric field gradient tensor has only two non-zero components (see Appendix A), namely

$$\nabla_x E_x = -\nabla_y E_y = E'.$$

Setting $\alpha = x, y, z$ in turn in (2.53), and considering propagation of the beam in the z-direction so that $\sigma_z = 1, \sigma_x = \sigma_y = 0$, we obtain, on performing the isotropic averages,

$$(\mu_0\varepsilon_0 - n^2c^{-2} + \tfrac{1}{3}\mu_0 N\alpha_{\alpha\alpha} + \mu_0 NsE')\mathscr{E}_x^{(0)} + \tfrac{2}{3}inc^{-1}\mu_0 NG'_{\alpha\alpha}\mathscr{E}_y^{(0)} = 0, \tag{2.54}$$

$$-\tfrac{2}{3}inc^{-1}\mu_0 NG'_{\alpha\alpha}\mathscr{E}_x^{(0)} + (\mu_0\varepsilon_0 - n^2c^{-2} + \tfrac{1}{3}\mu_0 N\alpha_{\alpha\alpha} - \mu_0 NsE')\mathscr{E}_y^{(0)} = 0, \tag{2.55}$$

$$(\mu_0\varepsilon_0 + \tfrac{1}{3}\mu_0 N\alpha_{\alpha\alpha})\mathscr{E}_z^{(0)} = 0, \tag{2.56}$$

where, relative to molecule-fixed axes,

$$s = \tfrac{1}{60}\{6b_{\alpha\beta\alpha\beta} - 2b_{\alpha\alpha\beta\beta} - \mathscr{b}_{\alpha\alpha\beta\beta} - 3\mathscr{b}_{\alpha\beta\beta\alpha} - 10\omega^{-1}\varepsilon_{\alpha\beta\gamma}J'_{\alpha\beta\gamma} + (kT)^{-1}[6q^{(0)}_{\alpha\beta}\alpha_{\alpha\beta} - 2q^{(0)}_{\alpha\alpha}\alpha_{\beta\beta} - \mu^{(0)}_{\alpha}(3a_{\alpha\beta\beta} + a_{\beta\beta\alpha} + 10\omega^{-1}\varepsilon_{\alpha\beta\gamma}G'_{\beta\gamma})]\}. \quad (2.57)$$

The solution of (2.56) is $\mathscr{E}^{(0)}_z = 0$, as expected. That of (2.54) and (2.55) is equally simple if we limit consideration to optically inactive molecules, since for them $G'_{\alpha\alpha} = 0$ [2]. Then, for the polarization eigenvectors,

$$\begin{aligned} \mathscr{E}^{(0)}_x \neq 0, \quad \mathscr{E}^{(0)}_y = 0: \quad & n_x^2 c^{-2} = \mu_0\varepsilon_0 + \tfrac{1}{3}\mu_0 N\alpha_{\alpha\alpha} + \mu_0 NsE', \\ \mathscr{E}^{(0)}_x = 0, \quad \mathscr{E}^{(0)}_y \neq 0: \quad & n_y^2 c^{-2} = \mu_0\varepsilon_0 + \tfrac{1}{3}\mu_0 N\alpha_{\alpha\alpha} - \mu_0 NsE', \end{aligned}$$

where n_y is the refractive index for light linearly polarized parallel to the plane of wires, and n_x for the perpendicular polarization. Thus the birefringence induced by the field gradient is

$$n_x - n_y = \mu_0 c^2 NsE' = \varepsilon_0^{-1} NsE', \quad (2.58)$$

since, for a dilute gas, $n_x + n_y = 2$ to a very good approximation. For a linear molecule, the symmetry axis of which is the z-axis of the molecular system, (2.57) and (2.58) yield

$$n_x - n_y = \tfrac{1}{2}\varepsilon_0^{-1} NE'\{b + 2(15kT)^{-1}[q^{(0)}\Delta\alpha - \tfrac{1}{2}\mu^{(0)}(2a_1 + a_2 + 3a_3 + 10\omega^{-1}G')]\}, \quad (2.59)$$

where

$$\begin{gathered} \mu^{(0)} = \mu^{(0)}_z, \\ q^{(0)} = q^{(0)}_{zz} - q^{(0)}_{xx}, \\ \Delta\alpha = \alpha_{zz} - \alpha_{xx}, \\ a_1 = a_{zzz}, \quad a_2 = a_{xxz} = a_{yyz}, \quad a_3 = a_{zxx} = a_{zyy}, \\ G' = G'_{xy} = -G'_{yx}. \end{gathered}$$

The form for a linear molecule of the temperature-independent term in (2.59) is not detailed, as there is evidence that it is negligible relative to the term in $(kT)^{-1}$ [37].

2.5 Effect of an Origin Shift

When the origin in a neutral molecule is displaced through $\mathbf{R}$, the multipole moment operators based on (1.2), (1.3), and (2.9) change by

$$\begin{aligned} \Delta\mu_\alpha &= 0, \\ \Delta q_{\alpha\beta} &= -R_\alpha\mu_\beta - R_\beta\mu_\alpha, \\ \Delta m_\alpha &= -\varepsilon_{\alpha\beta\gamma}R_\beta \sum_i (q_i/2m_i)\, p_{i\gamma}. \end{aligned}$$

The shifts in the polarizability tensors in (2.22), (2.23), (2.25), and (2.29)–(2.31) are then found to be

$$\begin{aligned}
\Delta\alpha_{\alpha\beta} &= 0, \\
\Delta a_{\alpha\beta\gamma} &= -R_\beta \alpha_{\alpha\gamma} - R_\gamma \alpha_{\alpha\beta}, \\
\Delta G'_{\alpha\beta} &= \tfrac{1}{2}\omega\, \varepsilon_{\beta\gamma\delta} R_\gamma \alpha_{\alpha\delta}, \\
\Delta b_{\alpha\beta\gamma\delta} &= -R_\gamma \beta_{\alpha\beta\delta} - R_\delta \beta_{\alpha\beta\gamma}, \\
\Delta \mathscr{b}_{\alpha\beta\gamma\delta} &= -R_\beta \beta_{\alpha\gamma\delta} - R_\gamma \beta_{\alpha\beta\delta}, \\
\Delta J'_{\alpha\beta\gamma} &= \tfrac{1}{2}\omega\, \varepsilon_{\beta\delta\varepsilon} R_\delta \beta_{\alpha\varepsilon\gamma}.
\end{aligned}$$

From these results and (2.57) and (2.58) it is readily shown that the birefringence expression obtained from the theory in §2.4 does not depend on the choice of origin in the molecule; the temperature-dependent and temperature-independent parts are, of course, separately origin-independent. These same results may also be used to show that the expression for the intensity (2.15) obtained from the forward-scattering theory discussed in §2.3 is also independent of the origin chosen.

Buckingham and Longuet-Higgins [12] present their theory in terms of the traceless quadrupole moment and obtain as the molecular part of the final expression for the intensity I_y

$$B_{\alpha\beta\alpha\beta} - \mathscr{B}_{\alpha\alpha\beta\beta} - 5\omega^{-1}\varepsilon_{\alpha\beta\gamma} J'_{\alpha\beta\gamma} + (kT)^{-1}[\theta^{(0)}_{\alpha\beta}\alpha_{\alpha\beta} - \mu^{(0)}_\alpha (A_{\beta\beta\alpha} + 5\omega^{-1}\varepsilon_{\alpha\beta\gamma} G'_{\beta\gamma})], \tag{2.60}$$

in which the polarizability tensors $B_{\alpha\beta\gamma\delta}$, $\mathscr{B}_{\alpha\beta\gamma\delta}$, and $A_{\alpha\beta\gamma}$ are the traceless-quadrupole analogues of $b_{\alpha\beta\gamma\delta}$, $\mathscr{b}_{\alpha\beta\gamma\delta}$, and $a_{\alpha\beta\gamma}$. This expression may also be shown to be independent of the choice of origin to which the multipole moments are referred. However, if the theory presented in §2.4 is repeated in terms of the traceless quadrupole moment, and (1.12) is taken as the form for the **D**-vector, then the molecular part of the birefringence expression is found to be

$$B_{\alpha\beta\alpha\beta} - \tfrac{1}{6}\mathscr{B}_{\alpha\alpha\beta\beta} - \tfrac{5}{2}\omega^{-1}\varepsilon_{\alpha\beta\gamma} J'_{\alpha\beta\gamma} + (kT)^{-1}[\theta^{(0)}_{\alpha\beta}\alpha_{\alpha\beta} - \mu^{(0)}_\alpha (\tfrac{1}{6}A_{\beta\beta\alpha} + \tfrac{5}{2}\omega^{-1}\varepsilon_{\alpha\beta\gamma} G'_{\beta\gamma})], \tag{2.61}$$

which is not origin-independent. This is not unexpected in view of the findings of Graham and Raab [5] who show that (1.12) is an incorrect form for the **D**-vector which leads to an origin-dependent set of Maxwell equations. Buckingham and Longuet-Higgins' result when expressed in terms of the primitive quadrupole moment is also origin-independent since their forward-scattering theory does not make explicit use of the **D**-vector.

Origin-independence is a necessary test for expressions describing observables in terms of molecular property tensors. Both molecular theories presented in this chapter pass this test despite giving different results. Therein lies a paradox, since these two different results cannot both describe the same observable. If we consider the special

case of non-polar molecules, then both expressions reduce to (2.3), the expression given by the original theory for non-polar molecules. We shall not attempt to resolve this paradox here, except to suggest that the solution may lie in the bounded range of detector-distance to beam-diameter ratios for which the approximations used in the forward-scattering theory are valid.

The need for a theory describing induced birefringence measurements in polar molecules arose out of the ambiguity concerning the origin to which quadrupole moments were referred, when these are evaluated by using (2.3). Since the expression $3a_{\alpha\beta\beta} + a_{\beta\beta\alpha} + 10\omega^{-1}\varepsilon_{\alpha\beta\gamma}G'_{\beta\gamma}$ in (2.57) depends on origin, there must exist at least one point at which it vanishes. This point is not unique but, in the case of a linear polar molecule, there exists only one point on the axis of the molecule at which the expression is zero. One may then interpret this point, called by Buckingham and Longuet-Higgins the *effective quadrupole centre*, as the origin to which $q^{(0)}$ in (2.59) is referred. One of the discrepancies between the two molecular theories discussed in this chapter is in the expression giving the location of the effective quadrupole centre.

2.6 Quantum Corrections to the Classical Birefringence Expressions

The use of classical Boltzmann averaging in (2.35) is valid only if the rotational energy levels of the molecules are sufficiently closely spaced as to give a good approximation of continuity. This is usually true for polyatomic molecules with large moments of inertia I, but may not hold for small diatomic molecules such as molecular hydrogen.

Buckingham and Pariseau [38] have given the quantum-mechanical derivation of an expression for the birefringence induced in a non-polar gas and its application to diatomic molecules. Not only is the temperature-dependent term in the classical expression modified due to the discrete nature of the rotational energy levels, but a further contribution arises as a consequence of the nuclear motion. If we ignore the latter effect then the birefringence may be written as

$$n_x - n_y = \frac{1}{4\pi\varepsilon_0}\frac{4\pi N_0 E'}{15V_m}\left[B' + (kT)^{-1}\theta\Delta\alpha f(T)\right],$$

in which the correction factor $f(T)$ is given by

$$f(T) = 1 - \frac{\hbar^2}{2IkT} + \tfrac{8}{15}\left(\frac{\hbar^2}{2IkT}\right)^2 + \cdots.$$

Chapter 3

BIREFRINGENCE MEASURING TECHNIQUES

3.1 Introduction

Having derived in the previous chapter an expression for the birefringence induced in a gas by an electric field gradient in terms of molecular property tensors, we consider in this chapter how best the induced birefringence might be measured.

References in this chapter to the azimuths of polarization states and the orientations of the axes of optical components are made with respect to the system of right-handed Cartesian axes shown in Figure 3.1. The z-axis is chosen to coincide with the path of the light beam propagating along the axis of the cell containing the gas in which birefringence has been induced, and which shall hereafter be referred to as the *quadrupole cell.* This light is monochromatic and linearly polarized at an azimuth, measured counterclockwise from the positive x-axis, which we define to be exactly $\frac{\pi}{4}$ radians. We have thus fixed the position of the x-axis, preferring to locate it relative to the polarization azimuth of the incident beam rather than with respect to the plane of the wires in the quadrupole cell in order that we may later consider the effects of a small rotational offset in the orientation of the cell. For the present, however, we shall assume that the plane of the wires coincides with the yz-plane as indicated in Figure 3.1.

The beam of light entering the cell may be resolved into two components having orthogonal electric vectors $\mathscr{E}_x$ and $\mathscr{E}_y$ which experience different refractive indices n_x and n_y. If the geometric path length of the beam in the gas is l, then the two components will emerge from the cell with a relative phase difference δ given by

$$\delta = \frac{2\pi l}{\lambda}(n_x - n_y), \tag{3.1}$$

in which λ is the wavelength of the light. We may therefore model the quadrupole cell as a linear retarder of azimuth 0 and retardation δ. Conventionally, the azimuth of a linear retarder is specified by the orientation of its fast axis; we have arbitrarily chosen this to be the axis lying perpendicular to the plane of the wires. We show later

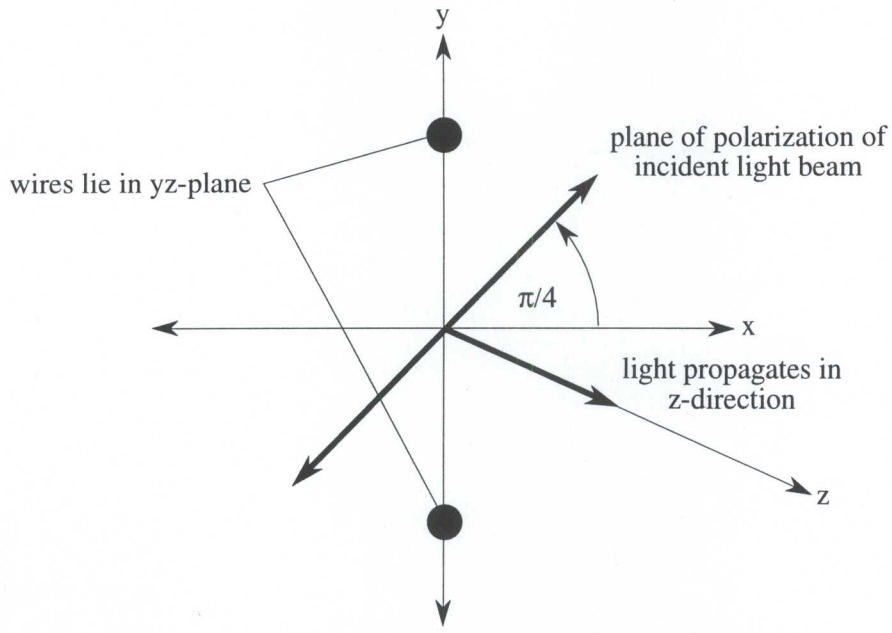

Figure 3.1 System of axes used in specifying all azimuths

that the experiment requires the electric field gradient to be modulated, in which case making an arbitrary choice for the fast-axis direction at this stage does not result in any loss of generality later.

Recombining $\mathscr{E}_x$ and $\mathscr{E}_y$ at the point of emergence of the light beam from the cell shows that the beam is now elliptically polarized in general, although its azimuth is still $\frac{\pi}{4}$. If the beam is next passed through a quarter-wave plate (hereafter called a $\frac{\lambda}{4}$-plate) with its fast axis set at an azimuth of $\frac{\pi}{4}$ and having retardation $\frac{\pi}{2}$, then, through the use of elementary analytical techniques, it may be shown that the light will emerge linearly polarized with azimuth $\frac{\pi}{4} + \frac{\delta}{2}$. The net effect of the quadrupole cell and the $\frac{\lambda}{4}$-plate has been to rotate the plane of polarization of the incident beam by $\frac{\delta}{2}$.

If δ was large then it could be measured as being twice the angle through which the analyser would have to be offset from its initial crossed position in order to achieve extinction. However, δ is not large; typically it is of the order 10^{-6} radians and must be determined to within 1%. This suggests the employment of the technique of phase-sensitive detection, which requires that the signal be modulated and an opto-electrical transducer be used to monitor the intensity of the light passing through the analyser. These requirements are met experimentally by applying a high ac voltage of angular frequency ω to the wires in the cell, and locating a photomultiplier behind the analyser.

Because of the smallness of δ, mechanical rotation of the analyser is not a viable method for nulling the effect due to the induced birefringence. A calibrated optical rotator capable of rotating the plane of polarization by small amounts is required. Because of the experience of Pierrus [39], a Faraday cell was chosen for this purpose in

preference to a Kerr cell. The Faraday cell is described in §4.5 but, for the purposes of this chapter, it will suffice to model it as an optical rotator capable of producing a variable but known rotation θ. This effect is also modulated at angular frequency ω but is in antiphase with δ.

With the polarizer and analyser crossed and the fast axis of the $\frac{\lambda}{4}$-plate set at an azimuth of $\frac{\pi}{4}$, the intensity of the light reaching the photomultiplier as a consequence of the induced birefringence alone is far too small to produce a signal which is discernible from the background noise inherent in the photomultiplier and the electronics. The solution is to amplify the optical signal by several orders of magnitude by deliberately allowing more light to reach the photomultiplier. Examples of how this might be achieved include: deliberately offsetting the $\frac{\lambda}{4}$-plate by a small angle; doing likewise with the analyser; passing a sufficient dc current through the windings of the Faraday cell; and introducing a $\frac{\lambda}{2}$-plate with a small offset between the $\frac{\lambda}{4}$-plate and the Faraday cell. Performing the analysis for any of these methods reveals that the expression for the intensity I at the photomultiplier now contains terms which are proportional to the product of the small offset angle and both δ and θ separately. Since any offset couples with δ and θ in exactly the same way, it is possible to measure I as a function of θ and then to find δ from a graphical analysis.

Deliberately allowing more light to pass through the analyser will also produce a very large dc term in the expression for I. However, the phase-sensitive detector (hereafter abbreviated to psd) is better at isolating a good signal in a large background of noise than it is at locking on to a very small signal hidden in a smaller background.

Two of the suggested methods for providing a small offset may be discarded at this point. The current required in the coil of the Faraday cell in order to produce a suitable rotation ($\sim 1°$) would dissipate sufficient heat to cause turbulence in the liquid in the cell. Introducing an additional component, the $\frac{\lambda}{2}$-plate, is also a poor idea because of complications that arise as a consequence of any small inaccuracies in its retardance, and because of the loss in transmitted intensity due to reflections off its surfaces. Thus we are left with the choice of offsetting either the $\frac{\lambda}{4}$-plate or the analyser.

Previous work on this apparatus [39] employed the option of offsetting the $\frac{\lambda}{4}$-plate by a small angle ε from the position in which the fast axis is at $\frac{\pi}{4}$. It was subsequently found that the value of δ measured in this way depended on the sign of ε. An explanation for this unexpected behaviour was put forward [39] in which the effect was attributed to the presence of small amounts of residual strain in the glass windows of the cell. This strain causes the windows to exhibit birefringence which, it was shown, can largely be eliminated by plotting graphs of I vs θ for offsets of $+\varepsilon_1$ and $-\varepsilon_2$, and then finding θ_{null} from the point where these lines intersect.

Results obtained using this method are not always in agreement with those obtained by other workers. For example, the quadrupole moment found for the carbon dioxide molecule differs by 8% from the best values reported at the time. In an attempt to explain this discrepancy a more comprehensive analysis of the optical cascade was undertaken, with the consequence that the experiment has now been redesigned and results obtained which are in good agreement with those of other workers. This analysis

of the optical cascade is presented in the remainder of this chapter.

3.2 The Jones Calculus

The effects which the components in the optical cascade have on the polarization state of the light beam could be determined by tracing the two orthogonal components of the incident beam $\mathscr{E}_x$ and $\mathscr{E}_y$ through each component in turn and then recombining them at the photomultiplier in order to determine the intensity there. Such an approach is both complicated and tedious, especially when one includes all the 'extra' effects such as the presence of strain in the cell windows. A more elegant approach is to make use of either the Mueller or the Jones calculus. In the Mueller calculus the polarization state of the incident beam is represented by a 4×1 column vector; that of the transmitted beam is found by multiplying the incident beam vector by a 4×4 Mueller matrix representing the optical component. The Jones calculus is similar but uses 2×1 column vectors for the polarization states and 2×2 matrices for the optical components. In our case either would serve the purpose but we choose to use the Jones calculus because of a useful property of some Jones matrices.

Piazza *et al* [40] have shown that the Jones matrices for certain optical components are expressible as linear combinations of the unit and Pauli matrices

$$\mathbf{I} = \begin{bmatrix} 1 & 0 \\ 0 & 1 \end{bmatrix}, \quad \mathbf{i} = \begin{bmatrix} i & 0 \\ 0 & -i \end{bmatrix}, \quad \mathbf{j} = \begin{bmatrix} 0 & 1 \\ -1 & 0 \end{bmatrix}, \quad \mathbf{k} = \begin{bmatrix} 0 & i \\ i & 0 \end{bmatrix}, \tag{3.2}$$

which combine in the following ways:

$$\begin{aligned} \mathbf{i}^2 = \mathbf{j}^2 = \mathbf{k}^2 = -\mathbf{I}, \\ \mathbf{ij} = \mathbf{k}, \quad \mathbf{jk} = \mathbf{i}, \quad \mathbf{ki} = \mathbf{j}. \end{aligned} \tag{3.3}$$

In the analysis of the optical cascade for the birefringence experiment we treat three types of components: polarizers, linear retarders, and optical rotators. The Jones matrix for a linear retarder of retardance ρ and azimuth ϕ is given by [40]

$$\mathbf{J}(\rho, \phi) = \cos\frac{\rho}{2}\mathbf{I} + \sin\frac{\rho}{2}\cos 2\phi\,\mathbf{i} + \sin\frac{\rho}{2}\sin 2\phi\,\mathbf{k}, \tag{3.4}$$

and that for an optical rotator having rotation ψ by

$$\mathbf{R}(\psi) = \cos\psi\,\mathbf{I} + \sin\psi\,\mathbf{j}. \tag{3.5}$$

The Jones matrix for a polarizer of azimuth σ has the form

$$\mathbf{P}(\sigma) = \begin{bmatrix} \cos^2\sigma & \cos\sigma\sin\sigma \\ \cos\sigma\sin\sigma & \sin^2\sigma \end{bmatrix}, \tag{3.6}$$

which cannot be expressed in terms of the $\mathbf{I}, \mathbf{i}, \mathbf{j}$, and $\mathbf{k}$ matrices. The normalised Jones vector for a linearly-polarized light beam of azimuth η is

$$\nu_\eta = \begin{bmatrix} \cos\eta \\ \sin\eta \end{bmatrix}. \tag{3.7}$$

3.3 An Optical Cascade Between Nearly-Crossed Polarizers

Suppose that we have, situated between two crossed polarizers, a series of optical components which are either linear retarders or optical rotators. A light source precedes the first polarizer and a photomultiplier detects the intensity of light which passes through the analyser.

We shall assume that light leaving the first polarizer is entirely linearly polarized at an azimuth of exactly $\frac{\pi}{4}$. From (3.7) the Jones vector for this beam is

$$\nu_0 = \frac{1}{\sqrt{2}} \begin{bmatrix} 1 \\ 1 \end{bmatrix}. \tag{3.8}$$

We now allow the azimuth of the analyser to deviate from its crossed position by a small angle α. This may be due either to a deliberate offset or to an unavoidable error in the crossing of the prisms. From (3.6) it follows that the Jones matrix for this analyser may be written

$$\begin{aligned} \mathbf{P}(-\tfrac{\pi}{4} + \alpha) &= \tfrac{1}{2} \begin{bmatrix} 1 + \sin 2\alpha & -\cos 2\alpha \\ -\cos 2\alpha & 1 - \sin 2\alpha \end{bmatrix} \\ &\approx \tfrac{1}{2} \begin{bmatrix} 1 + 2\alpha & -1 + 2\alpha^2 \\ -1 + 2\alpha^2 & 1 - 2\alpha \end{bmatrix}. \end{aligned} \tag{3.9}$$

In spite of the fact that α is small we initially retain terms which are quadratic in α, while neglecting terms of order α^3, pending a consideration of orders of magnitude in Appendix C.

Let the Jones matrices for the optical components between the polarizer and the analyser be $\mathbf{M_1}, \mathbf{M_2}, \ldots, \mathbf{M_n}$. Then the Jones vector for the light beam leaving the analyser is given by

$$\nu = \mathbf{P}(-\tfrac{\pi}{4} + \alpha)\mathbf{M_n}\mathbf{M_{n-1}} \cdots \mathbf{M_1}\nu_0, \tag{3.10}$$

in which $\mathbf{M_1}, \mathbf{M_2}, \ldots, \mathbf{M_n}$, being Jones matrices for linear retarders and optical rotators, are all expressible as linear combinations of the $\mathbf{I}, \mathbf{i}, \mathbf{j}$, and $\mathbf{k}$ matrices in (3.2). It is easily shown that these matrices form a closed set under the operation of matrix multiplication, from which it follows that the product $\mathbf{M_n}\mathbf{M_{n-1}} \cdots \mathbf{M_1}$ may also be expressed as a linear combination of these matrices. We write this as

$$\mathbf{M_n}\mathbf{M_{n-1}} \cdots \mathbf{M_1} = a\,\mathbf{I} + b\,\mathbf{i} + c\,\mathbf{j} + d\,\mathbf{k}. \tag{3.11}$$

From (3.2), and (3.8)–(3.11) we may show that the Jones vector for the beam at the

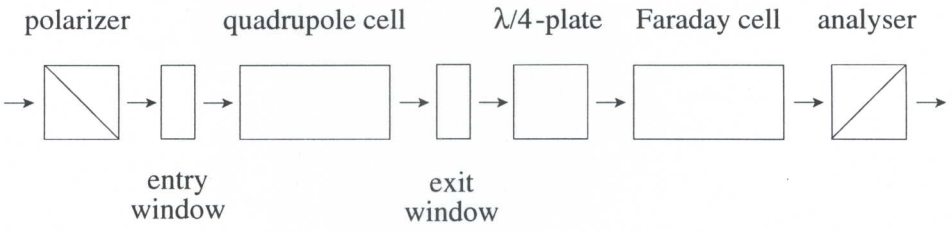

Figure 3.2 Optical components which lie between the crossed polarizers in the birefringence experiment

photomultiplier is given by

$$\begin{aligned}\nu &= \frac{1}{2\sqrt{2}}\begin{bmatrix} 1+2\alpha & -1+2\alpha^2 \\ -1+2\alpha^2 & 1-2\alpha \end{bmatrix} \\ &\qquad \times \left(a\begin{bmatrix} 1 & 0 \\ 0 & 1 \end{bmatrix} + b\begin{bmatrix} i & 0 \\ 0 & -i \end{bmatrix} + c\begin{bmatrix} 0 & 1 \\ -1 & 0 \end{bmatrix} + d\begin{bmatrix} 0 & i \\ i & 0 \end{bmatrix} \right) \begin{bmatrix} 1 \\ 1 \end{bmatrix} \\ &= \frac{1}{\sqrt{2}}\begin{bmatrix} bi+c+\alpha(a+bi+c+di)+\alpha^2(a-bi-c+di) \\ -bi-c+\alpha(-a+bi+c-di)+\alpha^2(a+bi+c+di) \end{bmatrix}.\end{aligned} \tag{3.12}$$

If I_0 is the intensity of the beam leaving the first polarizer, then the intensity of the beam at the photomultiplier is given by

$$I = \nu^* \nu I_0.$$

This, together with (3.12), gives

$$\frac{I}{I_0} = b^2 + c^2 + 2\alpha(ac+bd) + \alpha^2(a^2 - b^2 - c^2 + d^2), \tag{3.13}$$

in which we have again retained terms up to order α^2. The problem has now been reduced to finding the coefficients a, b, c, and d for a given optical cascade.

3.4 Jones Matrices for the Birefringence Experiment

The cascade of optical components lying between the polarizer and the analyser in the induced-birefringence experiment is shown in Figure 3.2. Included as separate components in the cascade are the windows of the quadrupole cell since Pierrus [39] has shown that the outcome of the experiment may be influenced by the existence of

birefringence in these windows. The glass from which the windows are cut is of the low-strain Pockels variety; so the manifestation of any birefringence in these components is attributed to mechanical strains caused largely by clamping the windows into their mountings and, to a lesser extent, by the high pressure difference which may exist across the glass. The windows of the Faraday cell are also cut from Pockels glass but are not subjected to conditions of high mechanical strain, so it is considered most unlikely that they can affect the polarization state of the light beam to anywhere near the same extent. Accordingly, the Faraday cell windows are not included in the cascade of optical components which we are considering here.

Assuming that the entry window of the quadrupole cell exhibits birefringence, we may model it as a linear retarder of small retardance β_1 and arbitrary azimuth θ_1. From (3.4) the Jones matrix for the entry window is given by

$$S_1(\beta_1, \theta_1) = \cos\frac{\beta_1}{2}\,\mathbf{I} + \sin\frac{\beta_1}{2}\cos 2\theta_1\,\mathbf{i} + \sin\frac{\beta_1}{2}\sin 2\theta_1\,\mathbf{k}. \tag{3.14}$$

A similar expression exists for the exit window.

The behaviour of the quadrupole cell as a linear retarder of retardance δ and an azimuth of 0 has been discussed in §3.1. Since the cell must be physically rotated in order to bring the wires into a vertical plane, there is bound to be some small error γ in the azimuth. However, the procedure for rotating the cell is very accurate (see §4.4.1) and it is therefore unlikely that γ ever exceeds 1°. The Jones matrix for the quadrupole cell is

$$J_q(\delta, \gamma) = \cos\frac{\delta}{2}\,\mathbf{I} + \sin\frac{\delta}{2}\cos 2\gamma\,\mathbf{i} + \sin\frac{\delta}{2}\sin 2\gamma\,\mathbf{k}. \tag{3.15}$$

The most complicated component to allow for is the $\frac{\lambda}{4}$-plate. Ideally this should, for a specified wavelength of light, have a retardance of $\frac{\pi}{2}$ radians; but in practice the retardance may deviate from this by a few degrees and also have some small temperature dependence. For this reason we allow for a retardance in the $\frac{\lambda}{4}$-plate of $\frac{\pi}{2}+\phi$ radians, where ϕ is not necessarily small and may be of either sign. The purpose of the $\frac{\lambda}{4}$-plate is to convert the elliptically-polarized light leaving the quadrupole cell back to a state of linear polarization, and it serves this purpose equally well with its fast axis at an azimuth of $-\frac{\pi}{4}$ or $+\frac{\pi}{4}$ radians. Besides accommodating both these possibilities we must also allow for a small offset ε from either of these nominal azimuths. Depending on the circumstances ε may represent either a deliberate offset or an unavoidable inaccuracy in the alignment; in either case it may be positive or negative, and checks made on the repeatability of this setting showed that it never exceeded 1°. The Jones

matrix for the $\frac{\lambda}{4}$-plate is thus given by

$$\begin{aligned} J_{\lambda/4}(\tfrac{\pi}{2}+\phi, \pm\tfrac{\pi}{4}+\varepsilon) &= \cos(\tfrac{\pi}{4}+\frac{\phi}{2})\,\mathbf{I} + \sin(\tfrac{\pi}{4}+\frac{\phi}{2})\cos(\pm\tfrac{\pi}{2}+2\varepsilon)\,\mathbf{i} \\ &\quad + \sin(\tfrac{\pi}{4}+\frac{\phi}{2})\sin(\pm\tfrac{\pi}{2}+2\varepsilon)\,\mathbf{k} \\ &= \frac{1}{\sqrt{2}}\cos\frac{\phi}{2}\,\mathbf{I} - \frac{1}{\sqrt{2}}\sin\frac{\phi}{2}\,\mathbf{I} \mp \frac{1}{\sqrt{2}}\cos\frac{\phi}{2}\sin 2\varepsilon\,\mathbf{i} \mp \frac{1}{\sqrt{2}}\sin\frac{\phi}{2}\sin 2\varepsilon\,\mathbf{i} \\ &\quad \pm \frac{1}{\sqrt{2}}\cos\frac{\phi}{2}\cos 2\varepsilon\,\mathbf{k} \pm \frac{1}{\sqrt{2}}\sin\frac{\phi}{2}\cos 2\varepsilon\,\mathbf{k}. \end{aligned} \tag{3.16}$$

Finally, we consider the Faraday cell which is simply an optical rotator giving a small rotation θ. From (3.5) the Jones matrix for the Faraday cell is given by

$$R(\theta) = \cos\theta\,\mathbf{I} + \sin\theta\,\mathbf{j}. \tag{3.17}$$

We now turn our attention to the solution of (3.11) which, for the particular cascade of optical components shown in Figure 3.2, may be written

$$R(\theta)\,J_{\lambda/4}(\tfrac{\pi}{2}+\phi, \pm\tfrac{\pi}{4}+\varepsilon)\,S_2(\beta_2,\theta_2)\,J_q(\delta,\gamma)\,S_1(\beta_1,\theta_1) = a\,\mathbf{I} + b\,\mathbf{i} + c\,\mathbf{j} + d\,\mathbf{k}\ . \tag{3.18}$$

The left-hand side of (3.18) comprises 324 terms when multiplied out. It is clear that these terms are not all of similar magnitude and so it has become necessary to decide the magnitude of the smallest term which we are to retain. Before doing so we must establish the relative magnitudes of the small angles which appear in (3.13) and (3.18). We have stated elsewhere that δ is typically of the order 10^{-6} radians; hence θ is of similar magnitude. A deliberate offset of the $\frac{\lambda}{4}$-plate or of the analyser is seldom more than $\frac{1}{2}^\circ$, so ε and α have maximum order 10^{-2} radians. The error in the orientation of the quadrupole cell is unlikely to be more than 1° so it, too, has order 10^{-2} radians. Estimating the magnitudes of β_1 and β_2 at this stage is difficult, but it is most unlikely that they are as great as 10^{-2} radians. Nonetheless, we shall make provision for them to be of the same order as ε, α, and γ.

The seven small angles in (3.13) and (3.18) have now been divided into two groups: the very small angles δ and θ, and the moderately small angles $\varepsilon, \alpha, \gamma, \beta_1$, and β_2. Grouping the last five angles together covers all possible circumstances, although it is improbable that all five will be of comparable size in any given experiment. For instance, if α is a deliberate offset of the analyser then ε is an unintentional alignment error in the azimuth of the $\frac{\lambda}{4}$-plate, and should therefore be considerably smaller.

In the final intensity expression (3.13) we need retain only those terms which are linear in either one of the modulated quantities δ and θ, since it is these terms alone which are detected by the psd. Thus the expression for the intensity will have the form

$$\frac{I}{I_0} = \delta(\cdots) + \theta(\cdots). \tag{3.19}$$

Terms in the brackets, being independent of δ and θ, have orders of magnitude determined by their dependence on $\varepsilon, \alpha, \gamma, \beta_1$, and β_2. Because these angles are all small we may make the approximations

$$\cos x \approx 1 - \tfrac{1}{2}x^2, \quad \sin x \approx x, \quad x \in \{\varepsilon, \alpha, \gamma, \beta_1, \beta_2\}.$$

In order to explain the behaviour discussed in §3.6, it is necessary to retain second order terms in the brackets in (3.19). This includes the possibility of terms such as ε^2 appearing in the intensity expression and it therefore appears that we must retain the $-\frac{1}{2}x^2$ term in the approximation for the cosine of these angles. On the other hand δ^2 and θ^2 do not appear in (3.19) and so for these angles we may make the approximations

$$\sin\delta = \delta, \quad \sin\theta = \theta, \quad \cos\delta = \cos\theta = 1.$$

With these approximations, (3.14)–(3.17) become, respectively,

$$S_n(\beta_n, \theta_n) = \mathbf{I} - \frac{\beta_n^2}{8}\mathbf{I} + \frac{\beta_n}{2}\cos 2\theta_n\,\mathbf{i} + \frac{\beta_n}{2}\sin 2\theta_n\,\mathbf{k}, \tag{3.20}$$

$$J_q(\delta, \gamma) = \mathbf{I} + \frac{\delta}{2}\mathbf{i} - \delta\gamma^2\,\mathbf{i} + \delta\gamma\,\mathbf{k}, \tag{3.21}$$

$$\begin{aligned} J_{\lambda/4}(\tfrac{\pi}{2} + \phi, \pm\tfrac{\pi}{4} + \varepsilon) = {} & \frac{1}{\sqrt{2}}\cos\frac{\phi}{2}\mathbf{I} - \frac{1}{\sqrt{2}}\sin\frac{\phi}{2}\mathbf{I} \mp \sqrt{2}\varepsilon\cos\frac{\phi}{2}\mathbf{i} \mp \sqrt{2}\varepsilon\sin\frac{\phi}{2}\mathbf{i} \\ & \pm \frac{1}{\sqrt{2}}\cos\frac{\phi}{2}\mathbf{k} \mp \sqrt{2}\varepsilon^2\cos\frac{\phi}{2}\mathbf{k} \pm \frac{1}{\sqrt{2}}\sin\frac{\phi}{2}\mathbf{k} \\ & \mp \sqrt{2}\varepsilon^2\sin\frac{\phi}{2}\mathbf{k}, \end{aligned} \tag{3.22}$$

$$R(\theta) = \mathbf{I} + \theta\,\mathbf{j}. \tag{3.23}$$

The use of these expressions in (3.18) produces 1024 terms on multiplying out. An argument is presented in Appendix C which shows that terms in equations (3.20)–(3.23) which are quadratic in any one of $\varepsilon, \gamma, \beta_1$, and β_2 do not contribute to the final intensity expression. Despite being rather lengthy this argument is very useful because it allows the quadratic terms to be dropped from (3.20)–(3.23), thereby simplifying the algebra considerably. It is further argued in Appendix C that there can be no term in α^2 in the final intensity expression, which means that we may drop this term from (3.13), giving

$$\frac{I}{I_0} = b^2 + c^2 + 2\alpha(ac + bd). \tag{3.24}$$

The final forms which we shall use for the Jones matrices in (3.18) are then

$$\begin{aligned} S_1(\beta_1,\theta_1) &= \mathbf{I} + \frac{\beta_1}{2}\cos 2\theta_1\,\mathbf{i} + \frac{\beta_1}{2}\sin 2\theta_1\,\mathbf{k} \\ &= \mathbf{I} + C_1\,\mathbf{i} + S_1\,\mathbf{k}, \end{aligned} \tag{3.25}$$

$$J_q(\delta,\gamma) = \mathbf{I} + \frac{\delta}{2}\mathbf{i} + \delta\gamma\,\mathbf{k}, \tag{3.26}$$

$$S_2(\beta_2,\theta_2) = \mathbf{I} + C_2\,\mathbf{i} + S_2\,\mathbf{k}, \tag{3.27}$$

$$\begin{aligned} J_{\lambda/4}(\tfrac{\pi}{2}+\phi,\pm\tfrac{\pi}{4}+\varepsilon) = {} & \frac{1}{\sqrt{2}}\cos\frac{\phi}{2}\,\mathbf{I} - \frac{1}{\sqrt{2}}\sin\frac{\phi}{2}\,\mathbf{I} \mp \sqrt{2}\varepsilon\cos\frac{\phi}{2}\,\mathbf{i} \\ & \mp \sqrt{2}\varepsilon\sin\frac{\phi}{2}\,\mathbf{i} \pm \frac{1}{\sqrt{2}}\cos\frac{\phi}{2}\,\mathbf{k} \pm \frac{1}{\sqrt{2}}\sin\frac{\phi}{2}\,\mathbf{k}, \end{aligned} \tag{3.28}$$

$$R(\theta) = \mathbf{I} + \theta\,\mathbf{j}, \tag{3.29}$$

in which we have adopted the following notation used by Pierrus [39]:

$$S_n = \frac{\beta_n}{2}\sin 2\theta_n, \quad C_n = \frac{\beta_n}{2}\cos 2\theta_n. \tag{3.30}$$

3.5 Performing the Algebra

The problem which remains is to multiply together the expressions for the Jones matrices given in (3.25)–(3.29), discard those terms which are smaller than the smallest order of magnitude that we are retaining, and then to use (3.3) to simplify the products of the $\mathbf{I}, \mathbf{i}, \mathbf{j}$, and $\mathbf{k}$ matrices which appear in each of the remaining terms. Coefficients of these matrices may then be identified as a, b, c, and d, and combined as shown in (3.24) to give an expression for the intensity that is 'seen' by the psd. In combining the coefficients a, b, c, and d, we must again discard small terms together with those which are not linear in δ or θ.

Apart from the tedium of performing these steps by hand, a pen-and-paper approach is also undesirable because of the ample opportunities that exist for errors to arise; even a single incorrect sign early on in the calculation can make a significant difference to the final result. This, together with the fact that the calculation may be broken up into a sequence of elementary steps, suggests that the aid of a computer might be enlisted. Commercially-available mathematics packages do not easily lend themselves to the solution of this problem because they are unable to make decisions regarding which terms to discard and which to retain. For this reason a symbolic manipulation program was written specifically to perform this calculation. A listing of this program appears in Appendix D together with a brief explanation of how it uses (3.18), (3.24), and (3.25)–(3.29) to yield an expression for the intensity at the photomultiplier,

which in this case is

$$\begin{aligned}\frac{I}{I_0} = \delta[&C_1 + C_2 + \varepsilon(\mp\cos\phi + 2S_2 + 2S_2\sin\phi) \\ &+ \alpha(\pm\cos\phi - 2S_2\sin\phi)] \\ &+ \theta[-2C_1S_1\sin\phi - 2C_2S_2\sin\phi - 4C_1S_2\sin\phi \\ &\pm 2C_1\cos\phi \pm 2C_2\cos\phi + \varepsilon(-2 - 2\sin\phi) + 2\alpha],\end{aligned} \tag{3.31}$$

in which the two nominal azimuths of the $\frac{\lambda}{4}$-plate of $+\frac{\pi}{4}$ and $-\frac{\pi}{4}$ radians are accounted for by the upper and lower signs, respectively.

3.6 Interpretation of the Intensity Expression

Suppose that we deliberately offset the $\frac{\lambda}{4}$-plate by a small angle ε_1 and then plot the psd output (which is proportional to the intensity I/I_0) as a function of θ. From (3.31) we see that zero psd output does not occur when $\theta = \frac{1}{2}\delta$, as we would like, but when

$$\theta = \tfrac{1}{2}\delta\frac{C_1 + C_2 + \varepsilon_1(\pm\cos\phi + 2S_2 + 2S_2\sin\phi) + \alpha(\pm\cos\phi - 2S_2\sin\phi)}{C_1S_1\sin\phi + C_2S_2\sin\phi + 2C_1S_1\sin\phi \mp C_1\cos\phi \mp C_2\cos\phi + \varepsilon_1(1 + \sin\phi) - 2\alpha}.$$

We shall refer to the value of θ which is equal to $\frac{1}{2}\delta$ as θ_{null}, since it is this rotation which, for ideal components in perfect orientations, is required to null the induced birefringence in the quadrupole cell. Because of strain in the cell windows, of alignment inaccuracies in the quadrupole cell and analyser, and of deviations from the ideal retardance of the $\frac{\lambda}{4}$-plate, it is clear that the intensity at θ_{null} is not zero. However, in the absence of any other procedure, the experimentalist is likely to conclude that θ_{null} is the value of θ corresponding to zero intensity.

Pierrus [39] has demonstrated an alternative procedure whereby θ_{null} may be found. By plotting a second line corresponding to a different offset ε_2 on the same graph, it follows from (3.31) that the two lines will intersect at a value of θ given by

$$\theta_{\text{int}} = -\tfrac{1}{2}\delta\frac{\pm\cos\phi - 2S_2 - 2S_2\sin\phi}{1 + \sin\phi}. \tag{3.32}$$

If ϕ is small then this approximates to

$$\theta_{\text{int}} = -\tfrac{1}{2}\delta\frac{\pm 1 - 2S_2}{1 + \phi}. \tag{3.33}$$

Although the two offsets ε_1 and ε_2 of the $\frac{\lambda}{4}$-plate may have the same sign, the statistical error in θ_{int} is minimized experimentally if they are arranged to have opposite signs and similar magnitudes.

The corresponding result obtained by Pierrus ((4.7) of [39]),

$$\theta_{\text{int}} = -\tfrac{1}{2}\delta(1 - 2S_2), \tag{3.34}$$

is a special case of (3.33) in which the effects of deviations from the ideal retardance of the $\frac{\lambda}{4}$-plate have not been considered, and in which the nominal azimuth of this component is assumed to be $+\frac{\pi}{4}$ radians. In that work it is stated that S_2 is small in comparison with 1 so that θ_{int} may be used as a good approximation of θ_{null}. However, if S_2 is not negligibly small then it may be seen from (3.33) to contribute additively for one position of the $\frac{\lambda}{4}$-plate and subtractively for the other[1]. It may therefore be eliminated by performing the experiment for both positions of the $\frac{\lambda}{4}$-plate and averaging the results. The retardance of the $\frac{\lambda}{4}$-plate may be measured using a Soleil-Babinet compensator and from this we may find a value for ϕ and use it to correct the averaged result. In this way it is possible to obtain a good value for θ_{null} which is certainly a better estimate than that found by using the method of two offsets for only one of the two possible nominal azimuths of the $\frac{\lambda}{4}$-plate.

The importance of performing the experiment for the two orthogonal azimuthal orientations of the $\frac{\lambda}{4}$-plate and then averaging the results depends on how large S_2 is in comparison with 1, and this may be experimentally gauged by comparing the results obtained with the $\frac{\lambda}{4}$-plate azimuth in both positions. Measurements carried out with carbon dioxide in the quadrupole cell have shown that these may differ by as much as 3.5%. Furthermore, the retardance of the $\frac{\lambda}{4}$-plate used by Pierrus has been measured at 632.8 nm to be $93.3 \pm 0.3°$. This fact alone suggests that the results reported in [39] are likely to be at least 5% too low. When the carbon dioxide results for the two $\frac{\lambda}{4}$-plate positions are averaged and then corrected for the imperfect $\frac{\lambda}{4}$-plate by multiplying by $1+\phi$, the result is found to be in good agreement with values measured by other workers.

Performing the experiment in this way is time-inefficient because it takes twice as long to obtain the same number of readings as before. Furthermore, it is implicitly assumed that the birefringence in the second window will remain constant over a period of several hours, which may not be case. For these reasons other experimental configurations for providing the offset previously provided by the $\frac{\lambda}{4}$-plate were investigated. The most satisfactory one found was to fix the azimuth of the $\frac{\lambda}{4}$-plate at either of the $\pm\frac{\pi}{4}$ settings and then to plot two lines corresponding to oppositely-signed offsets α_1 and α_2 of the analysing prism. From (3.31) it may be shown that these lines will intersect at

$$\theta_{\text{int}} = -\tfrac{1}{2}\delta(\pm\cos\phi - 2S_2\sin\phi). \tag{3.35}$$

In this case it is the term $2S_2\sin\phi$ which contributes additively for one $\frac{\lambda}{4}$-plate position and subtractively for the other. If ϕ is small then this term is at least two orders of magnitude smaller than the corresponding strain contribution $2S_2$ in (3.33). Since it was found to account for a few percent in that case, it appears that we may ignore it here. This was checked experimentally and it has been verified that the outcome of

[1]The overall change in sign on the right-hand side of (3.33), which occurs on changing between the two orthogonal $\frac{\lambda}{4}$-plate positions, is accommodated experimentally by introducing a phase lag of π radians between the driving signals which modulate δ and θ.

the experiment performed using this analyser-offset method does not depend on which of the two orthogonal $\frac{\lambda}{4}$-plate azimuths is used. For small ϕ we may approximate $\cos\phi \approx 1$ in which case (3.35) simplifies to

$$\theta_{\text{int}} = \mp\tfrac{1}{2}\delta. \tag{3.36}$$

Thus, if a $\frac{\lambda}{4}$-plate in which the retardance is very nearly $\frac{\pi}{2}$ radians is used in the experiment, the value of θ at the point of intersection of two graphs of intensity vs θ corresponding to two offsets α_1 and α_2 of the analyser provides an excellent estimate of θ_{null}. A mounted $\frac{\lambda}{4}$-plate having a measured retardance of $91.2 \pm 0.3°$ at 638.2 nm was used in obtaining all the measurements reported in Chapter 5, thereby ensuring that the error introduced by the approximation $\cos\theta \approx 1$ is less than 0.03%.

Chapter 4

DESCRIPTION OF THE EXPERIMENT

4.1 Introduction

The apparatus and techniques first used to measure electric quadrupole moments through induced birefringence have been described by Buckingham and Disch [41]. In the early 1980s a modified version of this early apparatus was manufactured in the Mechanical and Electronic Workshops of the Department of Physics at the University of Natal, Pietermaritzburg. Work carried out using this apparatus was reported first by Stuckenberg [42] and later by Pierrus and [39, 43]. Shortcomings of the apparatus were described by Pierrus which, together with the new theoretical considerations presented in the preceding chapter, led to modifications to the apparatus being carried out at the onset of the work reported here. Of greatest significance were the changes to the manner in which the experiment was performed and the addition of an extension to the existing quadrupole cell. This chapter describes the entire experimental set-up, paying particular attention to apparatus modifications.

4.2 The Gas Line

Gases were introduced to and exhausted from the quadrupole cell via a manifold constructed from $\frac{1}{4}$-inch 316-stainless steel tubing and Hoke Gyrolok fittings, also made of 316-stainless steel. Flow control was through needle valves selected from the Hoke 3700 series, with the most critical valves having soft Kel-F tips to ensure excellent sealing.

Before entering the cell the gas passed through two filters; a 1 μm sintered glass filter and a 0.22 μm Millipore paper filter. These filters could be bypassed when removing the gas from the cell.

For all the gases studied with the exception of chlorine, a Budenberg 0–4 MPa Master Test Gauge was used for measuring the gauge pressure of the gas. The accuracy of this gauge was checked periodically against a Budenberg dead-weight tester. In

searching for a pressure dependence in the results for nitrogen, pressures up to 6 MPa were used. To measure pressures in the range 4–6 MPa, special provision was made whereby the pressure of the gas in the cell was balanced directly against the dead-weight tester. Precautions were taken to ensure that oil vapours from the dead-weight tester did not contaminate the gas in the cell.

After work had been carried out on either the manifold or the cell, the entire system was checked for leaks. Occasionally, a helium leak-detector was used for this purpose, but a more effective method was to fill the cell and manifold with carbon dioxide at a pressure of 4 MPa and then to paint all joints with soap solution whilst looking for the formation of tell-tale bubbles. The pressure differential in this case is some 40 times greater than when testing the system under vacuum.

Before filling with gas, the cell and manifold were flushed out by repeatedly evacuating the cell and then filling it to about 1 MPa with the gas to be tested. Evacuation was achieved using a rotary oil pump, whilst gas was introduced into the cell in all cases under the pressure of the cylinder in which it was purchased.

Before measurements on chlorine were begun, an entirely new gas manifold was constructed and located close to the cell, thereby minimizing the length of tubing that would be exposed to the gas. For the purpose of measuring the pressure, a 0–600 kPa Blanes chlorine service gauge was acquired. This was calibrated frequently against the dead-weight tester in order to achieve an accuracy of measurement which was an order of magnitude better than that yielded by a face reading of this gauge.

4.3 The Light Source, Passive Optical Components, and Detector

The arrangement of the electronic and optical components used in the experiment is shown schematically in Figure 4.1. All the optical elements were securely mounted on an optical bench constructed from a 4 m length of 230 mm×90 mm mild steel channel. A 2 m-long side arm was butt-welded to the bench to provide stability, and the entire bench was supported on three rubber anti-vibration mounts resting on a massive free-standing concrete slab. This was of the same width as the optical bench and stood 600 mm high on a 50 mm-thick cork foundation. This arrangement served to provide adequate isolation of the optical components from the vibrations of the building in which the experiment was housed, and which would otherwise have contributed significantly to the signal noise.

Throughout the work reported here the light source employed was a Spectra-Physics model 107B-2 He-Ne laser having a nominal output power rating of 35 mW. Over the three year period during which it was used, the absolute power output of this laser was observed to fall from 38 mW to 30 mW. The separation of the $\frac{1}{e^2}$ points of the beam was specified as being 1.7 mm, which was an important consideration in deciding on a clear aperture of 1.6 mm for the passage of the beam through the quadrupole cell. An adjustable three-point support for the laser made provision for levelling and alignment

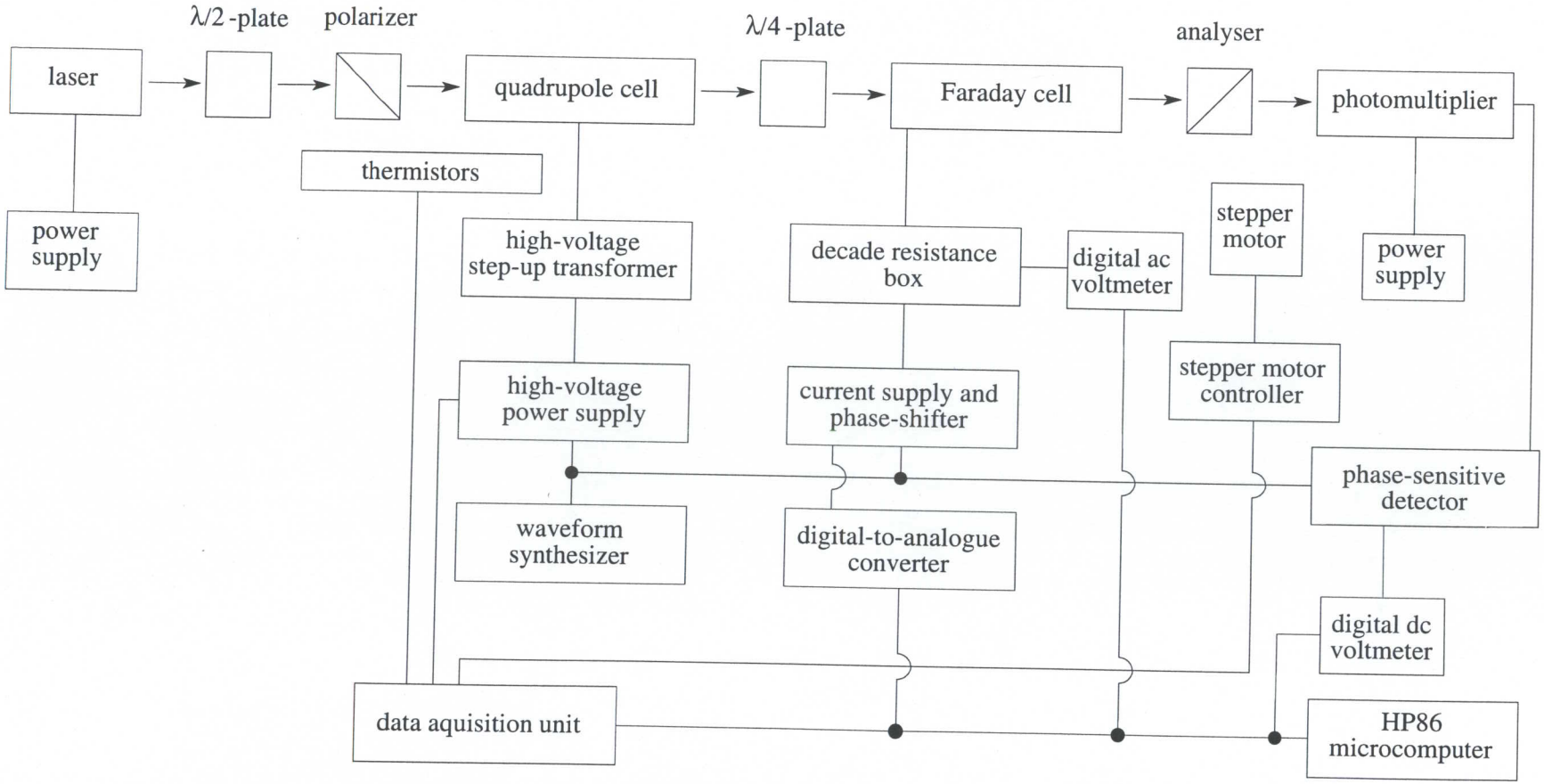

Figure 4.1 Schematic diagram of the experimental set-up

with respect to the optical bench.

The sensitivity of the experiment is partly dependent on the intensity of the light entering the cell; it is therefore desirable that as much of the laser light as possible should pass through the first polarizing prism. This was achieved by inserting a $\frac{\lambda}{2}$-plate between the laser and the polarizer and rotating the $\frac{\lambda}{2}$-plate until the plane of polarization of the laser light coincided with that of the polarizer. The $\frac{\lambda}{2}$-plate was a 25 mm-diameter disc cut from a sheet of mica selected for 632.8 nm and which had been sandwiched between two discs of low-strain Pockels glass. This arrangement was mounted in a divided circle and supported in a stand with a magnetic base.

The polarizing prisms used to polarize and analyse the light beam were of the air-spaced Glan-Taylor variety. That used as the polarizer was mounted in a divided circle having a resolution of 2 minutes of arc. In the Jones Calculus analysis presented in Chapter 3, departures of the azimuths of various optical components in the cascade from their ideal values are measured with respect to the plane of polarization of the light entering the quadrupole cell. It was therefore important that the polarizer be set up in such a manner as to permit these orientational errors to be minimized. To facilitate this a platform of surface-ground gauge plate was attached to the optical bench with a three-point support. This platform was levelled using an engineer's level before the magnetic base of the polarizer support was affixed to it. Through an iterative technique of rotating the polarizer about its stem, rotating the analyser for extinction of the beam, and then correcting the azimuth of the polarizer, it was possible to polarize the beam in a plane orthogonal to the platform. By then offsetting the polarizer by 45° a state was achieved in which the plane of the polarized beam entering the cell was at 45° to the level. This permitted a spirit-level to be used as a reference when orienting the plane of the wires within the cell.

Like the $\frac{\lambda}{2}$-plate, the $\frac{\lambda}{4}$-plate was cut from clear mica and was mounted and supported in similar fashion. Sandwiching the mica between discs of Pockels glass was found by Pierrus to reduce markedly the undesirable effects caused by differential reflection of the beam off the plate. A $\frac{\lambda}{4}$-plate having a measured retardance of $91.2 \pm 0.3°$ at 632.8 nm was used for this work.

A view, looking down the optical bench, of the analyser housing is shown in Figure 4.2. Two large taper-roller bearings are pulled up into their housings at opposite ends of a 200 mm-long thick-walled cylinder by lock nuts threaded on to a steel tube running through the centres of the bearings. The inside of this tube was painted matt black and the analyser prism was mounted in cork on the axis of the tube at the end nearest the laser. Attached to the other end was an arm of length 1300 mm cut from 5 mm-thick sheet aluminium. A 50 mm length of square section brass was mounted at a distance of 1000 mm from the axis of the bearings in such a way that a v-groove machined along its length was co-linear with the centre of rotation of the bearings. This v-groove served to locate a steel ball mounted on the end of a micrometer head which was coupled through a chain and sprocket arrangement to a stepper motor. A pulley and weight served to hold the arm against the micrometer with a constant force. By placing the stepper motor under computer control the micrometer could be advanced

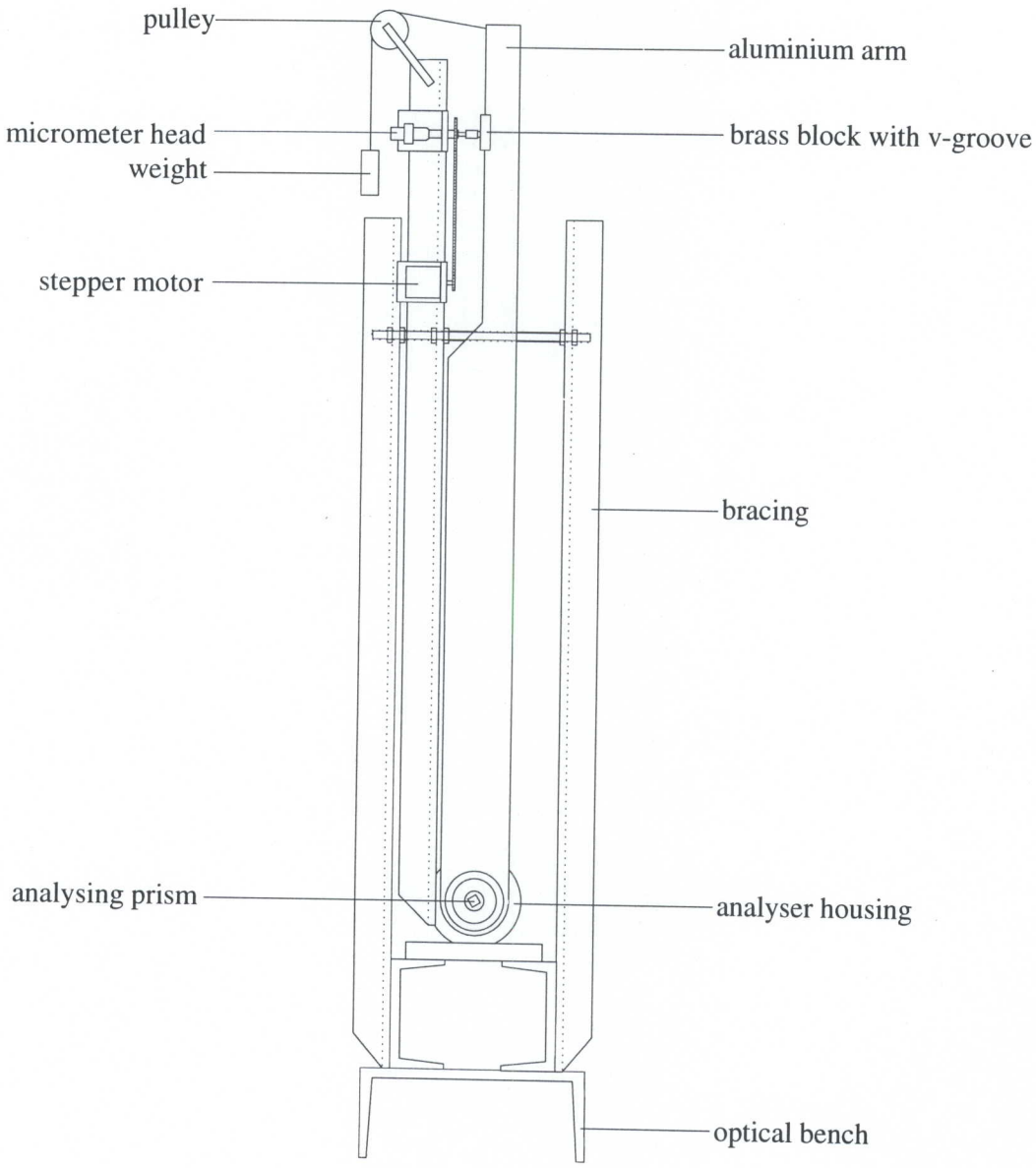

Figure 4.2 Front view of the housing for the analyser showing the mechanism whereby small rotations of this prism could be effected

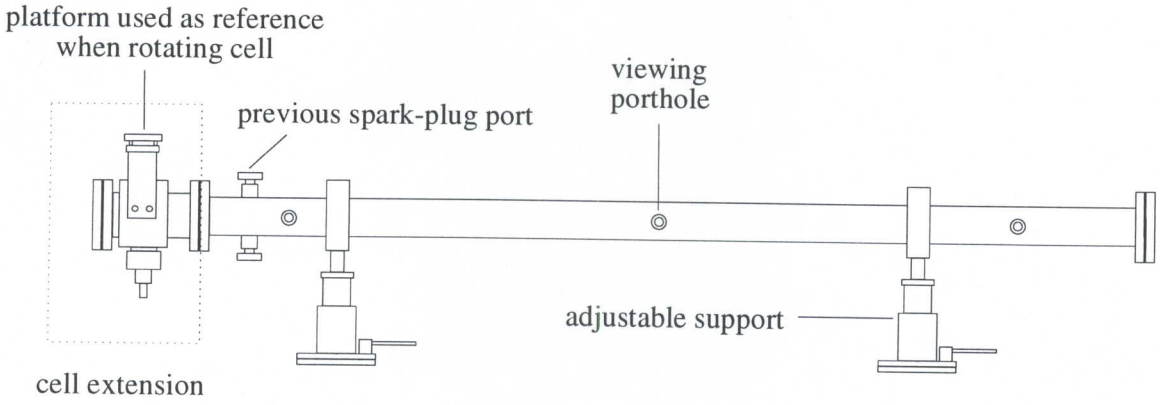

Figure 4.3 Side view of the quadrupole cell

in very small steps enabling small, known, and reproducible rotations of the analyser to be made.

An EMI 9698B photomultiplier tube, having its peak sensitivity in red light, was used as the detector throughout this work. The tube was well shielded from magnetic and electric fields, and baffled and shielded to detect light from the forward direction only. The photomultiplier was operated at 360 V—well within its region of linear response. Coherent radiation from the high-voltage supply to the quadrupole cell was excluded from the signal path by providing additional screening of the co-axial cables which carried the signal from the photomultiplier to the psd. Indeed, great care was taken with the earthing of all the components used in the experiment since an experiment of this sensitivity is particularly prone to picking up spurious earth-loop signals.

4.4 The Quadrupole Cell

4.4.1 Construction of the cell

A side view of the cell containing the gas in which birefringence was induced is shown in Figure 4.3, and the extension, enclosed in the broken line in this diagram, is shown sectioned in Figure 4.4. To understand fully the design and construction of the quadrupole cell, it is helpful to consider first its various functions. Most obviously it had to contain the gas on which measurements were to be performed without leaking. Because of the smallness of the effect being studied it was important to be able to work at small molar volumes which often implied working at high pressures; 4 MPa was typical, although pressures of 6 MPa were used for some measurements on nitrogen. In order to be able to contain these pressures, special consideration had to be given to the seals used. The quadrupole cell had also to contain the means for generating the high electric field gradient on its axis. Furthermore, this field gradient had to be

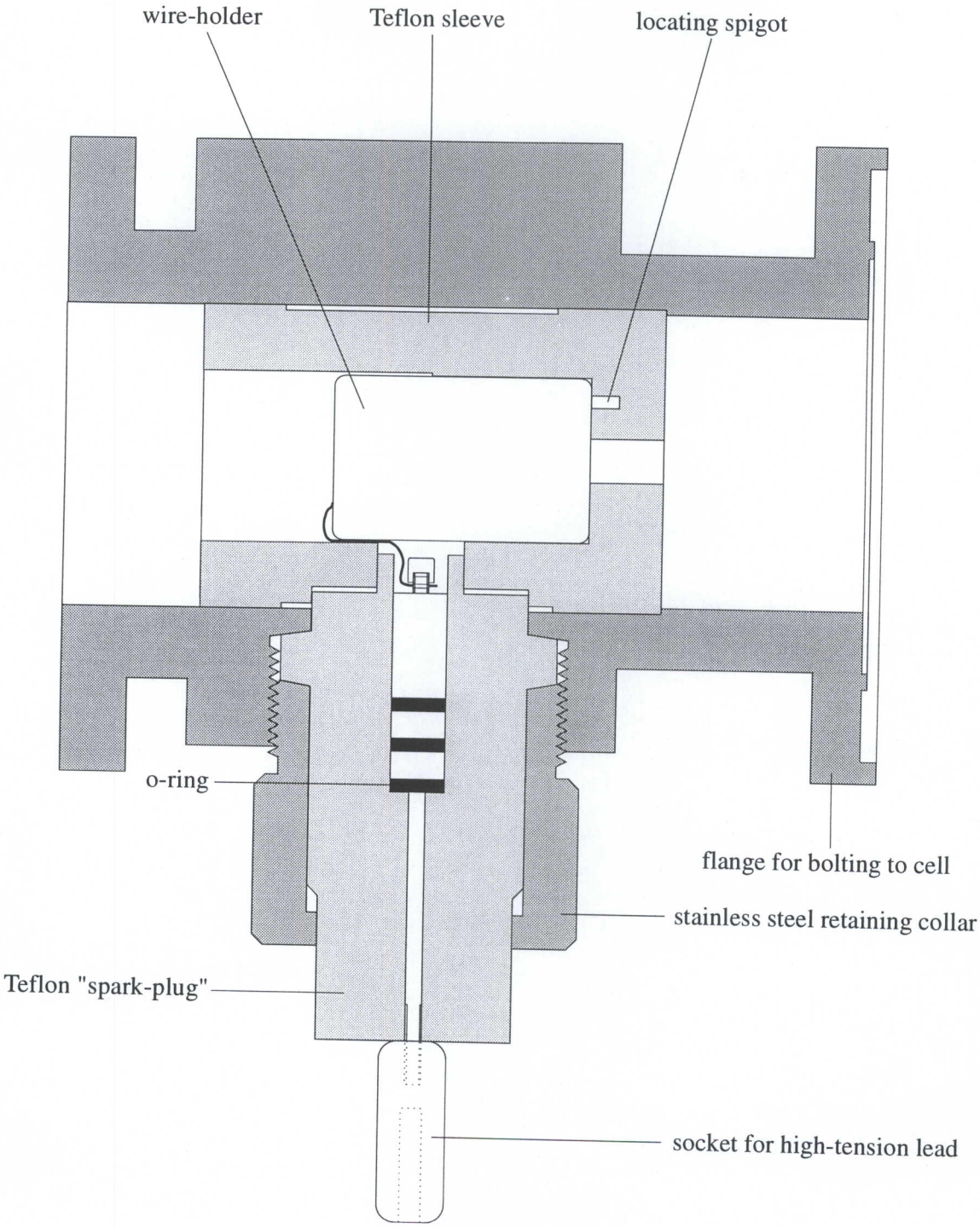

Figure 4.4 Section through the extension to the quadrupole cell

correctly oriented with respect to the plane of polarization of the incident beam. Since the electric field gradient was to be generated by earthing the cell and holding the wires at a high voltage, careful consideration had to be given to the means whereby this high voltage was led into the cell.

The original cell was constructed from a 1450 mm length of Hastelloy C-276 pipe having a 52.4 mm internal diameter and a wall thickness of 3.8 mm. Hastelloy C-276 (hereafter, Hastelloy) was selected for its excellent resistance to chemical attack by a large range of substances which are normally regarded as corrosive. Gases such as chlorine and boron trifluoride were used in this cell with no visible signs of surface degradation. To the ends of the pipe were welded the flanges on to which the end caps were bolted, and three uniformly-spaced observation portholes were drilled along the length of the tube on both sides. Threaded turrets were welded over these holes and into five of these were screwed stoppers which sealed against Teflon washers, whilst the sixth porthole served as the connection to the gas line. The portholes enabled the wire separation at high voltages to be measured using a travelling microscope. Two more threaded stoppers were made to seal off those holes in the cell which had previously been used to house the lead-through for the high-voltage line. These holes became redundant once the extension described in the next section had been fitted to the cell.

The cell was closed at its ends by bolting the window holders to the end flanges, and using a washer cut from 3 mm-thick Teflon sheet as a seal. Figure 4.5 shows a section through the end of the cell at which the beam exits. The window holders were machined from 12 mm Hastelloy plate and had a 6 mm hole drilled through their centres. Discs of clear, low-strain Pockels glass measuring 25 mm in diameter served as windows. From time to time these would be polished to remove a stained or etched surface and so their thickness decreased slightly over the duration of the work reported here. Typically, the windows were 5 mm thick making them the limiting factor in determining the greatest pressure which the cell could safely contain. The mounting of the windows is most easily understood by studying Figure 4.5. A disc of Hastelloy clamped the windows in place on the inside of the cell with Teflon washers again being used to seal and cushion the window. By mounting the window on the inside of the cell the pressure of the gas in the cell provided additional clamping of the window against the seal. A Teflon cap placed over the clamping plate reduced the likelihood of electrical arcing occurring between the plate and the wire-holder.

The entire cell was held by two supports which provided for independent vertical and lateral adjustments to the position of the cell. Once aligned, the position of the cell could be fixed by locking all the travelling mechanisms. The split-ring clamps which held the cell were lined with thin felt and were tightened by compression springs, thereby enabling the cell to be rotated about its axis. On to one of these mounts was bolted a 500 mm-long arm having an upright post attached to the outermost end. A second arm was clamped to the cell in an adjacent position, and at the end of this arm was mounted a micrometer head in such a way that the end of the micrometer thrust against a steel ball pressed into the end of the afore-mentioned post. The two arms were pulled together by tension springs, enabling small rotations of the cell in either

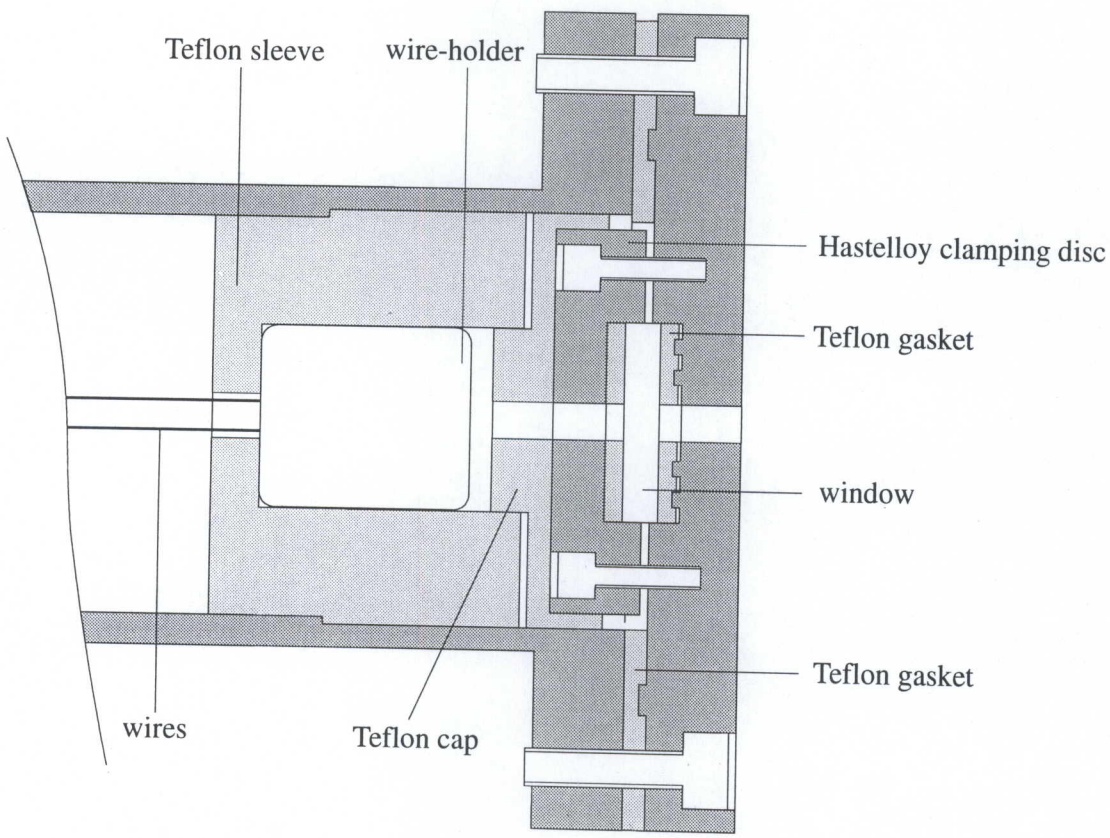

Figure 4.5 Longitudinal section through that end of the quadrupole cell at which the laser beam exits, in which the arrangement for clamping the window to the end of the cell is shown together with the use of Teflon gaskets for sealing

sense to be carried out by adjusting the micrometer.

4.4.2 The cell extension

Buckingham and Disch's [41] original quadrupole cell made use of a spark-plug to lead the high-voltage signal through the earthed cell and on to the wires. Although the apparatus described here does not make use of an actual spark-plug for this purpose, the term 'spark-plug' has been retained to describe the device which is used in its place. Pierrus [39] reports that the previous spark-plug design was prone to arcing at high voltages. That version consisted of a solid Teflon cylinder with a metal rod running through its centre to conduct the high voltage applied to the outer end to the wire-holder inside the cell. A decision was made to provide for a spark-plug of similar design but having superior insulation in the form of a greater diameter Teflon rod. This larger device could not easily be housed in the existing cell and so an extension was machined from a 150 mm length of 120 mm diameter Hastelloy round bar. The form of this extension and of the new spark-plug may be seen in Figure 4.4.

The spark-plug was held against the sealing surface on the extension by a threaded stainless steel collar. Flats machined on the collar enabled it to be tightened using a large shifting spanner. No problems were ever experienced with this seal, although several designs for the fitting of the conducting rod to the spark-plug were tried before arriving at the satisfactory design shown in the figure. The rod was turned from Hastelloy with a small threaded spigot at the upper end. A 0.5 mm hole was drilled through the spigot at its base, and a threaded cap was used to clamp in this hole the end of the short length of wire which conducted the high voltage to the wire-holder. Three Viton o-rings fitted to the broad part of the rod prevented the gas from seeping down the centre of the spark-plug. A 4 mm banana-plug socket was screwed on to the exposed end of the conducting rod providing a means whereby the pressure on the bottom o-ring could be increased in the event of a small leak developing, and a banana-plug soldered to the end of the high-voltage lead fitted tightly in this socket.

Not shown in Figure 4.4, but indicated in Figure 4.3, is a platform mounted above the extension. This platform was constructed from flat gauge plate and could be levelled by means of the adjustable three-point support on which it rested. The purpose of this platform is described in the following section.

4.4.3 The wires and wire-holders

Shown sectioned in Figure 4.6 are the two wire-holders which serve to maintain the wires at the correct orientation, separation, and tension. The keys to locating the wires accurately with respect to the axis of the cell are the 0.5 mm-thick plates which are located by short dowel pins in the shallow recesses at the inner ends of the holders. These pins also serve to locate the wire-holders in the Teflon sleeves.

The plates were produced by parting thin discs off a length of round bar, lapping them to a uniform thickness and good surface finish, and then drilling in a single pass

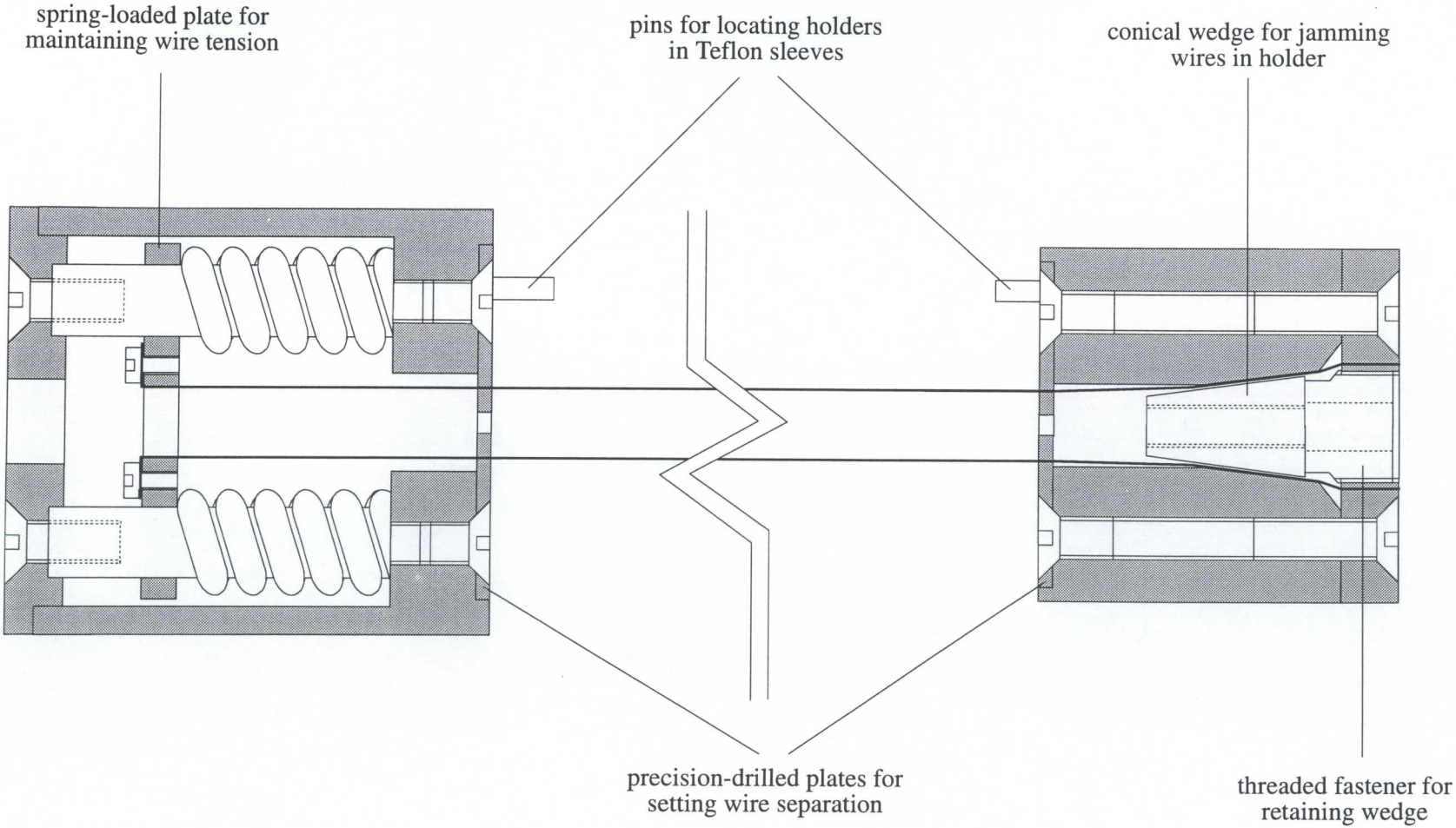

Figure 4.6 Sectioned view of the wire-holders showing the use of compression springs to maintain wire tension, and of precision-drilled plates to set the separation of the two wires

the holes required for the wires and the aperture through which the beam passed. This ensured that that the two wires were symmetrically disposed about the beam.

To ensure that the wires lay in a vertical plane, the following procedure was adopted. One wire-holder was located in its Teflon sleeve in an orientation which appeared to be vertical. This sleeve and wire-holder were then placed in the cell and the three holes at the centre of the plate were projected onto a screen using a He-Ne laser and a series of lenses. A plumb-line was set up near the screen and the cell was rotated until the centres of the three projected holes coincided with the shadow cast by the plumb-line. The platform atop the extension was then levelled using an engineer's level, and locked in this position. The position of the hole used to locate the second wire-holder in the other sleeve was then found by rotating this holder until its projected holes coincided with the plumb-line and then marking the sleeve with a pointed locating dowel. After assembly, the wires in the cell could be brought into a vertical plane by rotating the cell until the platform on the cell extension was level.

At the spark-plug end of the cell the wires were attached with threaded fasteners to a plate which rode on compression springs located on four posts inside the hollow wire-holder. When stringing the wires within the cell, these springs were compressed by the action of a bolt which screwed into the lid of the holder and forced down the plate to which the wires were attached. The wires, which were cut some 500 mm longer than the cell, were then threaded through the wire-holder at the other end of the cell before being attached to weight holders. With the cell firmly secured to the bench, the wires were hung over pulleys and tensioned by placing weights on the holders. The wires were each loaded to just below their breaking strain; 0.5 mm Hastelloy wire was loaded typically to 160 N. A conical plug was then secured in the second wire-holder by a threaded fastener having a hole bored through its centre and a slot cut into one end to enable it to be tightened using a screwdriver. Once the conical plug had securely jammed the wires in place, the wires were broken off at the surface of the wire-holder by fatiguing them. The bolt was then removed from the hollow wire-holder so that the tension in the wires was maintained by the four compression springs.

Measurements reported here for all gases except chlorine were carried out using wire-holder components made from Monel metal and fastened with stainless steel screws. Prior to the commencement of this work only stainless steel wires had been available for use in the cell. Measurements on chlorine gas are deemed to be of considerable theoretical interest and, since this had been the primary motivation in constructing the cell from Hastelloy, a roll of 0.500 mm-diameter Hastelloy wire was acquired at the beginning of this work for use with corrosive gases. Since chlorine gas will corrode both stainless steel and Monel metal, the wire-holder components were initially plated with silver in an attempt to form a silver chloride barrier against attack by the chlorine. An unexpected outcome of this was the formation of an unidentified deposit on the cell windows which severely blocked the passage of light through the cell. At this point a decision was made to remake all the wire-holder components, including the screws but excluding the springs, from Hastelloy. The springs were protected from attack by binding them tightly with Teflon tape. This proved to be a very satisfactory

arrangement since the only surfaces in the cell which were exposed to chlorine were of Hastelloy, Teflon, or glass.

Prior to the arrival of the Hastelloy wire, stainless steel wire of diameter 0.35 mm or 0.40 mm had been used at a spacing of 3.0 mm between centres. Before the plates for the new wire thickness could be prepared, a decision had to be made regarding the spacing of the thicker wires. There exist opposing criteria governing the optimal separation of wires of a given diameter. As shown in Appendix A, the strength of the electric field gradient on the axis of the cell is inversely proportional to the square of the distance separating the centres of the wires. Since the birefringence is proportional to the on-axis field gradient, we would like to place the wires as close together as possible. Two important factors oppose this. Firstly, since the wires carry equal charge, there exists a force of repulsion between them which also varies as the inverse square of their separation. A first-order correction is made for the resultant outward bowing of the wires, but the validity of this correction becomes doubtful if this bowing is too great.

Secondly, and more importantly, the derivation of the expression for the field gradient on the axis of the cell given in Appendix A makes implicit assumptions regarding the geometry of the conducting surfaces within the cell. Briefly, the derivation involves replacing the wires with line charges having magnitudes such that the potential at the surface of the wire, as determined by this model, is equal to the potential of the wire. This assumes the line charge equipotential at the wire surface to be circular so that it coincides with the entire wire surface. A computer program was written which plots the equipotential at the wire surface superimposed on the wire surface itself. It was found that this equipotential surface was very nearly round for large wire separations but became noticeably distorted as the wire separation was decreased. For a given wire thickness, a minimum separation was selected based on these plots, a selection of which is included in Appendix E. In the case of 0.5 mm wire a spacing of 4.0 mm between centres was used.

4.4.4 The high-voltage power supply

A Philips PM5190 LF synthesizer was used to generate the modulating signal used in the experiment. This signal was sinusoidal having a frequency chosen to be well away from the line frequency and from that at which resonance in the wires was observed to occur. Usually, a frequency of either 363 Hz or 463 Hz was used and the amplitude was set at an rms value of 50 mV, this being the optimum amplitude of the driving signal for the high-voltage power supply. This supply was essentially a two-stage high-voltage amplifier, the first stage of which fed into the primary coil of a high-voltage transformer immersed in oil. A Teflon-insulated high-voltage lead conducted the voltage from the secondary coil to the spark-plug of the quadrupole cell.

A feedback circuit was included in the amplifier to ensure that the output was kept constant to within 0.1%, as well as to provide a means whereby the high-voltage output could be accurately monitored. Part of the feed-back signal was rectified and attenuated so that a reading of 1 V dc on the digital voltmeter used to monitor this output

corresponded to 1 kV rms on the wires of the cell. After evaluating several different methods for performing this calibration, that chosen was to adjust the attenuation for an output of 1 kV, using a 1 kV ac $4\frac{1}{2}$-digit digital voltmeter as a standard, and then to assume that the linearity which was observed in the range 0–1 kV extended up to the operating voltage of, typically, 8 kV. Linearity was observed over the whole range using a high-voltage probe, whilst the ratio of input voltage of the primary coil to that of the secondary of the high-voltage transformer was observed to be constant to within 0.1% over the range 0–1 kV. With the calibration method described, the uncertainty in the high voltage was estimated to be no more than 0.2%.

4.4.5 Determining the electric field gradient

The electric field gradient on the axis of the cell was determined indirectly using the relationship derived in Appendix A together with an accurate knowledge of the cell geometry. An inside micrometer was used to measure the internal diameter of the cell whilst the wire thickness under tension was found with a micrometer screw gauge. Since the wires tended to repel each other when held at a high voltage it was necessary to measure the wire separation *in situ* with the high voltage applied. This was accomplished by using a travelling microscope to view the wires at each of the three viewing ports. A 1 μm dial-gauge indicator was fitted to the vertical axis of this instrument in order to achieve an accuracy of measurement which was an order of magnitude better than that which was possible using the vernier scale of the travelling stage.

Once the separation was known at three points along the wires an effective wire separation was calculated by fitting parabolas to these points and then integrating the difference along the length of the wires.

4.5 The Faraday Nulling Cell

4.5.1 Design and construction

The Faraday cell was of a comparatively simple design, being essentially a glass tube filled with toluene located on the axis of a solenoid. The glass tube was 400 mm long, had an internal diameter of 12 mm, and was closed at both ends by Teflon caps in which were located Pockels glass windows identical to those used in the quadrupole cell. The solenoid actually comprised two separate coils wound on a former having an outside diameter of 75 mm. The coil which was used to provide the magnetic field for nulling was of 100 turns of heavy-gauge wire, whilst the other consisted of 10 000 turns of much thinner wire and was used only in the set-up employed in calibrating the first coil.

Perspex holders located the cell at the centre of the solenoids and provided the means for applying sealing pressure to the windows. Standard optical bench traversing mechanisms were used to support these holders, thereby permitting the cell to be aligned with respect to the beam. To ensure that the light travelled down the centre

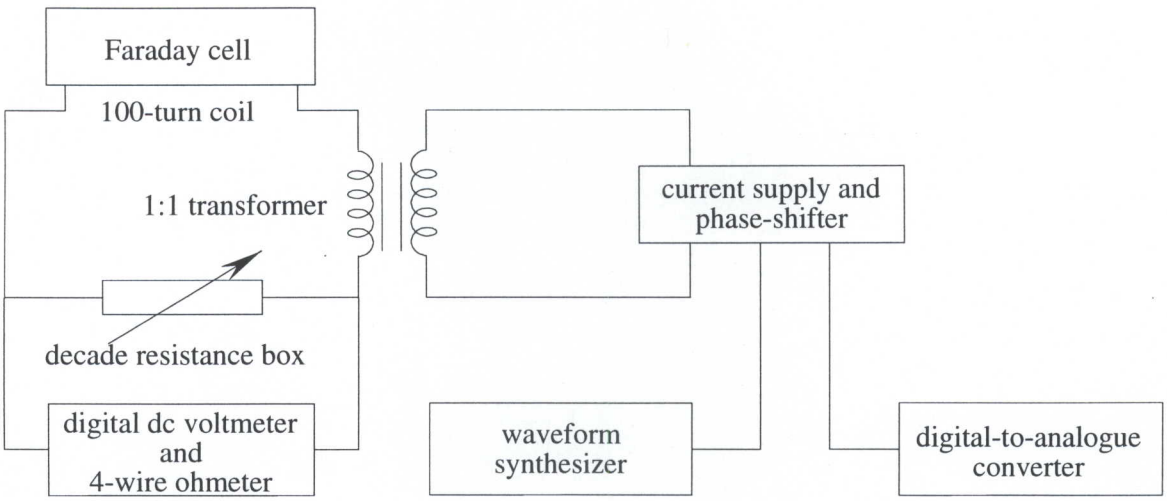

Figure 4.7 Schematic diagram of the Faraday cell circuit used in the experiment

of the cell, the Teflon caps which held the windows were machined to have a central clear aperture only slightly bigger than the waist diameter of the beam.

4.5.2 Circuit and power supply

The experimental arrangement for supplying current to the Faraday cell is shown in Figure 4.7. A decade resistance box was included as a current-limiting resistor in series with the 100-turn coil of the Faraday cell. Across this resistance was connected a high-impedance digital voltmeter to permit an accurate determination of the current flowing in the circuit. An AC power supply incorporating a phase-shifting circuit was used to supply current to the Faraday cell circuit via a 1:1 transformer; a feed-back path to the power supply maintained this current at a steady level. The waveform synthesizer which provided the signal for the high-voltage amplifier also supplied that for this ac current supply.

The high-voltage signal on the wires of the quadrupole cell was required to be in antiphase with the current in the Faraday cell. In order to achieve this the Lissajous figure of the two signals was monitored on an oscilloscope and the phase of the current was adjusted using the phase-shifting circuit.

Since the required experimental data were a set of psd output readings as a function of the current through the Faraday cell, a facility was needed whereby the computer would be able to control the current flowing in the Faraday cell circuit. To this end, the ac power supply was made 'programmable' through an input voltage, supplied in this case by a custom-built digital-to-analogue converter.

4.5.3 Calibration of the Faraday cell

Since the signal from the quadrupole cell was measured essentially by nulling it with that from the Faraday cell, it was important that the Faraday cell be accurately calibrated. This, too, was carried out using a nulling technique—in this case nulling the effect of a Faraday rotation of the plane of polarization with a mechanical rotation of the analysing prism. Small, known rotations of the analyser were achieved using a micrometer head acting on a 1 m-long arm used to pivot the prism, as described in §4.3. The micrometer was driven by a stepper motor under the control of the computer, presenting the possibility of automatically calibrating the Faraday cell. Attempts to achieve this were unsuccessful, due largely to the effects of the vibrations set up by the stepper motor which added greatly to the noise in the experiment. When running the main experiment, these effects were dealt with by allowing sufficient time for the vibrations to decay before taking measurements. In the case of the calibration procedure, this approach was impracticable because of the need to monitor constantly the output signal whilst rotating the analyser. On account of this, the micrometer was decoupled from the motor for purposes of calibration and could then be adjusted by hand. Calibrations were performed regularly and on each occasion many readings were taken and averaged.

The experimental set-up for calibrating the Faraday cell is depicted schematically in Figure 4.8. Optical components not directly involved in the calibration are not shown in this diagram, but in practice it was found that the outcome of the measurements was not affected if they remained in place, and for convenience they usually were. Cancelling the effect of a Faraday rotation of the plane of polarization of the light beam by physically rotating the analysing prism requires that the signal from the Faraday cell should be both static and large. When used in the experiment, the Faraday cell produces a modulated signal which is of the order 10^{-6} radians, clearly unsuitable for purposes of calibration. Since the Faraday cell could be be calibrated accurately only for rotations which were not smaller than about $\frac{1}{2}^{\circ}$, the assumption had to be made that the Faraday effect was linear in the current over this interval. Furthermore, in order that phase-sensitive detection techniques could still be used in the calibration procedure, a small ripple had to be superimposed on the dc signal to enable the psd to observe the coupled term in the intensity. This was achieved by driving a much smaller current through the second coil of the Faraday cell. A toroidal air-core inductor was included in the dc circuit to minimise coupling between this and the ac circuit.

A set of Faraday rotation vs current readings was obtained and fitted with the best least-squares line, the slope of which yielded the calibration constant F in units of radians per milliampere.

4.6 Experiment Control and Data Acquisition

Because of the smallness of the effect being measured and the fact that the signal was buried in a background of comparable noise, a great deal of data had to be processed

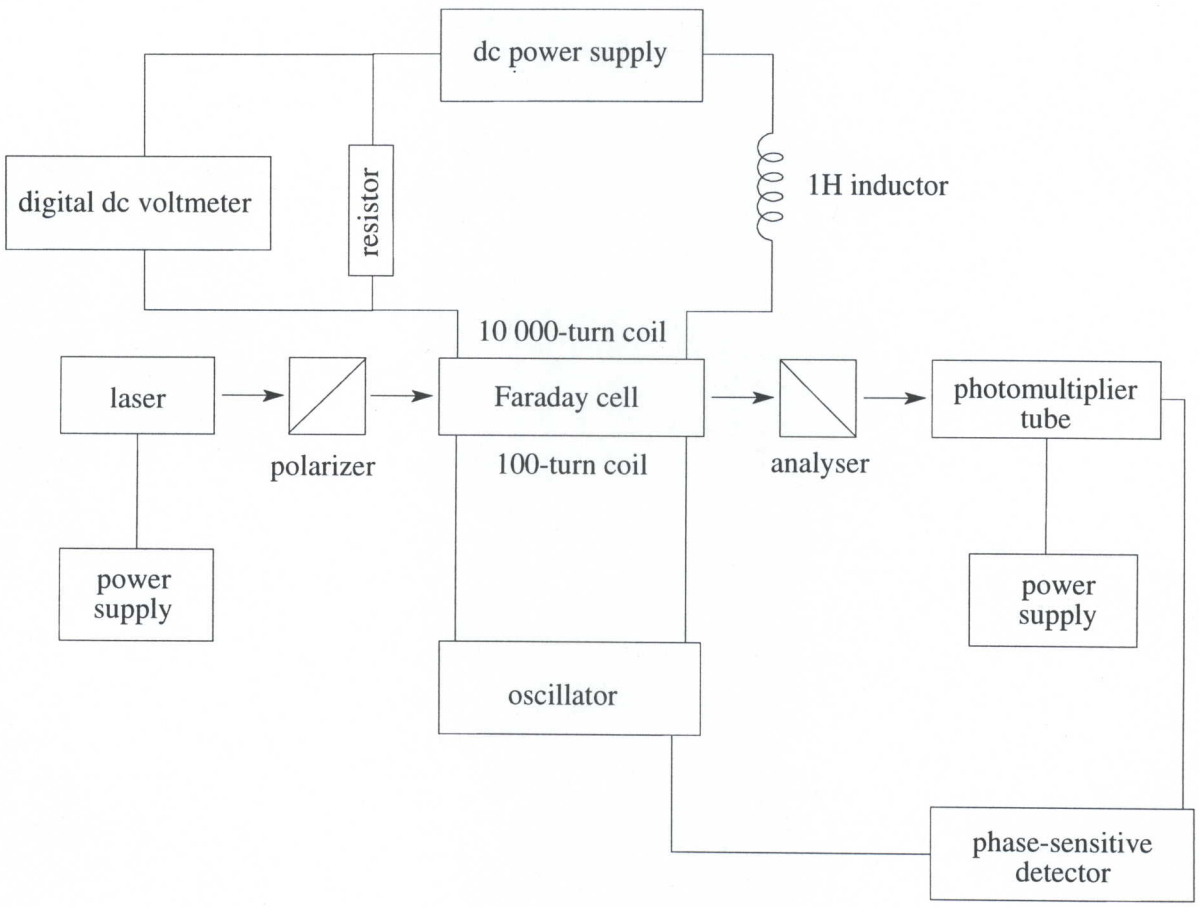

Figure 4.8 Schematic diagram of the set-up used in the calibration of the Faraday cell

in order to extract a meaningful result. This naturally suggested that the entire experiment should be placed under computer control and, because of the availability of Hewlett Packard equipment, an HP86 microcomputer was selected for the task. This was furnished with an HPIB interface, thereby enabling the data acquisition unit, HP multimeters and the custom-built digital-to-analogue converter to be addressed with ease.

The phase-sensitive detector used in this work was an EG&G Princeton Applied Research model 5210 Lock-In Amplifier. This model incorporated an integral current amplifier, thereby allowing the signal from the photomultiplier to be fed directly into the psd. Another useful feature of this model is the existence of several in-line filters in the signal path; those selected for this work were the bandpass filter, tuned to the frequency of the reference signal, and the line-frequency notch filters.

Throughout this work a current amplifier setting of $10^6\,\mathrm{VA}^{-1}$ was found to be most appropriate, whilst the sensitivity most frequently chosen was $100\,\mu\mathrm{V}$ full-scale deflection. A time constant of 1 s was selected for all but the very noisiest signals for which a 3 s time constant was sometimes used.

A facility was available whereby the phase difference between the reference signal and the detected signal could be displayed in degrees, and the phase of the reference signal could then be shifted to be exactly in phase with the signal from the photomultiplier. An output channel on the psd provided a dc signal in the range $-10\,\mathrm{V}$ to $+10\,\mathrm{V}$, corresponding to psd readings of -100% to $+100\%$ of the selected range. An HP3478A multimeter measured this output, and this reading, being proportional to the modulated light intensity at the photomultiplier, was then recorded by the computer. As mentioned in §4.5.2, the current through the Faraday cell was monitored by using an identical multimeter to measure the ac voltage across a known resistance in series with the Faraday cell. A four-wire measurement of this resistance was made each time the experiment was performed.

All other data were collected by an HP3421A data acquisition unit. This was fitted with the multiplexer card option configured to have eight multimeter channels and two channels which served as relays. In order to monitor the temperature of the cell three calibrated $10\,\mathrm{k}\Omega$ thermistors were attached along the length of the cell, and three of the data acquisition unit channels were used to monitor these resistances. These values were then used by the computer to obtain a mean value for the temperature of the gas in the cell. Another channel was used to monitor the dc voltage produced by the high-voltage amplifier in the ratio 1:1000 of the rms potential on the wires in the cell. The two relay channels provided the switching and direction control needed for the stepper motor, whilst another channel was configured as a counter to track the stepper motor position.

A listing of the HP86 program used to control the experiment is given in Appendix F. At the start of a series of measurements the alignment of the optical components would be checked to ensure that the maximum possible light intensity passed through the system. The current through the Faraday cell was then set in antiphase with the high voltage on the wires in the quadrupole cell, and the reference signal at

the psd was brought into phase with the signal from the quadrupole cell. A reading of the gauge pressure of the gas in the cell would then be entered into the computer together with the barometric pressure in the room. This information was logged in the same file as that in which the experimental data was stored. Other important variables such as the date, time, gas, wire separation, wire thickness, wire length, and Faraday cell constant were also recorded in the header of this file.

The computer would then proceed to find the positive and negative limits for the analyser offset which produced full scale deflection on the psd. Once these had been determined, the corresponding currents through the Faraday cell which yielded full scale deflections of the opposite sign were found. The program then began a cycle of measurements to find the current at the cross-over points which was repeated until interrupted by human intervention. In this cycle the analyser would first be positioned at one of its offset positions and the temperature of the gas in the cell would be measured and recorded. A reading of the high voltage in the cell was also taken. Twenty equally-spaced current values in the range from zero to that current giving full scale deflection in the opposite sense were then determined, and the current through the coil of the Faraday cell was set to each of these in turn. As a precaution these values were used in a non-sequential order thereby reducing the effect that any slow drift in other variables, such as the temperature of the gas, might have on the results.

At each current setting the computer waited for a fixed period equal to several times the time constant of the psd, and then took fifty readings of the psd output which were averaged and stored with a measured value for the current. After all twenty values for the current had been used, a least-squares linear regression was performed and the slope and intercept of the best-fit line were stored. The analyser would then be rotated to its second offset position and, after waiting for at least a minute for vibrations to decay, the process would be repeated and the slope and intercept of a second line were found. Finding I_{int}, the value of the current at the point of intersection of the second line with the first, enabled a value for θ_{int} in (3.36) to be calculated.

At the end of each cycle, the data would be written to magnetic disk and then printed on a line printer so that a copy was available in the event of the magnetic disk data being corrupted. Information contained in the HP86 magnetic disk files had to be processed in order to extract values for the electric quadrupole moments of the gas molecules from the measured cross-over points of the two lines. This analysis was performed using an IBM AT computer because of its greater convenience of use. A special program was used to convert the HP86 files to ones which could be read by this computer.

Chapter 5

PRESENTATION OF RESULTS

5.1 Theoretical Considerations

A general expression in terms of molecular quantities for the phase retardation induced between orthogonally-polarized components of the light beam on passing through the quadrupole cell may be found by substituting (2.58) in (3.1), to give

$$\delta = \frac{2\pi l}{\lambda}\frac{NE's}{\varepsilon_0} = \frac{2\pi l}{\lambda}\frac{N_0E's}{V_m\varepsilon_0}, \tag{5.1}$$

in which all symbols retain their previous meanings. In §4.6 it is noted that the output of the experiment is I_{int}, the value of the current through the Faraday cell at the point of intersection of the two graphs of psd output vs Faraday cell current. This may be related through the calibration constant F of the Faraday cell to θ_{int} in (3.36) by

$$\theta_{\text{int}} = FI_{\text{int}}. \tag{5.2}$$

Substituting this in (3.36) and solving for δ yields

$$\delta = \pm 2FI_{\text{int}}, \tag{5.3}$$

in which the sign is determined by the orientation of the fast axis of the $\frac{\lambda}{4}$-plate. In practice, an *ab initio* determination of signs in the experiment is difficult, so the sign of $3q^{(0)}_{\alpha\beta}\alpha_{\alpha\beta} - q^{(0)}_{\alpha\alpha}\alpha_{\beta\beta}$ for a given gas was determined by comparing the sign of the psd output for a given offset of the analyser with that found with the same analyser offset for carbon dioxide, for which the sign of $q^{(0)}_{zz} - q^{(0)}_{xx}$ is known to be negative [41]. In view of this we shall henceforth drop the sign from the notation.

Combining (5.3) and (5.1) allows us to solve for the molecular expression s in terms of experimental observables, yielding

$$s = \frac{FI_{\text{int}}\lambda\varepsilon_0V_m}{\pi lE'N_0}. \tag{5.4}$$

In order to extract from this an expression for the quadrupole moment of a molecule we must consider the special cases in which the expression for s may be simplified. For carbon dioxide, carbon monoxide, nitrogen, and chlorine, which are all linear molecules, and boron trifluoride, which is planar with an axis of 3-fold rotational symmetry, simplifying the molecular expression for s yields (2.59). We shall neglect at this stage the hyperpolarizability term b in comparison with the other terms, although we shall later consider the validity of doing so for each of the gases investigated. Furthermore, we may omit the term containing the permanent dipole moment $\mu^{(0)}$. In the case of carbon monoxide, a polar molecule, this is interpreted as referring the quadrupole moment to an origin located at that point in the molecule at which the origin-dependent coefficient of $\mu^{(0)}$ vanishes. The remaining part of (2.59) is substituted in (5.4) to yield

$$q^{(0)} = \frac{15\lambda V_m \varepsilon_0 F I_{\text{int}} kT}{\pi l N_0 E' \Delta\alpha}, \tag{5.5}$$

in which

$$\Delta\alpha = \alpha_{zz} - \alpha_{xx},$$
$$q^{(0)} = q^{(0)}_{zz} - q^{(0)}_{xx},$$

and the z-axis is the axis of highest symmetry of the molecule. We loosely refer to $q^{(0)}$ as the 'quadrupole moment' of a linear molecule.

The relationship between the primitive and traceless quadrupole moment definitions has been discussed at some length in §1.2. From (1.8) it is a simple matter to show that, for a linear molecule, $q^{(0)} = \theta_{zz}$. A direct comparison may therefore be made in this case between the θ_{zz}[1] 'quadrupole moment' reported by experimentalists using the traceless definition and the $q^{(0)}$ 'quadrupole moment' reported here.

Ethene is a non-polar molecule belonging to the symmetry point group D_{2h}. It therefore has three independent polarizabilities and its primitive quadrupole moment is also specified by three numbers. If we again assume that the hyperpolarizability terms are negligible then the appropriate form of (5.4) for ethene is

$$\tfrac{1}{2}[q^{(0)}_{xx}(2\alpha_{xx} - \alpha_{yy} - \alpha_{zz}) + q^{(0)}_{yy}(2\alpha_{yy} - \alpha_{zz} - \alpha_{xx}) + q^{(0)}_{zz}(2\alpha_{zz} - \alpha_{xx} - \alpha_{yy})] = \frac{15\lambda V_m \varepsilon_0 F I_{\text{int}} kT}{\pi l N_0 E'}. \tag{5.6}$$

The factor $\frac{1}{2}$ is introduced on the left-hand side of (5.6) so that the right-hand side differs from that of (5.5) only by the missing $\Delta\alpha$ in the denominator.

Further simplification of (5.6) is possible only if certain assumptions are made regarding the relationships between the quantities on the left-hand side. This appears to be common practice amongst experimentalists and is considered further in §5.3.6 where such approximations are made in order to compare the results reported here with those obtained by other workers.

[1] Often denoted simply by θ.

5.2 Experimental Variables

5.2.1 General considerations

The right-hand sides of (5.5) and (5.6) comprise several experimental variables and three fundamental physical constants. Values used for the latter were [44]:

$$\begin{aligned} \varepsilon_0 &= 8.8542 \times 10^{-12}\,\mathrm{C^2N^{-1}m^{-2}}, \\ k &= 1.38066 \times 10^{-23}\,\mathrm{JK^{-1}}, \\ N_0 &= 6.0220 \times 10^{23}\,\mathrm{mol^{-1}}. \end{aligned}$$

The wavelength λ of the He-Ne laser light used in the experiment is well known to be 632.8 nm; whilst the geometric path length of the light beam through the quadrupole cell was taken to be the distance between the exposed faces of the plates on the wire-holders. This distance was measured each time the cell was reassembled although it always fell within a one millimetre range centred on 1466 mm. The maximum error in this measurement was estimated to be 0.1%.

Another experimental variable which was checked frequently but varied little was the calibration constant of the Faraday cell. A typical value for this constant would be 3.31×10^{-6} radians per milliampere having a standard deviation of the mean of 0.6%, due almost entirely to the uncertainty in finding the null position during the calibration procedure, since the current through the cell and the rotation of the analyser could both be determined with far greater precision. By the same token, the error in determining I_{int} was also due to uncertainties in finding the point of intersection of the the two graphs of psd output vs Faraday cell current, rather than an uncertainty in measuring the Faraday cell current itself.

The remaining variables, temperature, molar volume, and electric field gradient, require a more detailed discussion.

5.2.2 Temperature

Since the quadrupole cell was not designed to be heated or cooled, all measurements were made at room temperature. Over the course of a year this temperature ranged from 15°C to 32°C whereas the thermal insulation encasing the cell ensured that the temperature of the gas seldom varied by more than 0.2°C over the period required to determine a single null point.

An accurate determination of the gas temperature was vital since it not only appears in its own right in (5.5) but also plays an important role in determining the molar volume and, to a lesser extent, the dielectric constant of the gas. The temperature of the gas in the cell was found by measuring the resistance of the three thermistors mentioned in §4.6. These had been individually calibrated in a constant-temperature oil bath against a Beckman mercury thermometer over a slightly wider temperature range than was encountered experimentally. Discrepancies between the temperatures inferred from resistance measurements made on each of the three thermistors were

generally of the order of 0.1°C. Confidence could therefore be placed in the temperature measurement obtained by averaging the three individual readings, the maximum error in which was estimated to be 0.1%.

5.2.3 The molar volume

Measurements on most of the gases reported in this chapter were made over a range of gas densities. An exception was chlorine, largely because the condition of the windows deteriorated steadily from the moment the gas entered the cell, thereby presenting a need to obtain accurate results as swiftly as possible. For this reason, measurements on chlorine were made at the highest usable pressures. Even in the cases of the remaining gases, higher pressures were favoured as it is at the smallest molar volumes that the birefringence induced in a gas is greatest. The highest pressure used was generally just below the critical pressure of the gas, providing that this was less than the 4 MPa upper limit imposed by the Budenberg Master Test Gauge.

Deviations in the behaviour of a gas from the ideal gas law are described by the virial equation of state,

$$\left(\frac{PV_m}{RT} - 1\right) = \frac{B_p}{V_m} + \frac{C_p}{V_m^2} + \frac{D_p}{V_m^3} + \cdots,$$

in which B_p, C_p, and D_p are, respectively, the second, third, and fourth pressure virial coefficients, and are, in general, functions of the temperature of the gas. Other symbols in this equation have their usual meanings. If the virial equation of state is truncated after the term in $\frac{1}{V_m^2}$ then it becomes an equation which is cubic in the molar volume and for which V_m may, therefore, be solved exactly.

Dymond and Smith [45] have compiled extensive tables of reported virial coefficient data for most gases. This data is tabulated over a range of temperatures, thereby permitting the user to select the data which are considered to be the most reliable over a given temperature range and then to fit to them a smooth curve for purposes of interpolation. For the work reported here, polynomials of typically fifth order were fitted by 'least-squares' to selected data for the second and, where available, the third pressure virial coefficient. The coefficients so found were stored in the computer program used to analyse the results so that the virial coefficients of the gas could be found at the recorded temperature. These values were then substituted, together with the absolute pressure of the gas, into an exact expression for the required root of the truncated virial equation of state in order to determine the molar volume V_m of the gas.

Based on maximum error of 0.3% in the pressure measurement at a typical pressure of 3 MPa the maximum error in V_m was estimated to be 0.5%.

5.2.4 The electric field gradient

The principle used to calculate the electric field gradient on the axis of the cell is outlined in §4.4.5. Measured values for the wire spacing at three places along the cell

were passed to the analysis program along with the other experimental data so that the average wire separation could be calculated for each experimental run. Line charges which are used to model the set-up as described in Appendix A were then positioned so that those equipotential surfaces at the potential of the measured high voltage on the wires coincided with the wire surfaces. Once the geometry had been established the field gradient per volt was calculated, thereby enabling the electric field gradient to be found from the value of the high voltage recorded for each cycle of the experiment. In practice, drift in the high voltage output was inconsequential over a typical 12-hour run period.

The point is made in Appendix A that a factor $\frac{1}{\varepsilon_r}$ should be included in the expression for the electric field gradient to account for the dielectric properties of the gas. Pierrus [39] has noted that this correction can amount to several percent in certain cases. The dielectric constant of a gas has a density-dependence described by expanding the Clausius-Mosotti function $\frac{\varepsilon_r - 1}{\varepsilon_r + 2} V_m$ in inverse powers of the molar volume:

$$\frac{\varepsilon_r - 1}{\varepsilon_r + 2} V_m = A_\varepsilon + \frac{B_\varepsilon}{V_m} + \frac{C_\varepsilon}{V_m^2} + \cdots ,$$

in which $A_\varepsilon, B_\varepsilon$, and C_ε are, respectively, the first, second, and third dielectric virial coefficients. Unfortunately, there is a relative paucity of data giving the temperature dependence of dielectric virial coefficients for gases. Where such data exists they have usually been carefully measured in order to infer from them the value of some molecular quantity such as the electric quadrupole moment, and in these cases the approach used to determine ε_r was analogous to that employed in finding the molar volume.

In the cases of carbon monoxide, chlorine, and boron trifluoride, no dielectric virial coefficient data were available. The dielectric constant of carbon monoxide was calculated using the expression [46]

$$A + \frac{B}{T} = \frac{\varepsilon_r - 1}{\varepsilon_r + 2} V_m. \tag{5.7}$$

A tabulated value for A and the permanent electric dipole moment $\mu^{(0)}$ were available [46], the latter enabling B to be found using the expression

$$B = \frac{4\pi N_0 \mu^2}{9k}.$$

In the cases of chlorine and boron trifluoride, published values of the polarizability α were used to approximate the first dielectric virial coefficient A_ε as $\frac{N_0 \alpha}{3\varepsilon_0}$.

Taking into consideration the maximum uncertainty of 0.2% in the measured value of the high voltage and the method of calculating a mean wire spacing, the maximum uncertainty in the electric field gradient is estimated to be 0.4%.

5.3 Results

5.3.1 Statistical analysis

The apparatus and techniques described in the previous chapter were used to perform induced-birefringence measurements on six gases: carbon dioxide, carbon monoxide, nitrogen, ethene, boron trifluoride, and chlorine.

In order that these results, presented in the subsections which follow, serve as useful a purpose as possible, it is important that careful attention be paid to assigning them the most realistic bounds of uncertainty. This uncertainty contains elements of both random scatter and of a 'scale-limited' nature. In evaluating and combining the uncertainties from various sources, the writings of Baird [47] have proved helpful. The theory which follows is necessarily based on the assumption that measurements of the quadrupole moment in this experiment are normally distributed about the mean. Histograms of runs of measurements on carbon dioxide have shown that this is a reasonable assumption. For convenience, we will use the notation pertaining specifically to the case of a linear molecule. The statistical treatment of other cases is exactly analogous.

We begin by considering the process of arriving at a measured value of the quadrupole moment of a molecule. Before starting a run of the experiment, the pressure of the gas in the cell was set to the desired value, the apparatus was left to stand in order to allow the turbulence in the gas to decay, and the optical components were realigned in order to maximize the light intensity passing through them. After determining limits for the offset of the analyser, the computer would begin to take readings of the psd output for various currents passing through the Faraday cell. Since these currents were actively maintained at a steady level and were measured by a $5\frac{1}{2}$-digit ac voltmeter connected across a resistance which was known to a precision of better than 0.01%, the most important uncertainties in these readings were entirely due to the noise in the psd output. To counter this noise, which necessarily depended on the signal strength and was therefore greatest at lower pressures and was more significant in some gases than in others, a number of psd output readings were taken in quick succession and averaged. This number was typically twenty but as many as fifty readings per point were taken in particularly noisy cases.

In all instances, readings were taken for twenty uniformly-spaced current settings for both offsets of the analyser. Straight lines were fitted to these data sets using least-squares linear regression and a correlation coefficient r was calculated for each line. From the slopes and intercepts of these two lines, the current at the point of intersection was calculated. A single spurious reading, due, say, to a spike in the mains supply, could introduce considerable error into the value of the current at the point of intersection. For this reason, if either line had a correlation coefficient which was less than 0.99 then the quadrupole moment calculated from the current at that cross-over point was not included in the average for that run.

A run would be terminated by human intervention, whereupon the mean quadrupole

moment $\bar{q}^{(0)}$ and standard deviation s of the sample were calculated from those n measurements which had been accepted on the basis of the above test. The standard deviation was calculated, not as a measure of the standard deviation of a single reading from the mean of the sample, given by

$$s = \sqrt{\frac{\sum(\bar{q}^{(0)} - q_i^{(0)})^2}{n}},$$

but as the best estimate of the standard deviation σ of a single measurement in the universe of measurements for that particular configuration of the experiment, given by

$$\sigma \approx s = \sqrt{\frac{\sum(\bar{q}^{(0)} - q_i^{(0)})^2}{n-1}}. \tag{5.8}$$

However, the quadrupole moment quoted is an average of several independent measurements so the measure of probable deviation of this value from the 'true' quadrupole moment that would be measured with this particular experimental configuration is σ_m, the standard deviation of the mean of a random sample of n measurements, which is best estimated in this case by

$$\sigma_m = \frac{\sigma}{\sqrt{n}} \approx \sqrt{\frac{\sum(\bar{q}^{(0)} - q_i^{(0)})^2}{n(n-1)}}. \tag{5.9}$$

It is this value which has been recorded with the mean in the last column of Table 5.1, and in all the tables of results which follow. There is, of course, inherent uncertainty in estimating σ and, therefore, in estimating σ_m based on only a small sample of measurements. The standard deviations of sets of n measurements of quadrupole moments for a given experimental configuration will themselves be normally distributed about σ with an uncertainty σ_s given by

$$\sigma_s = \frac{\sigma}{\sqrt{2(n-1)}}.$$

In view of this, greater confidence may be placed in those estimates of σ_m which are based on many readings.

A brief inspection of the last column of Table 5.1 reveals that the the best estimate of σ_m in almost every run is considerably smaller than a typical deviation between a randomly chosen run and the mean of all the runs, recorded at the foot of the table. This suggests that each σ_m and the corresponding value of the mean quadrupole moment are applicable only to the universe of measurements for that particular experimental configuration. Between runs of the experiment, variables such as the pressure and temperature of the gas and the electric field gradient changed. Every effort was made to account for these changes but residual effects such as slightly differing wire separation, misalignment of the optics, temperature of the Faraday Cell, and scattering

from deteriorated inner surfaces of the cell windows are virtually impossible to measure and model and will therefore give rise to small differences between runs. It does not seem unreasonable to assume that the results for $\bar{q}^{(0)}$ from all the runs run are normally distributed about some value: presumably the quadrupole moment which would be considered correct if there were no uncertainties in the other variables such as the electric field gradient and Faraday cell constant.

If these values had all been measured under the same, or nearly similar, conditions, then the recommended course of action would be to obtain from this data an average quadrupole moment weighted by the inverse square of each of the σ_m values. Under the circumstances described above, the validity of doing so is highly questionable. The most prudent strategy is probably to discard the individual σ_m values and to treat the mean values from each run as individual measurements of $q^{(0)}$. An overall value for $\bar{q}^{(0)}$ and for σ_m may then be calculated in exactly the same way as before. The benefit of having performed many measurements in each run is not lost in this way since the universe of measurements to which the mean values of $q^{(0)}$ from each run belong must necessarily have a smaller standard deviation σ than would be the case had just one measurement been made in each run.

The above procedure was adopted in analysing the data shown in each of the tables of results which follow. The mean value is shown together with the best estimate of σ_m in the bottom row of each table. This value of σ_m is merely the uncertainty due to effects which may be considered to be random and does not include the uncertainties of a more systematic nature.

Uncertainties in the measured and calculated quantities appearing in (5.5) have been discussed in §5.2. Briefly, these are :

T The absolute temperature of the gas has a maximum uncertainty of 0.1%.

V_m The molar volume of the gas was calculated from measurements of the absolute pressure and temperature of the gas and has a maximum uncertainty of 0.5%.

l The length of the wires in the cell was measured with a maximum uncertainty of 0.1%.

E' The on-axis electric field gradient was calculated from measurements of the wire spacing and of the potential difference between the cell and the wires. It has a maximum uncertainty of 0.4%.

F The calibration constant of the Faraday cell was found by averaging a large number of readings. A statistical treatment of this data yields a value for the standard deviation of the mean which was never greater than 0.6%.

The uncertainty in the anisotropy in the polarizability $\Delta\alpha$ also contributes to the uncertainty in the value of $q^{(0)}$ calculated using (5.5). Bogaard *et al.* [48] have performed light-scattering measurements from which the anisotropy in the molecular polarizability may be deduced, and it is from this source that $\Delta\alpha$ values for all the gases

investigated, excepting chlorine and boron trifluoride, were taken. The value for chlorine was taken from an earlier paper by Bridge and Buckingham [49] in which the same technique was employed. Light-scattering experiments measure the intensity of light scattered by a molecule in a direction perpendicular to the incident beam in two orthogonal polarization planes. Suppose that the molecule is located at the origin of a set of right-handed axes and that the incident beam is polarized in the x-direction and propagates along the z-axis. Then the ratio of the intensity of light scattered by the molecule in the y-direction and polarized in the z-direction to that scattered in the y-direction and polarized in the x-direction is known as the depolarization ratio ρ_0, and is related to the polarizability of a linear molecule via the expressions [48]

$$\rho_0 = \frac{3\kappa^2}{5+4\kappa^2}, \quad \kappa = \frac{\Delta\alpha}{3\alpha}, \tag{5.10}$$

from which may be deduced the expression

$$\Delta\alpha = 3\alpha\sqrt{\frac{5}{3-4\rho_0}}. \tag{5.11}$$

Bogaard *et al.* [48] state that one should assume their values of ρ_0 to contain an error of $\approx \pm 3\%$. Of all the gases considered here, that having the greatest depolarization ratio is carbon dioxide, for which $\Delta\alpha$ is 0.00405 at 632.8 nm [48]. It is immediately apparent that the maximum error in $\sqrt{\frac{5}{3-4\rho_0}}$ will be considerably smaller than that in ρ_0. Indeed, a $\pm 3\%$ range in the ρ_0 value for carbon dioxide causes an uncertainty of only 0.02% in the value of this quantity. Clearly, the greatest source of uncertainty in $\Delta\alpha$ in (5.11) must stem from that in the polarizability α. Bogaard *et al.* [48] deduce these values from refractivity data obtained from a number of sources but do not discuss the uncertainties associated with them. In an earlier paper Bridge and Buckingham [49] suggest that realistic uncertainties in α range from 0.5% for diatomic gases to 5% in the case of heavy vapours. In view of this, an uncertainty of 2% for all cases is probably over-cautious, but this is the maximum error which has been assigned to $\Delta\alpha$ in calculating the overall uncertainty in $q^{(0)}$ in the present study.

Baird [47] has pointed out the difficulties in combining uncertainties of both the maximum error and standard deviation types. He has outlined an approach for doing so which yields an uncertainty in the calculated quantity having a $\frac{2}{3}$ probability associated with it. This is the approach which has been adopted in this work to produce the final uncertainty quoted for the quadrupole moment of each gas studied. It must be borne in mind that this uncertainty is neither a maximum error nor a standard deviation of the mean, but instead represents an interval over which the probability of finding the true quadrupole moment is estimated to be $\frac{2}{3}$.

5.3.2 Carbon dioxide

Being a 'well-behaved' gas and having as it does a comparatively large value for the product of $q_{zz}^{(0)} - q_{xx}^{(0)}$ and $\Delta\alpha$, carbon dioxide is a useful gas for checking the behaviour of

apparatus designed to measure quadrupole moments of gases. Indeed, the first induced-birefringence measurements made for this purpose were performed on carbon dioxide [41]. Since then, many workers have reported values for the quadrupole moment of this molecule found using the birefringence technique [37, 39] as well as a variety of other methods [32, 50, 16, 51, 52, 15]. Establishing the quadrupole moment of carbon dioxide with great certainty is an appealing idea since it would then provide a standard against which apparatus could be calibrated and techniques evaluated. For these reasons, a great many measurements spanning a period of about three years were made on carbon dioxide in the present study.

Coleman-grade (99.99% minimum purity) carbon dioxide was used in all the measurements reported here. The second and third virial coefficient data used in calculating the molar volume were taken from Butcher and Dadson [53], whilst the dielectric constant ε_r was found using the dielectric virial coefficient data of Bose and Cole [16]. A value of $2.350 \times 10^{-40}\,\mathrm{C^2m^2J^{-1}}$ for $\Delta\alpha$ of carbon dioxide as measured by Bogaard *et al.* [48] at 632.8 nm was used to calculate $q^{(0)}$.

A feature of the carbon dioxide measurements is the variety of conditions under which they were made. Especially noteworthy are the two different combinations of wire thicknesses and spacings which were used in performing the measurements. These two sets of data have been tabulated separately in Table 5.1 and Table 5.2. Since the mean values obtained from these two tables are not significantly different, both sets of data have been used to obtain a mean value for the quadrupole moment of carbon dioxide, this being $(-14.53 \pm 0.22) \times 10^{-40}\,\mathrm{Cm^2}$.

Battaglia *et al.* [37] have reported a value of $(-14.98 \pm 0.50) \times 10^{-40}\,\mathrm{Cm^2}$ for the quadrupole moment of carbon dioxide measured using the same induced-birefringence technique. By making measurements over a range of temperatures they showed that the hyperpolarizability term b in (2.59) contributes less than 2% to the induced birefringence. Calculations of an *ab initio* nature performed by Amos [54] suggest that the hyperpolarizability contribution may be less than 0.5%. Ignoring this contribution in comparison with that of the quadrupole moment term is then well justified. The discrepancy between our value and that of $(-13.4 \pm 0.4) \times 10^{-40}\,\mathrm{Cm^2}$ reported by Pierrus [39, 43] has been considered in §3.6.

Amos [54] has reported an *ab initio* calculated value for the quadrupole moment of carbon dioxide of $-15.2 \times 10^{-40}\,\mathrm{Cm^2}$. A more recently calculated value due to Maroulis and Thakkar [55] of $-14.54 \times 10^{-40}\,\mathrm{Cm^2}$ is in excellent agreement with the value reported here. These authors obtain this value using an *SDQ*-MP4 calculation which they suggest is accurate to within 3%.

Table 5.1 Carbon dioxide results for 0.5 mm wire thickness

Number of null points	T (K)	P (MPa)	V_m ($cm^3 mol^{-1}$)	ε_r	E'_{xx} ($10^8\ V m^{-2}$)	$q^{(0)} \pm \sigma_m$ ($10^{-40}\ C m^2$)
22	293.3	2.574	796.7	1.028	5.76	-14.68 ± 0.03
19	292.2	2.546	802.5	1.028	5.76	-14.38 ± 0.01
5	293.3	2.555	803.7	1.028	5.76	-14.51 ± 0.02
15	294.0	2.564	804.2	1.028	5.77	-14.48 ± 0.03
5	294.2	2.481	837.9	1.027	6.05	-14.21 ± 0.05
7	292.0	2.440	844.3	1.027	6.05	-14.16 ± 0.04
16	293.7	2.454	846.8	1.027	6.06	-14.25 ± 0.01
7	292.9	2.437	850.2	1.026	6.06	-14.32 ± 0.02
16	293.6	2.440	852.0	1.026	6.05	-14.28 ± 0.01
6	292.1	2.415	855.4	1.026	6.05	-14.36 ± 0.03
15	292.2	2.413	856.7	1.026	6.05	-14.30 ± 0.01
7	290.2	2.379	861.8	1.026	6.03	-14.18 ± 0.02
15	291.4	2.389	863.1	1.026	6.03	-14.29 ± 0.02
9	290.4	2.370	866.6	1.026	6.03	-14.20 ± 0.02
13	291.7	2.380	868.9	1.026	6.03	-14.60 ± 0.07
12	296.9	4.005	446.4	1.051	6.07	-14.37 ± 0.02
7	295.7	3.910	458.4	1.051	6.06	-14.78 ± 0.16
12	295.4	3.812	475.6	1.048	6.06	-14.24 ± 0.03
6	294.0	3.705	490.4	1.046	6.06	-15.34 ± 0.05
12	294.6	3.600	514.8	1.044	6.06	-14.61 ± 0.02
13	295.2	3.402	561.0	1.040	6.06	-14.69 ± 0.05
6	293.6	3.305	577.1	1.039	6.06	-15.32 ± 0.03
7	294.7	3.105	633.0	1.036	6.06	-14.46 ± 0.04
12	295.8	2.993	669.2	1.034	6.06	-14.23 ± 0.01
6	295.6	2.901	695.7	1.032	6.07	-14.52 ± 0.01
18	296.9	2.907	699.7	1.032	6.07	-14.34 ± 0.04
36	297.7	2.802	736.7	1.031	6.07	-14.35 ± 0.03
7	299.5	4.027	454.1	1.050	6.08	-14.27 ± 0.09
11	299.6	4.014	456.7	1.050	6.07	-14.35 ± 0.04
9	296.5	3.928	458.7	1.050	6.09	-14.44 ± 0.02
9	296.0	3.889	463.1	1.049	6.09	-14.41 ± 0.01
11	295.3	3.865	465.1	1.049	6.09	-15.23 ± 0.17
12	299.0	3.637	526.2	1.043	6.18	-14.41 ± 0.02
30	298.1	3.617	526.5	1.043	6.18	-14.40 ± 0.04
15	298.0	3.613	529.9	1.043	6.18	-14.64 ± 0.03
27	297.6	3.604	527.1	1.043	6.18	-14.39 ± 0.04

continued

continued from previous page						
Number of null points	T (K)	P (MPa)	V_m (cm^3mol^{-1})	ε_r	E'_{xx} ($10^8\ Vm^{-2}$)	$q^{(0)} \pm \sigma_m$ ($10^{-40}\ Cm^2$)
40	298.6	3.620	528.1	1.043	6.18	-15.13 ± 0.07
26	301.1	3.669	528.4	1.043	6.19	-14.42 ± 0.02
16	301.2	3.667	529.4	1.043	8.27	-14.34 ± 0.01
28	302.3	3.691	528.9	1.043	8.27	-14.17 ± 0.02
31	301.5	3.673	529.2	1.043	8.95	-14.50 ± 0.01
15	300.9	3.663	528.8	1.043	8.95	-14.45 ± 0.05
25	301.6	3.675	529.3	1.043	8.95	-14.23 ± 0.02
17	302.0	3.682	529.6	1.043	9.60	-14.05 ± 0.20
25	300.5	3.652	529.5	1.043	6.98	-14.84 ± 0.02
17	300.2	3.644	529.9	1.043	6.98	-14.59 ± 0.11
25	300.8	3.654	530.2	1.043	7.50	-14.56 ± 0.01
29	301.8	3.227	631.6	1.036	8.31	-14.16 ± 0.06
6	304.2	3.707	533.4	1.043	7.58	-14.44 ± 0.01
33	304.0	3.704	533.2	1.043	7.59	-14.52 ± 0.02
30	305.8	3.734	534.4	1.042	8.90	-14.76 ± 0.06
10	307.0	3.754	535.3	1.042	8.18	-15.16 ± 0.05
41	306.7	3.747	535.5	1.042	8.87	-14.45 ± 0.02
18	302.5	3.655	537.1	1.042	9.58	-14.66 ± 0.05
25	302.8	3.663	536.8	1.042	9.58	-14.58 ± 0.02
					mean	-14.49 ± 0.04

5.3.3 Carbon monoxide

Shown in Table 5.3 are the results for measurements performed on CP-grade (minimum 99.5% purity) carbon monoxide. The pressure virial coefficient data of Michels *et al.* [56] were used in determining the molar volume of the gas. No dielectric virial coefficient data for carbon monoxide could be found, so the dielectric constant of the gas was calculated using the method described in §5.2.4 and the tables of dielectric constants and dipole moments in [46]. A value of $0.592 \times 10^{-40}\ C^2m^2J^{-1}$ for $\Delta\alpha$ as reported by Bogaard *et al.* [48] at 632.8 nm was used to calculate $q^{(0)}$. The quadrupole moment of carbon monoxide measured in this way had a mean value of $(-9.47 \pm 0.15) \times 10^{-40}\ Cm^2$.

This result is somewhat greater than the value of $(-8.34 \pm 1.00) \times 10^{-40}\ Cm^2$ reported in 1968 by Buckingham *et al.* [57]. That of $(-8.58 \pm 0.35) \times 10^{-40}\ Cm^2$ obtained by Pierrus [39, 43] is in good agreement with the Buckingham value, but differs from that reported here by approximately the same percentage (-9%) as did his value for carbon dioxide (-8%).

No comparisons with data from other experiments can be made since these measure the quadrupole moment with respect to an origin located at the centre of mass of the molecule. However, knowing the quadrupole moment of carbon monoxide with respect to both the centre of mass and the effective quadrupole centre of the molecule permits additional information to be calculated. If the permanent electric dipole moment is

Table 5.2 Carbon dioxide results for 0.4 mm wire thickness

Number of null points	T (K)	P (MPa)	V_m ($cm^3\,mol^{-1}$)	ε_r	E'_{xx} ($10^8\,V\,m^{-2}$)	$q^{(0)} \pm \sigma_m$ ($10^{-40}\,C\,m^2$)
9	294.2	3.985	437.5	1.052	8.72	-14.80 ± 0.46
7	294.4	4.002	435.4	1.052	8.70	-15.13 ± 0.26
11	296.6	4.052	436.6	1.052	9.83	-14.51 ± 0.07
9	295.4	4.019	437.1	1.052	9.92	-14.53 ± 0.10
9	295.4	4.021	436.6	1.052	9.92	-14.70 ± 0.45
8	295.2	4.012	437.3	1.052	9.94	-14.49 ± 0.18
10	296.5	3.104	641.3	1.035	9.99	-13.84 ± 0.31
10	295.7	3.081	644.0	1.035	9.92	-14.25 ± 0.21
5	298.4	3.125	643.8	1.035	9.96	-14.49 ± 0.07
9	299.7	3.149	643.1	1.035	9.96	-14.40 ± 0.04
22	300.0	3.161	641.2	1.035	9.96	-14.39 ± 0.18
8	301.4	3.175	643.5	1.035	8.79	-13.63 ± 0.40
11	297.5	3.935	461.8	1.049	9.94	-14.90 ± 0.28
11	298.4	3.954	462.4	1.049	9.96	-14.94 ± 0.19
20	300.9	3.990	466.6	1.049	8.65	-14.77 ± 0.10
6	301.8	3.970	473.9	1.048	9.88	-14.89 ± 0.05
5	300.5	4.092	447.1	1.051	9.89	-15.13 ± 0.18
21	301.1	2.693	789.3	1.028	9.87	-14.43 ± 0.20
13	301.1	2.704	785.2	1.029	9.87	-14.61 ± 0.21
20	302.1	2.714	786.2	1.029	9.87	-14.61 ± 0.22
20	302.5	2.725	784.1	1.029	9.87	-14.73 ± 0.12
9	299.3	2.685	783.8	1.029	9.89	-14.63 ± 0.29
7	295.9	2.645	782.7	1.029	9.85	-14.75 ± 0.07
22	295.8	2.644	782.7	1.029	9.87	-14.57 ± 0.10
9	296.7	2.654	783.1	1.029	9.87	-14.42 ± 0.04
14	297.7	2.667	783.0	1.029	9.88	-14.45 ± 0.13
21	299.3	2.691	781.7	1.029	9.89	-14.73 ± 0.10
13	298.9	2.685	782.2	1.029	9.89	-14.49 ± 0.08
14	299.7	2.694	782.7	1.029	9.89	-14.95 ± 0.05
5	299.5	2.693	781.8	1.029	9.88	-14.54 ± 0.09
21	300.5	2.704	782.5	1.029	9.92	-14.45 ± 0.13
9	300.3	2.703	782.0	1.029	9.92	-14.73 ± 0.11
23	301.8	2.723	781.6	1.029	9.92	-14.74 ± 0.07
9	302.1	2.726	781.9	1.029	9.92	-14.47 ± 0.08
34	303.6	2.745	782.0	1.029	9.93	-14.91 ± 0.10
18	303.8	2.746	782.7	1.029	9.93	-14.67 ± 0.15
					mean	-14.60 ± 0.05

Table 5.3 Carbon monoxide results

Number of null points	T (K)	P (MPa)	V_m ($cm^3\ mol^{-1}$)	ε_r	E'_{xx} ($10^8\ V\ m^{-2}$)	$q^{(0)} \pm \sigma_m$ ($10^{-40}\ C\ m^2$)
13	293.0	4.052	594.2	1.027	9.39	-9.26 ± 0.08
7	291.9	4.044	593.0	1.027	9.40	-9.50 ± 0.13
18	293.0	4.064	592.5	1.027	9.40	-9.53 ± 0.15
17	293.1	4.037	596.7	1.026	9.38	-9.50 ± 0.20
9	291.3	4.026	594.3	1.027	9.37	-9.51 ± 0.12
17	293.4	4.059	594.1	1.027	9.38	-9.50 ± 0.09
6	292.2	4.034	595.1	1.026	9.38	-9.60 ± 0.06
17	293.9	3.829	631.3	1.025	9.38	-9.51 ± 0.09
8	293.0	3.811	632.2	1.025	9.38	-9.52 ± 0.09
17	292.5	3.804	632.1	1.025	9.37	-9.54 ± 0.20
6	290.6	3.557	671.4	1.023	9.37	-9.37 ± 0.21
16	291.1	3.565	671.2	1.023	9.37	-9.44 ± 0.15
16	290.3	3.548	672.5	1.023	9.36	-9.28 ± 0.21
9	289.7	3.540	672.5	1.023	9.37	-9.47 ± 0.21
14	299.5	3.951	624.6	1.025	8.93	-9.21 ± 0.09
25	299.9	3.949	625.8	1.025	9.56	-9.27 ± 0.07
12	301.6	3.964	627.3	1.025	9.27	-9.58 ± 0.04
4	301.4	3.956	628.2	1.025	8.59	-9.59 ± 0.03
28	302.1	3.956	629.7	1.025	9.61	-9.77 ± 0.06
					mean	-9.47 ± 0.03

known then (1.15) may be used to establish the displacement of the effective quadrupole centre from the centre of mass in the molecule. Several *ab initio* calculations of the centre-of-mass quadrupole moment of carbon monoxide have been reported [58, 59, 60, 61, 62]. Maroulis and Thakkar [61] report the results of coupled cluster calculations for a variety of different basis sets; that which they appear to consider most reliable is a CCD+ST(CCD) value of $-6.74 \times 10^{-40}\ Cm^2$, which is identical to the value obtained by Amos [58] using an SCF calculation. This may be used in (1.15) together with the quadrupole moment reported here and a value of $-3.659 \times 10^{-31}\ Cm$ (C^-O^+) [63] for the dipole moment of carbon monoxide to yield $3.7 \times 10^{-10}\ m$ for the displacement of the effective quadrupole centre from the centre of mass in the direction of the carbon nucleus.

5.3.4 Nitrogen

Ultra High Purity grade nitrogen (99.998% minimum purity) was used in obtaining the results presented in Table 5.4. It was suspected at one stage that the results for nitrogen exhibited some small pressure dependence and for this reason provision was made for making measurements using pressures of up to 6 MPa. However, further measurements provided no statistically significant evidence of a trend in the results,

and so they have simply been grouped together and averaged in obtaining the result below.

The molar volume was calculated using pressure virial coefficient data taken from Michels *et al.* [64], whilst the data of Johnston *et al.* [65] were used to calculate the dielectric constant of the gas. A value of $0.783 \times 10^{-40}\,\mathrm{C^2m^2J^{-1}}$ for $\Delta\alpha$ as measured by Bogaard *et al.* [48] at 632.8 nm was used in calculating $q^{(0)}$ for nitrogen, the mean value of which was found to be $(-5.25 \pm 0.08) \times 10^{-40}\,\mathrm{Cm^2}$.

In terms of the traceless quadrupole moment the quantity measured by the experiment is $\frac{15}{2}B + \frac{1}{kT}\Theta_{\alpha\beta}\alpha_{\alpha\beta}$, in which $\frac{15}{2}B$ represents the hyperpolarizability term [12], calculated by Amos [54] to have a value of $-0.43 \times 10^{-60}\,\mathrm{C^3m^4J^{-2}}$. Although the theory used in the present work has been cast in terms of the primitive quadrupole moment, there is no reason why Amos' value for the total contribution of the hyperpolarizability term to the birefringence should not also be used to correct the present result. The effect of doing so is to decrease the value for $q^{(0)}$ measured at 300 K by $-0.23 \times 10^{-40}\,\mathrm{Cm^2}$, giving a corrected value of $(-5.02 \pm 0.07) \times 10^{-40}\,\mathrm{Cm^2}$.

Buckingham *et al.* [66] have measured the quadrupole moment of nitrogen and found it to be $(-4.90 \pm 0.3) \times 10^{-40}\,\mathrm{Cm^2}$. No correction for the hyperpolarizability terms was made in obtaining this value. The uncorrected quadrupole moment reported by Pierrus [39, 43] is $(-4.72 \pm 0.26) \times 10^{-40}\,\mathrm{Cm^2}$, this being 10% less in absolute magnitude than the uncorrected figure presented here.

Calculated values of the quadrupole moment of nitrogen [59, 60, 67, 62] and those found using techniques other than induced birefringence [68, 32, 22] are free from hyperpolarizability contributions and may, therefore, be more usefully compared with the corrected value quoted above. Making use of an MPPT(4) calculation, Maroulis and Thakker [67] obtained a value of $-4.99 \times 10^{-40}\,\mathrm{Cm^2}$ which is in good agreement with our corrected value. Woliński *et al.* [62] have recently reported a value of $-5.10 \times 10^{-40}\,\mathrm{Cm^2}$ obtained from an *SDQ*-MBPT(4) calculation, also in good agreement with the corrected value reported here. Based on measurements of the second dielectric virial coefficient, Huot and Bose [22] have recently deduced the quadrupole moment of nitrogen to be $(-4.90 \pm 0.23) \times 10^{-40}\,\mathrm{Cm^2}$.

Table 5.4 Nitrogen results

Number of null points	T (K)	P (MPa)	V_m ($cm^3 mol^{-1}$)	ε_r	E'_{xx} (10^8 Vm^{-2})	$q^{(0)} \pm \sigma_m$ (10^{-40} Cm^2)
8	295.0	3.956	614.7	1.022	6.07	-5.35 ± 0.03
7	290.4	3.978	600.8	1.022	6.07	-5.12 ± 0.08
9	291.1	3.942	607.9	1.022	6.07	-5.18 ± 0.09
7	292.2	3.911	615.2	1.022	6.07	-5.22 ± 0.05
8	293.3	3.893	620.8	1.021	6.07	-5.22 ± 0.08
8	293.4	3.859	626.6	1.021	6.07	-5.26 ± 0.13
9	292.1	3.804	637.7	1.021	6.07	-5.24 ± 0.18
7	291.1	3.752	639.1	1.021	6.07	-5.27 ± 0.19
10	292.2	3.666	657.0	1.020	6.04	-5.32 ± 0.06
8	292.4	3.595	670.5	1.020	6.05	-5.38 ± 0.04
6	294.5	3.380	719.0	1.018	6.05	-5.40 ± 0.02
10	295.1	3.199	761.7	1.017	6.05	-5.30 ± 0.08
8	290.8	3.006	798.2	1.017	6.04	-5.38 ± 0.06
10	292.1	2.881	837.2	1.016	6.04	-5.52 ± 0.06
8	292.6	2.777	870.4	1.015	6.05	-5.45 ± 0.09
10	295.0	2.654	919.0	1.014	6.05	-5.37 ± 0.05
7	295.4	2.531	965.4	1.014	6.05	-5.44 ± 0.03
11	295.9	2.385	1026.4	1.013	6.05	-5.32 ± 0.04
11	295.9	4.044	603.3	1.022	6.38	-5.27 ± 0.06
13	294.9	3.911	621.7	1.021	6.38	-5.16 ± 0.06
8	294.0	3.756	645.4	1.021	6.37	-5.33 ± 0.03
11	295.2	3.578	680.8	1.019	6.37	-5.27 ± 0.08
10	296.6	3.367	727.6	1.018	6.38	-5.22 ± 0.05
8	295.2	3.201	761.6	1.017	6.38	-5.23 ± 0.07
10	295.1	3.046	800.3	1.017	6.38	-5.20 ± 0.06
8	294.1	2.921	831.6	1.016	6.38	-5.15 ± 0.06
11	295.6	2.761	885.1	1.015	6.38	-5.16 ± 0.06
8	296.0	2.644	925.8	1.014	6.38	-5.17 ± 0.09
10	297.4	2.505	982.2	1.013	6.39	-5.20 ± 0.11
8	296.3	2.394	1024.2	1.013	6.38	-5.18 ± 0.07
11	296.0	3.695	661.1	1.020	6.35	-5.18 ± 0.05
8	296.0	3.557	686.9	1.019	6.35	-5.15 ± 0.05
10	296.5	3.380	724.3	1.018	6.35	-5.19 ± 0.04
8	295.9	3.171	770.7	1.017	6.35	-5.19 ± 0.06
10	298.3	2.964	832.1	1.016	6.35	-5.11 ± 0.08
8	298.9	2.788	887.0	1.015	6.35	-5.09 ± 0.06

continued

continued from previous page						
Number of null points	T (K)	P (MPa)	V_m (cm^3mol^{-1})	ε_r	E'_{xx} ($10^8\,Vm^{-2}$)	$q^{(0)} \pm \sigma_m$ ($10^{-40}\,Cm^2$)
10	297.0	2.600	944.8	1.014	6.35	-5.02 ± 0.06
6	304.3	4.083	616.2	1.022	9.90	-5.26 ± 0.08
18	304.8	4.099	614.8	1.022	9.90	-5.29 ± 0.09
9	303.5	4.084	614.2	1.022	9.87	-5.45 ± 0.37
19	304.3	4.094	614.5	1.022	9.89	-5.23 ± 0.16
8	302.6	4.073	613.9	1.022	9.89	-5.22 ± 0.25
19	303.2	4.081	614.1	1.022	9.89	-5.36 ± 0.14
13	299.2	5.158	477.9	1.028	8.64	-5.39 ± 0.04
7	298.1	5.178	474.1	1.028	8.69	-5.35 ± 0.05
17	298.5	5.184	474.2	1.028	8.67	-5.29 ± 0.06
8	295.5	5.143	472.7	1.028	9.90	-5.17 ± 0.09
18	297.1	5.168	473.2	1.028	9.91	-5.14 ± 0.05
9	293.8	6.134	392.8	1.034	8.69	-5.22 ± 0.07
17	296.1	6.153	395.1	1.034	8.83	-5.23 ± 0.04
10	294.3	6.107	395.3	1.034	8.83	-5.21 ± 0.03
18	295.6	6.131	395.8	1.034	9.69	-5.16 ± 0.07
9	294.5	6.110	395.5	1.034	9.90	-5.14 ± 0.07
16	295.7	6.123	396.5	1.034	8.64	-5.21 ± 0.04
					mean	-5.25 ± 0.01

5.3.5 Chlorine

The special modifications made to the apparatus for the purpose of performing measurements on chlorine have been discussed in §4.2 and §4.4.3. Chlorine gas with a minimum purity of 99.5% was used in obtaining the measurements shown in Table 5.5. A second pressure virial coefficient of $-274 \times 10^{-6} m^3 mol^{-1}$ due to Morrison [69] was used to calculate the gas density. Bridge and Buckingham [49] have reported a value for the anisotropy in the polarizability $\Delta\alpha$ at 632.8 nm of $2.89 \times 10^{-40} C^2 m^2 J^{-1}$. In the absence of any published dielectric virial coefficient data for chlorine the polarizability α, which at this wavelength is $5.13 \times 10^{-40} C^2 m^2 J^{-1}$ [46], was used to estimate the first dielectric virial coefficient as $\frac{N_0 \alpha}{3\varepsilon_0}$. A mean value of $(+9.99 \pm 0.16) \times 10^{-40}\,Cm^2$ was obtained for $q^{(0)}$ for chlorine.

Emrich and Steele [70] were the first to perform induced-birefringence measurements of the quadrupole moment of chlorine, reporting a value of $(+16.6 \pm 1.7) \times 10^{-40}\,Cm^2$. The result obtained by Buckingham *et al.* [66], $(+10.79 \pm 0.54) \times 10^{-40}\,Cm^2$, is in better agreement with that reported here. Pierrus [39] has reported a quadrupole moment of $(10.57 \pm 0.95) \times 10^{-40}\,Cm^2$, which runs contrary to the expectation that his measurements should be some 9% lower than those reported here. No explanation could be found for this, although our value is based on considerably more readings than was the case with Pierrus. The modifications to the cell made it possible to use field gradients some 50% higher than those used by Pierrus without any sign of electrical breakdown

Table 5.5 Chlorine results

Number of null points	T (K)	P (MPa)	V_m (cm^3mol^{-1})	ε_r	E'_{xx} ($10^8\ Vm^{-2}$)	$q^{(0)} \pm \sigma_m$ ($10^{-40}\ Cm^2$)
5	299.0	0.605	3815	1.009	8.87	$+10.16 \pm 0.22$
22	298.6	0.606	3804	1.009	9.62	$+10.43 \pm 0.26$
19	300.3	0.609	3803	1.009	9.56	$+9.92 \pm 0.42$
11	299.5	0.605	3816	1.009	9.64	$+10.27 \pm 0.29$
22	299.2	0.605	3818	1.009	9.64	$+9.94 \pm 0.09$
16	300.2	0.606	3825	1.009	9.65	$+9.81 \pm 0.14$
25	300.7	0.606	3833	1.009	9.60	$+9.81 \pm 0.16$
17	301.0	0.606	3836	1.009	9.60	$+9.64 \pm 0.17$
18	298.9	0.612	3762	1.009	9.58	$+10.17 \pm 0.16$
24	300.9	0.606	3835	1.009	8.88	$+9.76 \pm 0.28$
16	299.8	0.613	3767	1.009	9.59	$+10.19 \pm 0.20$
26	300.6	0.614	3772	1.009	9.59	$+9.79 \pm 0.19$
19	300.1	0.612	3783	1.009	9.59	$+9.98 \pm 0.24$
22	300.2	0.605	3832	1.009	9.59	$+10.00 \pm 0.35$
					mean	$+9.99 \pm 0.06$

occurring within the cell.

Amos [54] has reported the results of *ab initio* calculations of the quadrupole moment of chlorine and of the contribution of the hyperpolarizability term to the induced birefringence, showing the latter to be less than 1% of the entire effect. He obtained a quadrupole moment of $+11.9 \times 10^{-40}\ Cm^2$.

5.3.6 Ethene

Ethene having a minimum purity of 99% was used in obtaining the measurements presented in Table 5.6. Pressure virial coefficient data reported by Douslin and Harrison [71] were used to determine the gas density. The first and second dielectric virial coefficient data of David *et al.* [72] was used to calculate the dielectric constant of the gas.

The measured quantity Γ tabulated in the right-hand column of Table 5.6 is the left-hand side of (5.6), that is,

$$\Gamma = \tfrac{1}{2}[q_{xx}^{(0)}(2\alpha_{xx} - \alpha_{yy} - \alpha_{zz}) + q_{yy}^{(0)}(2\alpha_{yy} - \alpha_{zz} - \alpha_{xx}) + q_{zz}^{(0)}(2\alpha_{zz} - \alpha_{xx} - \alpha_{yy})]. \tag{5.12}$$

The mean value of Γ obtained here is $(+15.59 \pm 0.14) \times 10^{-80}\ C^3m^2s^2kg^{-1}$. Amos [54] has performed calculations which suggest that this value is likely to be underestimated by about 3.5% due to hyperpolarizability effects which contribute subtractively to the induced birefringence.

Because ethene lacks axial symmetry (5.12) can be simplified further only by making certain approximations. We begin by choosing axes such that the molecule lies in the

xz-plane with the carbon double bond coinciding with the z-axis. In terms of the traceless quadrupole moment $\theta_{\alpha\beta}$,

$$\begin{aligned}\Gamma &= \theta_{xx}\alpha_{xx} + \theta_{yy}\alpha_{yy} + \theta_{zz}\alpha_{zz} \\ &= (\alpha_{zz} - \alpha_{yy})\left(\theta_{zz} + \theta_{xx}\frac{\alpha_{xx} - \alpha_{yy}}{\alpha_{zz} - \alpha_{yy}}\right),\end{aligned} \tag{5.13}$$

in which we have made use of the traceless nature of $\theta_{\alpha\beta}$. An estimate of $\frac{\alpha_{xx}-\alpha_{yy}}{\alpha_{zz}-\alpha_{yy}}$ of 0.019 has been communicated privately by Buckingham to Stogryn and Stogryn [73]. Maroulis [74] has calculated very similar values for θ_{xx} and θ_{zz} which suggests that we may safely make the approximation in (5.13) that $\Gamma \approx (\alpha_{zz} - \alpha_{yy})\theta_{zz}$. This is equivalent to treating ethene as though it were a linear molecule with $\alpha_{xx} = \alpha_{yy}$. In order to solve for θ_{zz} (or $q^{(0)}$, in the case of the primitive quadrupole moment), we require a value for $\alpha_{zz} - \alpha_{xx}$. Bogaard *et al.* [48] have deduced from gas-phase refractivity data given in [75] a value for the polarizability of ethene at 632.8 nm of $4.70 \times 10^{-40}\,\mathrm{C^2m^2J^{-1}}$, and have obtained from light-scattering measurements a value of $2.014 \times 10^{-40}\,\mathrm{C^2m^2J^{-1}}$ for the quantity $3\alpha|\kappa|$, in which

$$\kappa^2 = \frac{3\alpha_{\beta\gamma}\alpha_{\beta\gamma} - \alpha_{\beta\beta}\alpha_{\gamma\gamma}}{2\alpha_{\beta\beta}\alpha_{\gamma\gamma}}.$$

In the case of a linear molecule this simplifies to

$$\kappa = \frac{\alpha_{zz} - \alpha_{xx}}{3\alpha}.$$

Buckingham *et al.* [57] have used a value of $3\alpha|\kappa|$ obtained from earlier light-scattering measurements reported by Bridge and Buckingham [49] to obtain an estimate for θ_{zz} of $(+6.6 \pm 0.5) \times 10^{-40}\,\mathrm{Cm^2}$. If we use the value of $3\alpha|\kappa|$ quoted above together with our value for Γ then our estimate of θ_{zz} is $(+7.74 \pm 0.12) \times 10^{-40}\,\mathrm{Cm^2}$. This agrees rather poorly with the estimate of Buckingham *et al.* and even less well with Maroulis' [74] calculated value of $(+5.56 \pm 0.22) \times 10^{-40}\,\mathrm{Cm^2}$. It is worth noting that the dielectric constant of ethene rises fairly rapidly with increasing pressure—more so than is the case with the other gases in the present study. At room temperature and a pressure of 40 atmospheres it is about 1.08, at 80 atmospheres it has climbed to 1.38 [72]. It appears that the effect of the dielectric constant has not been considered by Buckingham *et al.* [57] in arriving at their value, which could lead to their value being somewhat too low since they report using pressures up to 80 atmospheres for measurements performed on certain gases, of which ethene may have been one.

5.3.7 Boron trifluoride

Boron trifluoride having a minimum purity of 99.5% was used in obtaining the results shown in Table 5.7. Measurements of the anisotropy in the polarizability of boron

Table 5.6 Ethene results

Number of null points	T (K)	P (MPa)	V_m (cm^3mol^{-1})	ε_r	E'_{xx} ($10^8\,Vm^{-2}$)	$\Gamma \pm \sigma_m$ ($10^{-80}\,C^3m^2s^2kg^{-1}$)
8	295.6	4.025	433.7	1.077	7.42	$+15.81 \pm 0.21$
10	297.7	4.080	433.6	1.077	8.70	$+16.10 \pm 0.66$
8	296.7	4.054	433.6	1.077	8.70	$+15.58 \pm 0.10$
5	298.4	4.095	434.1	1.077	8.70	$+15.74 \pm 0.46$
6	296.7	4.053	433.8	1.077	9.90	$+15.78 \pm 0.24$
3	294.8	4.004	433.8	1.077	8.68	$+15.09 \pm 0.30$
6	297.4	4.071	433.7	1.077	8.69	$+15.05 \pm 0.17$
8	295.8	4.026	434.7	1.077	8.74	$+16.07 \pm 0.15$
18	297.5	4.073	434.0	1.077	8.64	$+15.84 \pm 0.16$
7	296.1	4.034	434.3	1.077	8.64	$+15.34 \pm 0.16$
5	296.9	4.054	434.4	1.077	8.64	$+16.12 \pm 0.42$
13	296.1	3.229	596.4	1.055	8.84	$+15.78 \pm 0.38$
12	294.9	3.206	596.9	1.055	8.84	$+15.16 \pm 0.27$
15	296.5	3.234	596.9	1.055	8.84	$+15.57 \pm 0.43$
10	295.0	3.211	596.2	1.055	8.84	$+15.04 \pm 0.14$
15	295.1	2.285	915.3	1.035	8.80	$+15.37 \pm 0.39$
9	294.3	2.284	911.9	1.036	8.80	$+15.50 \pm 0.34$
16	295.4	2.291	913.9	1.036	8.80	$+15.61 \pm 0.41$
					mean	$+15.59 \pm 0.08$

trifluoride appear not to have been performed, which has made it necessary to quote a value for the combined quantity $q^{(0)}\Delta\alpha$. The second pressure virial coefficient data of Schramm and Gehrmann [76] were used to calculate the molar volume of the gas. No dielectric virial coefficient data for boron trifluoride could be found, so, as was the case with chlorine, the dielectric constant was estimated as $\frac{N_0\alpha}{3\varepsilon_0}$. Tabulations of polarizabilities [46] list the polarizability of boron trifluoride as $3.68 \times 10^{-40}\,C^2m^2J^{-1}$.

As far as is known, these are the first measurements of this nature to be performed on boron trifluoride. Once a value for $\Delta\alpha$ becomes available, it may be used to deduce the value for $q^{(0)}$ from the value $(-7.93 \pm 0.08) \times 10^{-80}\,C^3m^2s^2kg^{-1}$ obtained here as the mean value of $q^{(0)}\Delta\alpha$ for boron trifluoride.

5.4 Discussion

The results reported in §5.3.2–§5.3.7 are summarised in Table 5.8.

Before making any new birefringence measurements, the initial aim of this study was to reproduce the results for carbon dioxide which had previously been obtained with this apparatus [39], or to explain the large discrepancy between these results and those obtained by other workers [57, 37]. Re-examining the experiment using the Jones calculus suggested a better way to perform the experiment in which it is the analyser,

Table 5.7 Boron trifluoride results

Number of null points	T (K)	P (MPa)	V_m (cm^3mol^{-1})	ε_r	E'_{xx} ($10^8\ Vm^{-2}$)	$q^{(0)}\Delta\alpha \pm \sigma_m$ ($10^{-80}\ C^3m^2s^2kg^{-1}$)
10	294.2	3.100	655.3	1.039	9.44	-7.88 ± 0.17
8	294.0	3.093	656.3	1.039	9.44	-8.27 ± 0.03
13	294.7	3.102	656.8	1.039	9.44	-8.20 ± 0.02
14	293.6	3.093	654.4	1.039	9.44	-8.16 ± 0.03
11	293.3	3.090	654.0	1.039	9.44	-8.08 ± 0.06
18	294.4	3.104	655.0	1.039	9.44	-7.84 ± 0.03
18	294.4	3.622	535.9	1.047	9.44	-7.92 ± 0.23
4	294.1	3.612	536.7	1.047	9.61	-8.06 ± 0.05
18	294.3	3.614	537.1	1.047	9.60	-8.03 ± 0.03
5	292.8	3.584	536.9	1.047	9.60	-7.92 ± 0.20
16	293.5	3.622	532.2	1.048	9.60	-7.92 ± 0.04
19	291.4	3.856	478.6	1.053	8.80	-7.79 ± 0.02
10	290.4	3.834	478.2	1.053	8.81	-7.83 ± 0.03
14	291.1	3.844	479.4	1.053	8.80	-7.46 ± 0.02
8	290.3	3.842	476.3	1.054	8.81	-7.62 ± 0.07
					mean	-7.93 ± 0.06

Table 5.8 Summary of results

Gas	Quantity determined	$\bar{x} \pm \sigma_m$	units
Carbon dioxide	$q^{(0)}$	-14.53 ± 0.22	$10^{-40}\ Cm^2$
Carbon monoxide	$q^{(0)}$	-9.47 ± 0.15	$10^{-40}\ Cm^2$
Nitrogen	$q^{(0)}$	-5.25 ± 0.08	$10^{-40}\ Cm^2$
Chlorine	$q^{(0)}$	$+9.99 \pm 0.16$	$10^{-40}\ Cm^2$
Ethene	Γ (see (5.12))	$+15.59 \pm 0.14$	$10^{-80}\ C^3m^2s^2kg^{-1}$
Boron Trifluoride	$q^{(0)}\Delta\alpha$	-7.93 ± 0.08	$10^{-80}\ C^3m^2s^2kg^{-1}$

rather than the $\frac{\lambda}{4}$-plate, as was previously the case, which is deliberately offset in order to amplify the signal. The quadrupole moment of carbon dioxide obtained using the new method is in much better agreement with the measured values of other workers, and is in excellent agreement with the figure predicted by Maroulis and Thakkar [55] using what is probably the most elaborate calculation of this quantity to date.

It is of some importance that the measurements of the quadrupole moment of carbon dioxide which were made using two different wire thicknesses and separations have been shown to be essentially the same. This is strong evidence that the method used to calculate the electric field gradient on the axis of the cell is sound.

After demonstrating that Pierrus' measurement of the quadrupole moment of carbon dioxide was likely to be too low by about 8%, it was essential to perform new measurements on the more important gases which had been included in the previous study. In the cases of nitrogen and carbon monoxide the new measurements are again greater than the previous ones by about the same margin. The value for nitrogen is in fair agreement with that reported by Buckingham *et al.* [66], and, after correcting for the contribution of hyperpolarizability terms to the induced birefringence, is in excellent concurrence with that predicted by Maroulis and Thakkar [67]. The only other birefringence measurement of the quadrupole moment of carbon monoxide was reported in 1968 by Buckingham *et al.* [57] and is in poor agreement with that reported here. Calculations of this quantity and those values measured using other techniques generally refer the quadrupole moment to the centre of mass of the molecule and are, therefore, of little help in deciding which of the two birefringence values is more likely to be correct. Another independent birefringence measurement of this quantity might help to resolve this matter.

The poor agreement between Maroulis' [74] calculated value of $q^{(0)}$ for ethene and that obtained from the birefringence measurement by treating ethene as a linear molecule casts doubt on the validity of the latter approximation. It is probably best, therefore, to place confidence only in the measured quantity Γ in (5.12). A theoretical check of this quantity will be possible once *ab initio* calculations of α_{xx}, α_{yy}, and α_{zz} have been performed.

The most recent *ab initio* calculation of the quadrupole moment of chlorine appears to be that of Amos [54] and is some 20% higher than that measured in this study. That reported by Buckingham *et al.* [66] is 8% higher than our value but is in better agreement with that reported by Pierrus [39]. The fact that the latter value is higher than that reported here runs contrary to the trend predicted by the analysis in Chapter 3 and confirmed experimentally in the cases of carbon dioxide, carbon monoxide, and nitrogen. Our result was obtained with very good repeatability and the analysis of the results was performed using the same data to find the molar volume, dielectric constant, and polarizability anisotropy as were used by Pierrus [39].

The measurements performed on boron trifluoride are believed to be new, and await only a measurement of $\Delta\alpha$ to enable the quadrupole moment to be extracted. No *ab initio* calculations of this quadrupole moment appear to have been made.

The birefringence experiment remains a difficult one to perform, accounting for the

apparently few sets of apparatus in existence. Great care has been taken in the present study to eliminate systematic errors so that the results may be presented with 67% confidence intervals of less than 2% of the mean. Nonetheless, discrepancies between these results and those measured with other apparatus using the same technique are as great as 8% in some cases. These differences highlight the need for measurements to be repeated by independent workers, preferably using independent apparatus.

Appendix A

CALCULATION OF THE ELECTRIC FIELD GRADIENT

The method used here to calculate the on-axis electric field gradient in the quadrupole cell was communicated privately by Graham to Pierrus [39], and was described in full by the latter. It is repeated here only for completeness.

A section through the quadrupole cell is shown in Figure A.1 in which the size and position of the wires have been exaggerated for clarity. If the length of the wires is large in comparison with the diameter of the cell, then the problem is one of determining the electric field gradient due to two infinitely-long and equally-charged conducting cylinders symmetrically disposed about the axis of a hollow cylinder of radius R which is earthed. The problem is more easily solved by replacing the charged wires and earthed cylinder with infinitely-long line charges in such a way as to ensure that the boundary conditions of the two problems are very nearly identical. In other words, the line charges must be positioned so as to produce equipotential surfaces which coincide as closely as possible with the surfaces of the wires, and the line charge density must be chosen to give the correct potential difference between this equipotential surface and one coinciding with the inner surface of the cell.

The symmetry of the infinitely-long line charges reduces the problem to one in only two dimensions. We locate a set of Cartesian axes as shown in Figure A.1 so that the centres of the wires are located on the y-axis at $(0, d)$ and $(0, -d)$. From symmetry it is clear that the line charges should also be located on the y-axis, in this case at $(0, d')$ and $(0, -d')$ as shown in Figure A.2. We shall consider later how these positions are to be determined.

The vacuum electric field due to a single infinitely-long line charge of uniform charge density λ is radial, given at a distance r by

$$E(r) = \frac{1}{4\pi\varepsilon_0}\frac{2\lambda}{r}. \tag{A.1}$$

The potential at a point a distance r from the line charge relative to one at a distance

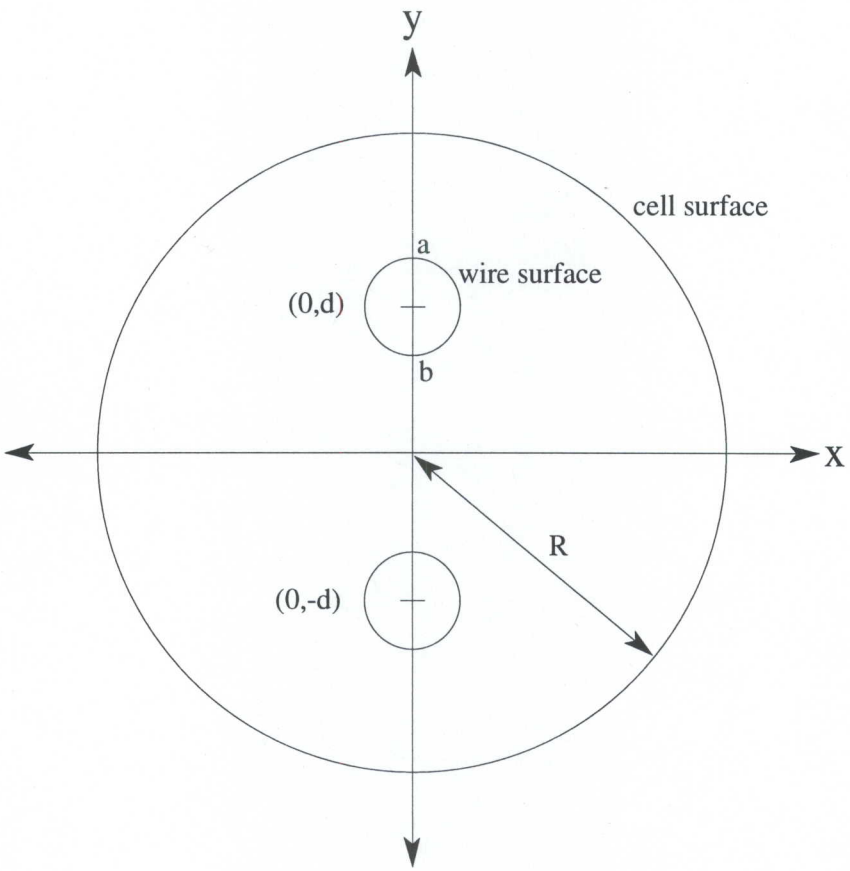

Figure A.1 Section through the quadrupole cell (not to scale) showing the orientation of the axes used in the electric field-gradient calculation

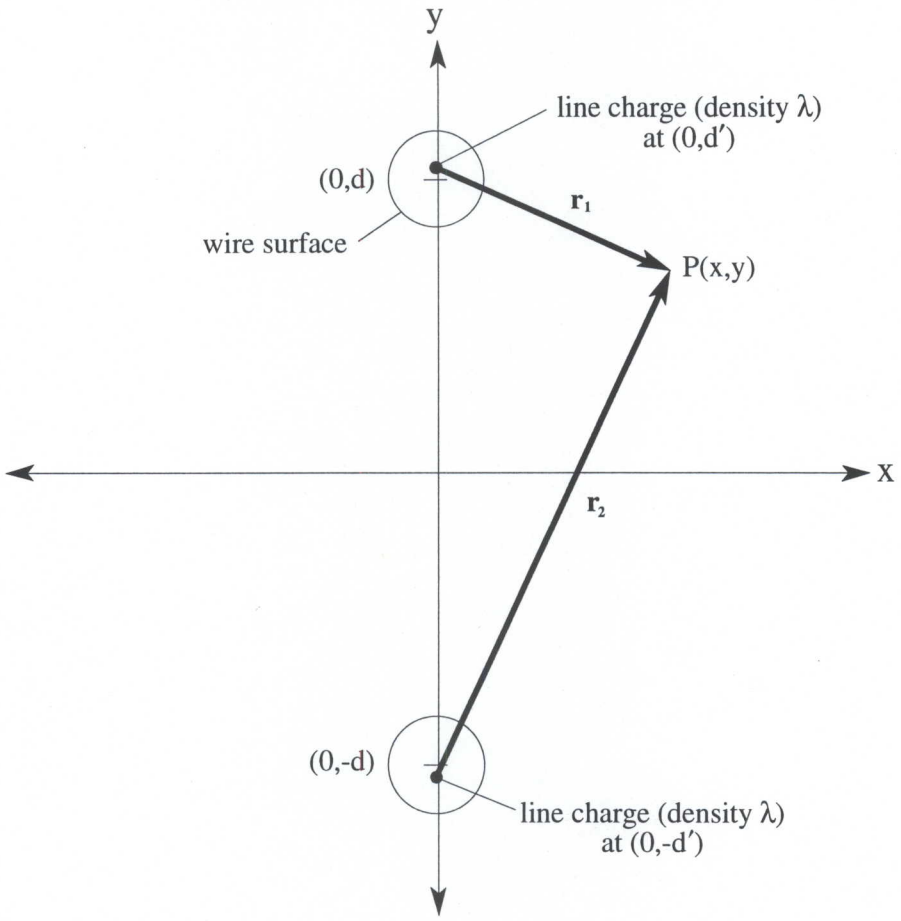

Figure A.2 Positions of the line charges with which the high-voltage wires are replaced in calculating the electric field gradient in the quadrupole cell

R is then given by

$$\phi(r) = -\int_R^r E(r)\,dr = \frac{2\lambda}{4\pi\varepsilon_0}\ln\frac{R}{r}. \tag{A.2}$$

Now consider the case shown in Figure A.2 in which we seek the potential at the point $P(x, y)$ relative to that at a distant point (not shown) which is displaced by $\mathbf{R}_1$ from one line charge and by $\mathbf{R}_2$ from the other. The point P is displaced from these line charges by the much smaller distances r_1 and r_2. By superposition the potential at P

relative to that at the more distant point is given by

$$\begin{aligned}\phi(x,y) &= \frac{2\lambda}{4\pi\varepsilon_0}\left\{\ln\frac{R_1}{r_1}+\ln\frac{R_2}{r_2}\right\}\\ &= \frac{2\lambda}{4\pi\varepsilon_0}\ln\frac{R_1R_2}{r_1r_2}\\ &\approx \frac{2\lambda}{4\pi\varepsilon_0}\ln\frac{R^2}{r_1r_2}\\ &= \frac{\lambda}{4\pi\varepsilon_0}\ln\left\{\frac{R^4}{[(y-d')^2+x^2][(y+d')^2+x^2]}\right\},\end{aligned} \tag{A.3}$$

in which R is the distance from the point midway between the two line charges to the distant point. By evaluating the function $\frac{R^2-R_1R_2}{R^2}$ around the circumference of the cell the effect of this approximation may be shown to be very small. For the 'worst case' in the present research, in which the wire separation is 4 mm, this function varies between $+0.0058$ and -0.0058. The approximation is therefore an undercorrection for some regions and an overcorrection for others, suggesting that the overall error will be considerably smaller than these 0.6% extremes.

Using the potential in (A.3) to find the the electric field $\mathbf{E}(x,y) = -\nabla\phi(x,y)$ gives

$$\begin{aligned}\mathbf{E}(x,y) = \frac{2\lambda}{4\pi\varepsilon_0}\Bigg[&\left\{\frac{x}{(y-d')^2+x^2}+\frac{x}{(y+d')^2+x^2}\right\}\hat{\mathbf{x}}\\ &+\left\{\frac{y-d'}{(y-d')^2+x^2}+\frac{y+d'}{(y+d')^2+x^2}\right\}\hat{\mathbf{y}}\Bigg],\end{aligned} \tag{A.4}$$

from which the electric field gradient $E'_{\alpha\beta} = \nabla_\alpha E_\beta$ may be shown to have non-zero components

$$E'_{xx} = \frac{2\lambda}{4\pi\varepsilon_0}\left\{\frac{(y-d')^2-x^2}{[(y-d')^2+x^2]^2}+\frac{(y+d')^2-x^2}{[(y+d')^2+x^2]^2}\right\}, \tag{A.5}$$

$$E'_{xy} = \frac{-4\lambda}{4\pi\varepsilon_0}\left\{\frac{x(y-d')}{[(y-d')^2+x^2]^2}+\frac{x(y+d')}{[(y+d')^2+x^2]^2}\right\}, \tag{A.6}$$

$$E'_{yx} = E'_{xy}, \quad \text{and} \quad E'_{yy} = -E'_{xx}.$$

Buckingham and Disch [41] have shown that the average of these quantities over the circular area which is sampled by the laser beam is equal to their value on the axis of the cell. Thus E'_{xy} and E'_{yx} vanish on averaging, whilst

$$\bar{E}'_{xx} = E'_{xx}(0,0) = \frac{1}{4\pi\varepsilon_0}\frac{4\lambda}{(d')^2}. \tag{A.7}$$

In practice the wires are located in a dense gas which acts as a dielectric having a relative permittivity ε_r greater than 1. This is accounted for by replacing the permittivity

of free space ε_0 in (A.7) with the permittivity of the gas $\varepsilon_r\varepsilon_0$ to yield

$$\bar{E'}_{xx} = \frac{1}{4\pi\varepsilon_0}\frac{4\lambda}{\varepsilon_r(d')^2}. \tag{A.8}$$

It is this quantity which is referred to in the main body of this text simply as 'the electric field gradient', and is given the symbol E'.

The remaining problem is to position the line charges and to assign them a charge density. The computer program which analyses the data determines the most suitable position for the line charges by moving them outwards from the centres of the wires in very small increments until the potential evaluated using (A.3) at point a in Figure A.1 is within a given tolerance of that evaluated at point b. We may then be assured that the equipotential line passing through these two points coincides very closely with the entire wire surface because the separation of the two wires for any given wire thickness was chosen so as to ensure that that such an equipotential is circular.

Finally, (A.3) describes an electrostatic potential which is necessarily zero at a distance R, so the line charge density λ may be found by setting the potential at either point a or point b in Figure A.1 to the voltage on the wires, and then solving for λ. In practice the electric field gradient per volt was calculated for a given cell geometry and then scaled by the measured high voltage to yield the absolute field gradient.

Appendix B

PERTURBATION THEORY CALCULATIONS

B.1 Time-Dependent Perturbation Theory Calculation

Time-dependent perturbation theory is concerned with the solution of the time-dependent Schrödinger equation

$$H(t)|n(t)\rangle = i\hbar\frac{\partial}{\partial t}|n(t)\rangle$$

for the case in which the Hamiltonian may be expressed as $H(t) = H^{(0)} + H'(t)$, where $H^{(0)}$ is a time-independent contribution whose eigenvalue problem has been solved, and $H'(t)$ is a small time-dependent perturbation. We assume that $H'(t)$ may be expanded in powers of the perturbation,

$$H'(t) = H^{(1)}(t) + H^{(2)}(t) + \cdots,$$

and that a similar expansion exists for the eigenket $|n(t)\rangle$, so that

$$|n(t)\rangle = |n^{(0)}(t)\rangle + |n^{(1)}(t)\rangle + |n^{(2)}(t)\rangle + \cdots.$$

The example which we will consider here is to find the effect of the laser beam on the electric dipole moment of a molecule in the quadrupole cell. In this case, $H^{(0)}$ is the Hamiltonian for an isolated molecule and $H^{(1)}(t)$ is that for the linear components of a weak electromagnetic field. We begin by expressing the expectation value of the dipole moment $\langle\mu_\alpha\rangle$ in terms of the expanded eigenkets,

$$\begin{aligned}
\langle\mu_\alpha\rangle &= \langle n(t)|\mu_\alpha|n(t)\rangle \\
&= \langle n^{(0)}(t) + n^{(1)}(t) + \cdots|\mu_\alpha|n^{(0)}(t) + n^{(1)}(t) + \cdots\rangle \\
&= \langle n^{(0)}(t)|\mu_\alpha|n^{(0)}(t)\rangle + \langle n^{(0)}(t)|\mu_\alpha|n^{(1)}(t)\rangle + \langle n^{(1)}(t)|\mu_\alpha|n^{(0)}(t)\rangle + \cdots \\
&= \langle\mu_\alpha^{(0)}\rangle + 2\,\mathrm{Re}\{\langle n^{(0)}(t)|\mu_\alpha|n^{(1)}(t)\rangle\} + \cdots.
\end{aligned} \tag{B.1}$$

Since the eigenkets $|j^{(0)}\rangle$ of $H^{(0)}$ form a basis set it is possible to express $|n^{(1)}(t)\rangle$ and $\langle n^{(1)}(t)|$ as

$$|n^{(1)}(t)\rangle = c|n^{(0)}(t)\rangle + \sum_{j\neq n} a_j(t)|j^{(0)}(t)\rangle, \quad \text{and}$$
$$\langle n^{(1)}(t)| = c^*\langle n^{(0)}(t)| + \sum_{j\neq n} a_j^*(t)\langle j^{(0)}(t)|. \tag{B.2}$$

From the normalization condition $\langle n(t)|n(t)\rangle = 1$, it follows that $\langle n^{(0)}(t)|n^{(0)}(t)\rangle = 1$ and $\langle n^{(0)}(t)|n^{(1)}(t)\rangle + \langle n^{(1)}(t)|n^{(0)}(t)\rangle = 0$. Using (B.2) in the latter equation, together with the orthogonality result $\langle n^{(0)}(t)|j^{(0)}(t)\rangle = 0$ for $j \neq n$, one obtains the result $c + c^* = 0$. Hence c in (B.2) is imaginary.

For a perturbation applied at time $t = 0$, the mixing coefficients $a_j(t)$ in (B.2) are given by [77]

$$a_j(t) = -\frac{i}{\hbar}\int_0^t e^{-i\omega_{nj}t} H_{jn}^{(1)}(t)\, dt, \quad j \neq n, \tag{B.3}$$

where

$$H_{jn}^{(1)} = \langle j^{(0)}(0)|H^{(1)}|n^{(0)}(0)\rangle,$$

and

$$\omega_{nj} = \hbar^{-1}(E_n^{(0)} - E_j^{(0)}).$$

In this, $E_j^{(0)}$ is the unperturbed energy of state j. It may be shown that [77]

$$|n^{(0)}(t)\rangle = e^{-iE_n^{(0)}t/\hbar}|n^{(0)}(0)\rangle, \tag{B.4}$$

which, when used with (B.2) in (B.1), gives

$$\begin{aligned}\langle \mu_\alpha \rangle &= \langle \mu_\alpha^{(0)} \rangle + 2\,\mathrm{Re}\left\{\sum_{j\neq n} a_j(t) e^{i(E_n^{(0)} - E_j^{(0)})t/\hbar}\langle n^{(0)}(0)|\mu_\alpha|j^{(0)}(0)\rangle\right\} + \cdots \\ &= \langle \mu_\alpha^{(0)} \rangle + 2\,\mathrm{Re}\left\{\sum_{j\neq n} a_j(t) e^{i\omega_{nj}t}\mu_{\alpha_{nj}}\right\} + \cdots .\end{aligned} \tag{B.5}$$

Because μ_α is Hermitian, so that $\langle n^{(0)}(t)|\mu_\alpha|n^{(0)}(t)\rangle$ is real, the effect of taking the real part in (B.1) is to eliminate the imaginary c in (B.2). It is for this reason that $j = n$ is not included in the summation in (B.5).

To the order of electric quadrupole and magnetic dipole the form of the perturbation Hamiltonian in (B.3), when expressed in the Barron-Gray gauge [78], is

$$H^{(1)} = q[\phi(\mathbf{r},t)]_0 - \mu_\alpha[\mathscr{E}_\alpha(\mathbf{r},t)]_0 - \tfrac{1}{2}q_{\alpha\beta}[\nabla_\beta \mathscr{E}_\alpha(\mathbf{r},t)]_0 - m_\alpha[\mathscr{B}_\alpha(\mathbf{r},t)]_0 - \cdots, \tag{B.6}$$

in which $[\ ]_0$ indicates a value taken at the origin.

We take as an explicit form for the oscillating electric field

$$\mathscr{E}_\alpha = \mathscr{E}_\alpha^{(0)} \cos\omega(t - \frac{r_\beta \sigma_\beta}{c}), \tag{B.7}$$

which, when used in (B.6) together with the Maxwell equation $\nabla \times \mathscr{E} = -\dot{\mathscr{B}}$, yields from (B.3) the explicit form of the mixing coefficients

$$a_j(t) = \frac{e^{-i\omega_{nj}t}}{\hbar(\omega^2 - \omega_{nj}^2)}[\mu_{\alpha_{jn}}(\omega_{nj}\mathscr{E}_\alpha - i\dot{\mathscr{E}}_\alpha) + \tfrac{1}{2}q_{\alpha\beta_{jn}}(\omega_{nj}\nabla_\beta\mathscr{E}_\alpha - i\nabla_\beta\dot{\mathscr{E}}_\alpha) + m_{\alpha_{jn}}(\omega_{nj}\mathscr{B}_\alpha - i\dot{\mathscr{B}}_\alpha) + \cdots]. \tag{B.8}$$

When (B.8) is substituted in (B.5) the resultant expression for $\langle\mu_\alpha\rangle$ may be compared with the total dipole moment implicit in (2.16), namely

$$\mu_\alpha = \mu_\alpha^{(0)} + \alpha_{\alpha\beta}\mathscr{E}_\beta + \tfrac{1}{2}a_{\alpha\beta\gamma}\nabla_\gamma\mathscr{E}_\beta + \omega^{-1}G'_{\alpha\beta}\dot{\mathscr{B}}_\beta + \cdots, \tag{B.9}$$

to obtain the expressions

$$\alpha_{\alpha\beta} = 2\hbar^{-1}\sum_{j\neq n}\frac{\omega_{jn}}{\omega_{jn}^2 - \omega^2}\,\mathrm{Re}\{\langle n^{(0)}(0)|\mu_\alpha|j^{(0)}(0)\rangle\langle j^{(0)}(0)|\mu_\beta|n^{(0)}(0)\rangle\} = \alpha_{\beta\alpha}, \tag{B.10}$$

$$a_{\alpha\beta\gamma} = 2\hbar^{-1}\sum_{j\neq n}\frac{\omega_{jn}}{\omega_{jn}^2 - \omega^2}\,\mathrm{Re}\{\langle n^{(0)}(0)|\mu_\alpha|j^{(0)}(0)\rangle\langle j^{(0)}(0)|q_{\gamma\beta}|n^{(0)}(0)\rangle\} = a_{\alpha\gamma\beta}, \tag{B.11}$$

$$G'_{\alpha\beta} = -2\hbar^{-1}\sum_{j\neq n}Z_{jn}\omega\,\mathrm{Im}\{\langle n^{(0)}(0)|\mu_\alpha|j^{(0)}(0)\rangle\langle j^{(0)}(0)|m_\beta|n^{(0)}(0)\rangle\}. \tag{B.12}$$

These are the expressions given in (2.22), (2.23), and (2.25). The remaining relationships contained in (2.24) and (2.26) may be derived in a similar manner by finding the expectation values of the electric quadrupole and magnetic dipole moment operators in perturbed states.

B.2 Time-Independent Perturbation Theory Calculation

The distorting effect that the applied electric field gradient has on a molecule in the quadrupole cell is essentially electrostatic in nature and may, therefore, be investigated using time-independent perturbation theory. As an example of this type of calculation we shall consider the perturbations due to the applied field $\mathbf{E}$ and field gradient $\boldsymbol{\nabla}\mathbf{E}$ on the polarizability $\alpha_{\alpha\beta}$ of the molecule. A quantum-mechanical expression for $\alpha_{\alpha\beta}$ has been derived in §B.1 and is given in (B.10). We begin by considering the effect of the perturbation on the transition frequency ω_{jn} through which the transition energy enters this expression.

Shankar [77] shows that the eigenvalue problem may be solved approximately if the time-independent perturbation Hamiltonian H' is small in comparison with the

unperturbed Hamiltonian $H^{(0)}$. The procedure is to assume that the eigenvalues and eigenkets of the Hamiltonian $H = H^{(0)} + H'$ may be expanded in a convergent perturbation series and then to extract terms of similar order from the eigenvalue equation so expressed. We need consider here only those terms of zeroth and first order, and will quote [77] any general results that are needed.

The perturbation Hamiltonian for a system of charges in a non-uniform electrostatic field is

$$H' = q\phi_0 - \mu_\alpha E_\alpha - \tfrac{1}{2} q_{\alpha\beta} \nabla_\beta E_\alpha - \cdots . \tag{B.13}$$

Since all the field terms are linear, the second- and higher-order terms in the general expansion

$$H' = H^{(1)} + H^{(2)} + H^{(3)} + \cdots$$

are zero, and $H' = H^{(1)}$. It then follows that

$$\begin{aligned}
\hbar\omega_{jn} &= E_j - E_n \\
&= E_j^{(0)} + E_j^{(1)} + \cdots - (E_n^{(0)} + E_n^{(1)} + \cdots) \\
&= E_j^{(0)} - E_n^{(0)} + \langle j^{(0)}|H^{(1)}|j^{(0)}\rangle - \langle n^{(0)}|H^{(1)}|n^{(0)}\rangle + \cdots \\
&= \hbar\omega_{jn}^{(0)} + \langle j^{(0)}|q\phi_0 - \mu_\alpha E_\alpha - \tfrac{1}{2} q_{\alpha\beta}\nabla_\beta E_\alpha + \cdots |j^{(0)}\rangle \\
&\qquad - \langle n^{(0)}|q\phi_0 - \mu_\alpha E_\alpha - \tfrac{1}{2} q_{\alpha\beta}\nabla_\beta E_\alpha + \cdots |n^{(0)}\rangle,
\end{aligned} \tag{B.14}$$

in which the result $E_j^{(1)} = \langle j^{(0)}|H^{(1)}|j^{(0)}\rangle$ [77] was used. From (B.14) it is a simple matter to show that

$$\begin{aligned}
\omega_{jn} = \omega_{jn}^{(0)} &- \hbar^{-1} E_\alpha(\langle j^{(0)}|\mu_\alpha|j^{(0)}\rangle - \langle n^{(0)}|\mu_\alpha|n^{(0)}\rangle) \\
&- \tfrac{1}{2}\hbar^{-1}\nabla_\beta E_\alpha(\langle j^{(0)}|q_{\alpha\beta}|j^{(0)}\rangle - \langle n^{(0)}|q_{\alpha\beta}|n^{(0)}\rangle) + \cdots ,
\end{aligned} \tag{B.15}$$

and

$$\begin{aligned}
\omega_{jn}^2 = (\omega_{jn}^{(0)})^2 &- 2\hbar^{-1}\omega_{jn}^{(0)} E_\gamma(\langle j^{(0)}|\mu_\gamma|j^{(0)}\rangle - \langle n^{(0)}|\mu_\gamma|n^{(0)}\rangle) \\
&- \hbar^{-1}\omega_{jn}^{(0)}\nabla_\delta E_\gamma(\langle j^{(0)}|q_{\gamma\delta}|j^{(0)}\rangle - \langle n^{(0)}|q_{\gamma\delta}|n^{(0)}\rangle) + \cdots .
\end{aligned} \tag{B.16}$$

For $\omega \gg |\omega_{jn}|$ it follows from (B.15) and (B.16) that

$$\begin{aligned}
\frac{\omega_{jn}}{\omega_{jn}^2 - \omega^2} \approx &- \frac{\omega_{jn}^{(0)}((\omega_{jn}^{(0)})^2 + \omega^2)}{\omega^4} + \frac{3(\omega_{jn}^{(0)})^2 + \omega^2}{\hbar\omega^4} E_\gamma(\langle j^{(0)}|\mu_\gamma|j^{(0)}\rangle - \langle n^{(0)}|\mu_\gamma|n^{(0)}\rangle) \\
&+ \frac{3(\omega_{jn}^{(0)})^2 + \omega^2}{2\hbar\omega^4}\nabla_\delta E_\gamma(\langle j^{(0)}|q_{\gamma\delta}|j^{(0)}\rangle - \langle n^{(0)}|q_{\gamma\delta}|n^{(0)}\rangle) + \cdots .
\end{aligned} \tag{B.17}$$

Furthermore, if $\omega \gg |\omega_{jn}^{(0)}|$ then, to a very good approximation,

$$\frac{(\omega_{jn}^{(0)})^2+\omega^2}{((\omega_{jn}^{(0)})^2-\omega^2)^2} \approx \frac{3(\omega_{nj}^{(0)})^2+\omega^2}{\omega^4}. \tag{B.18}$$

Substituting (B.18) in (B.17) gives

$$\begin{aligned}\frac{\omega_{jn}}{\omega_{jn}^2-\omega^2} = \frac{\omega_{jn}^{(0)}}{(\omega_{jn}^{(0)})^2-\omega^2} + \frac{(\omega_{jn}^{(0)})^2+\omega^2}{\hbar((\omega_{jn}^{(0)})^2-\omega^2)^2} E_\alpha(\langle j^{(0)}|\mu_\alpha|j^{(0)}\rangle - \langle n^{(0)}|\mu_\alpha|n^{(0)}\rangle) \\ + \frac{(\omega_{jn}^{(0)})^2+\omega^2}{2\hbar((\omega_{jn}^{(0)})^2-\omega^2)^2} \nabla_\beta E_\alpha(\langle j^{(0)}|q_{\alpha\beta}|j^{(0)}\rangle - \langle n^{(0)}|q_{\alpha\beta}|n^{(0)}\rangle) + \cdots,\end{aligned} \tag{B.19}$$

which is the expression we shall use for the perturbed form of $\frac{\omega_{jn}}{\omega_{jn}^2-\omega^2}$ in (B.10).

In order to perturb the remaining part of the expression for $\alpha_{\alpha\beta}$ we use from Chapter 17 of [77] the eigenket expansions

$$|j\rangle = c|j^{(0)}\rangle + \sum_{k\neq j} a_{kj}|k^{(0)}\rangle, \quad \langle j| = c^*\langle j^{(0)}| + \sum_{k\neq j} a_{kj}^*\langle k^{(0)}|, \tag{B.20}$$

in which c is imaginary and

$$a_{kj} = \frac{H_{kj}^{(1)}}{E_j^{(0)}-E_k^{(0)}} = \frac{H_{kj}^{(1)}}{\hbar\omega_{jk}^{(0)}}. \tag{B.21}$$

Combining (B.10) and (B.19)–(B.21) gives

$$\begin{aligned}\alpha_{\alpha\beta} = \tfrac{1}{2}\hbar^{-1}\,\mathrm{Re}\Bigg\{\sum_j \Bigg[\Bigg(\frac{\omega_{jn}}{\omega_{jn}^2-\omega^2} + \frac{\omega_{jn}^2+\omega^2}{\hbar(\omega_{jn}^2-\omega^2)^2} E_\gamma(\langle j|\mu_\gamma|j\rangle - \langle n|\mu_\gamma|n\rangle) \\ + \frac{\omega_{jn}^2+\omega^2}{2\hbar(\omega_{jn}^2-\omega^2)^2}\nabla_\delta E_\gamma(\langle j|q_{\gamma\delta}|j\rangle - \langle n|q_{\gamma\delta}|n\rangle) + \cdots\Bigg) \\ \times\Bigg(\langle n|\mu_\alpha|j\rangle + \sum_{k\neq j}\frac{H_{kj}^{(1)}}{\hbar\omega_{jk}}\langle n|\mu_\alpha|k\rangle + \sum_{k\neq n}\frac{H_{kn}^{(1)}}{\hbar\omega_{nk}}\langle k|\mu_\alpha|j\rangle + \cdots\Bigg) \\ \times\Bigg(\langle j|\mu_\alpha|n\rangle + \sum_{k\neq j}\frac{H_{kj}^{(1)}}{\hbar\omega_{jk}}\langle k|\mu_\beta|n\rangle + \sum_{k\neq n}\frac{H_{kn}^{(1)}}{\hbar\omega_{nk}}\langle j|\mu_\beta|k\rangle + \cdots\Bigg)\Bigg]\Bigg\},\end{aligned} \tag{B.22}$$

in which we have dropped all the superscripted (0)s on the understanding that only unperturbed quantities and states are referred to in this expression. Expanding (B.22)

and grouping terms which are linear in the applied field and field gradient yields

$$\begin{aligned}
\alpha_{\alpha\beta} = {} & 2\,\mathrm{Re}\left\{\sum_j \frac{\omega_{jn}}{\hbar(\omega_{jn}^2-\omega^2)}\langle n|\mu_\alpha|j\rangle\langle j|\mu_\beta|n\rangle\right\} \\
& + 2E_\gamma\,\mathrm{Re}\left\{\sum_j \frac{\omega_{jn}^2+\omega^2}{\hbar^2(\omega_{jn}^2-\omega^2)^2}(\langle j|\mu_\gamma|j\rangle - \langle n|\mu_\gamma|n\rangle)\langle n|\mu_\alpha|j\rangle\langle j|\mu_\beta|n\rangle\right. \\
& \quad + \sum_{j,k\neq n} \frac{\omega_{jn}}{\hbar^2\omega_{kn}(\omega_{jn}^2-\omega^2)}(\langle n|mu_\gamma|k\rangle\langle k|\mu_\alpha|j\rangle\langle j|\mu_\beta|n\rangle \\
& \qquad\qquad + \langle k|mu_\gamma|n\rangle\langle j|\mu_\beta|k\rangle\langle n|\mu_\alpha|j\rangle) \\
& \quad + \sum_{j,k\neq j} \frac{\omega_{jn}}{\hbar^2\omega_{kj}(\omega_{jn}^2-\omega^2)}(\langle k|mu_\gamma|j\rangle\langle n|\mu_\alpha|k\rangle\langle j|\mu_\beta|n\rangle \\
& \qquad\qquad \left. + \langle j|mu_\gamma|k\rangle\langle k|\mu_\beta|n\rangle\langle n|\mu_\alpha|j\rangle)\right\} \\
& + \nabla_\delta E_\gamma\,\mathrm{Re}\left\{\sum_j \frac{\omega_{jn}^2+\omega^2}{\hbar^2(\omega_{jn}^2-\omega^2)^2}(\langle j|q_{\gamma\delta}|j\rangle - \langle n|q_{\gamma\delta}|n\rangle)\langle n|\mu_\alpha|j\rangle\langle j|\mu_\beta|n\rangle\right. \\
& \quad + \sum_{j,k\neq n} \frac{\omega_{jn}}{\hbar^2\omega_{kn}(\omega_{jn}^2-\omega^2)}(\langle n|q_{\gamma\delta}|k\rangle\langle k|\mu_\alpha|j\rangle\langle j|\mu_\beta|n\rangle \\
& \qquad\qquad + \langle n|mu_\alpha|j\rangle\langle k|q_{\gamma\delta}|n\rangle\langle j|\mu_\beta|k\rangle) \\
& \quad + \sum_{j,k\neq j} \frac{\omega_{jn}}{\hbar^2\omega_{kj}(\omega_{jn}^2-\omega^2)}(\langle k|q_{\delta\gamma}|j\rangle\langle n|\mu_\alpha|k\rangle\langle j|\mu_\beta|n\rangle \\
& \qquad\qquad \left. + \langle n|mu_\alpha|j\rangle\langle j|q_{\gamma\delta}|k\rangle\langle k|\mu_\beta|n\rangle)\right\} + \cdots .
\end{aligned} \tag{B.23}$$

Comparison of this with the expansion implicit in (2.19), namely

$$\alpha_{\alpha\beta}(E_\gamma, \nabla_\delta E_\gamma) = \alpha_{\alpha\beta}^{(0)} + \beta_{\alpha\beta\gamma}E_\gamma + \tfrac{1}{2}b_{\alpha\beta\gamma\delta}\nabla_\delta E_\gamma + \cdots , \tag{B.24}$$

allows one to extract the following quantum-mechanical expressions for the hyperpo-

larizability tensors:

$$\beta_{\alpha\beta\gamma} = \beta_{\beta\alpha\gamma} = 2\hbar^{-2}\mathrm{Re}\left\{\sum_j \frac{(\omega_{jn}^2+\omega^2)}{(\omega_{jn}^2-\omega^2)^2}[\langle j|\mu_\gamma|j\rangle - \langle n|\mu_\gamma|n\rangle]\langle n|\mu_\alpha|j\rangle\langle j|\mu_\beta|n\rangle \right.$$
$$+ \sum_{j,k\neq n} \frac{\omega_{jn}}{\omega_{kn}(\omega_{jn}^2-\omega^2)}[\langle n|\mu_\gamma|k\rangle\langle k|\mu_\alpha|j\rangle\langle j|\mu_\beta|n\rangle + \langle n|\mu_\alpha|j\rangle\langle j|\mu_\beta|k\rangle\langle k|\mu_\gamma|n\rangle]$$
$$\left. + \sum_{j,k\neq j} \frac{\omega_{jn}}{\omega_{kj}(\omega_{jn}^2-\omega^2)}[\langle n|\mu_\alpha|k\rangle\langle k|\mu_\gamma|j\rangle\langle j|\mu_\beta|n\rangle + \langle n|\mu_\alpha|j\rangle\langle j|\mu_\gamma|k\rangle\langle k|\mu_\beta|n\rangle]\right\}, \tag{B.25}$$

$$b_{\alpha\beta\gamma\delta} = b_{\beta\alpha\gamma\delta} = b_{\alpha\beta\delta\gamma} = 2\hbar^{-2}\mathrm{Re}\left\{\sum_j \frac{\omega_{jn}^2+\omega^2}{(\omega_{jn}^2-\omega^2)^2}[\langle j|q_{\gamma\delta}|j\rangle - \langle n|q_{\gamma\delta}|n\rangle]\right.$$
$$\times \langle n|\mu_\alpha|j\rangle\langle j|\mu_\beta|n\rangle + \sum_{j,k\neq n} \frac{\omega_{jn}}{\omega_{kn}(\omega_{jn}^2-\omega^2)}[\langle n|q_{\gamma\delta}|k\rangle\langle k|\mu_\alpha|j\rangle\langle j|\mu_\beta|n\rangle$$
$$+ \langle n|\mu_\alpha|j\rangle\langle j|\mu_\beta|k\rangle\langle k|q_{\gamma\delta}|n\rangle]$$
$$+ \sum_{j,k\neq j} \frac{\omega_{jn}}{\omega_{kj}(\omega_{jn}^2-\omega^2)}[\langle n|\mu_\alpha|k\rangle\langle k|q_{\gamma\delta}|j\rangle\langle j|\mu_\beta|n\rangle$$
$$\left. + \langle n|\mu_\alpha|j\rangle\langle j|q_{\gamma\delta}|k\rangle\langle k|\mu_\beta|n\rangle]\right\}. \tag{B.26}$$

These expressions are, respectively, (2.28) and (2.29). A similar treatment of (2.24) and (2.25) yields (2.30) and (2.31), respectively.

Appendix C

COSINE APPROXIMATIONS FOR THE ANALYSIS IN CHAPTER 3

An argument is presented in this appendix in which it is shown that terms quadratic in $\varepsilon, \gamma, \beta_1, \beta_2$, and α in (3.13) and (3.20)–(3.23), and which we shall hereafter refer to as the *small angles*, do not contribute to the expression for the intensity at the photomultiplier. We recall that we retain in this expression only those terms which are linear in either δ or θ, hereafter referred to as the *modulated angles*, and for which the remaining factor is of an order less than or equal to that of α^2.

In Table C.1 are listed (3.20)–(3.23) together with the terms in them, each term being assigned a label in the form of a number. In multiplying the five Jones matrices together to obtain expressions for a, b, c, and d in (3.18) we must consider all combinations in which one term is selected from each matrix. We shall refer to these terms by the appropriate combination of the afore-mentioned labels. For example, we would write

$$[1][4][11][16][19] = (\mathbf{I}) \times (-\frac{1}{\sqrt{2}} \sin\frac{\phi}{2}\,\mathbf{I}) \times (\mathbf{I}) \times (\frac{\delta}{2}\,\mathbf{i}) \times (\mathbf{I}).$$

Combining the matrices which appear in this example gives $\mathbf{I}\,\mathbf{I}\,\mathbf{I}\,\mathbf{i}\,\mathbf{I} = \mathbf{i}$, so this particular term contributes to the coefficient b which appears in (3.18). Shown in Table C.2 are all possible combinations which are independent of δ and θ or which are linear in only one of them, and which are either independent of $\varepsilon, \gamma, \beta_1$, and β_2 or which have a quadratic dependence on either ε or β_1 and on no other small quantity except possibly δ or θ. These terms have also been labelled so that they can be referred to in the discussion which follows.

The expression for the intensity at the photomultiplier as given by (3.13) is

$$\frac{I}{I_0} = b^2 + c^2 + 2\alpha(ac + bd) + \alpha^2(a^2 - b^2 - c^2 + d^2). \tag{C.1}$$

The only way in which ε^2 can enter this expression is via b^2 or c^2, otherwise it will contribute to a term which has at least a third-order small-angle dependence. Suppose

Table C.1 Labels assigned to terms in the expressions for the Jones matrices

$$
\begin{aligned}
R(\theta) &= \mathbf{I} && [1]\\
&\quad + \theta\,\mathbf{j}, && [2]\\
J_{\lambda/4}\left(\tfrac{\pi}{2}+\phi, \pm\tfrac{\pi}{4}+\varepsilon\right) &= \frac{1}{\sqrt{2}}\cos\frac{\phi}{2}\,\mathbf{I} && [3]\\
&\quad - \frac{1}{\sqrt{2}}\sin\frac{\phi}{2}\,\mathbf{I} && [4]\\
&\quad \mp \sqrt{2}\varepsilon\cos\frac{\phi}{2}\,\mathbf{i} && [5]\\
&\quad \mp \sqrt{2}\varepsilon\sin\frac{\phi}{2}\,\mathbf{i} && [6]\\
&\quad \pm \frac{1}{\sqrt{2}}\cos\frac{\phi}{2}\,\mathbf{k} && [7]\\
&\quad \mp \sqrt{2}\varepsilon^2\cos\frac{\phi}{2}\,\mathbf{k} && [8]\\
&\quad \pm \frac{1}{\sqrt{2}}\sin\frac{\phi}{2}\,\mathbf{k} && [9]\\
&\quad \mp \sqrt{2}\varepsilon^2\sin\frac{\phi}{2}\,\mathbf{k}, && [10]\\
S_2(\beta_2, \theta_2) &= \mathbf{I} && [11]\\
&\quad - \frac{\beta_2^2}{8}\,\mathbf{I} && [12]\\
&\quad + \frac{\beta_2}{2}\cos 2\theta_2\,\mathbf{i} && [13]\\
&\quad + \frac{\beta_2}{2}\sin 2\theta_2\,\mathbf{k}, && [14]\\
J_q(\delta, \gamma) &= \mathbf{I} && [15]\\
&\quad + \frac{\delta}{2}\,\mathbf{i} && [16]\\
&\quad - \delta\gamma^2\,\mathbf{i} && [17]\\
&\quad + \delta\gamma\,\mathbf{k}, && [18]\\
S_1(\beta_1, \theta_1) &= \mathbf{I} && [19]\\
&\quad - \frac{\beta_1^2}{8}\,\mathbf{I} && [20]\\
&\quad + \frac{\beta_1}{2}\cos 2\theta_1\,\mathbf{i} && [21]\\
&\quad + \frac{\beta_1}{2}\sin 2\theta_1\,\mathbf{k} && [22]
\end{aligned}
$$

Table C.2 Terms through which ε^2 and β_1^2 could enter the intensity expression

Small angle	Modulated angle	Term	Coefficient	Label
none	none	[1][3][11][15][19]	a	[A]
none	none	[1][4][11][15][19]	a	[B]
none	none	[1][7][11][15][19]	d	[C]
none	none	[1][9][11][15][19]	d	[D]
none	δ	[1][3][11][16][19]	b	[E]
none	δ	[1][4][11][16][19]	b	[F]
none	δ	[1][7][11][16][19]	c	[G]
none	δ	[1][9][11][16][19]	c	[H]
none	θ	[2][3][11][15][19]	c	[I]
none	θ	[2][4][11][15][19]	c	[J]
none	θ	[2][7][11][15][19]	b	[K]
none	θ	[2][9][11][15][19]	b	[L]
ε^2	none	[1][8][11][15][19]	d	[M]
ε^2	none	[1][10][11][15][19]	d	[N]
ε^2	δ	[1][8][11][16][19]	c	[O]
ε^2	δ	[1][10][11][16][19]	c	[P]
ε^2	θ	[2][8][11][15][19]	b	[Q]
ε^2	θ	[2][10][11][15][19]	b	[R]
β_1^2	none	[1][3][11][15][20]	a	[S]
β_1^2	none	[1][4][11][15][20]	a	[T]
β_1^2	none	[1][7][11][15][20]	d	[U]
β_1^2	none	[1][9][11][15][20]	d	[V]
β_1^2	δ	[1][3][11][16][20]	b	[W]
β_1^2	δ	[1][4][11][16][20]	b	[X]
β_1^2	δ	[1][7][11][16][20]	c	[Y]
β_1^2	δ	[1][9][11][16][20]	c	[Z]
β_1^2	θ	[2][3][11][15][20]	c	[AA]
β_1^2	θ	[2][4][11][15][20]	c	[BB]
β_1^2	θ	[2][7][11][15][20]	b	[CC]
β_1^2	θ	[2][9][11][15][20]	b	[DD]

strings are internally separated by a single space so that the variables of which they are composed may be easily identified later on. The results must then pass an order-of-magnitude test in the subroutine in lines 540–640 before being stored in the array `T$()`.

Execution then jumps to line 710 which is the start of a procedure to filter out and simplify the products of the **I**, **i**, **j**, and **k** matrices. These are referred to in the program as the *quaternians* because they form a mathematical group which is isomorphic to the quaternian group, the multiplication rules for which are given in lines 940–1230. In these lines, `RM$` is the string to be removed, and `RP$` is the one which replaces it. This operation is carried out in the subroutine at lines 3240–3280. Each entry in the `T$()` array now has a corresponding entry in `Q$()` which must correspond to one of the options listed in lines 1440–1510. The occurrence of the matrices in `T$` is now superfluous, so these are removed in lines 1270–1370. Depending on the matrix remaining in `Q$()`, the terms in `T$` are assigned in lines 1380–1580 to a row in the two-dimensional array `E$( , )`. The rows of this array correspond to the unknowns $a, b, c,$ and d in (3.18).

Further multiplication is carried out in lines 1700–2220 in which the elements of `E$` are combined according to (3.24) and the results stored in the array `SQ$`, which essentially stores the expression for the intensity at the photomultiplier. Small-order terms and terms which are not linear in either of the modulated quantities, but not both, are discarded and then each term is rearranged so that its factors appear in a standard order. This enables similar terms to be identified and combined with due regard for the sign and numeric constant. Lines 2450–2970 perform these tasks.

Finally, terms in each of the modulated quantities are separated and the final intensity expression is printed to the line printer. This is, of course, encoded in the same manner as the data in lines 650–690, leaving a small amount of decoding to be done by hand before the expression may be interpreted. The program terminates at line 3180; the code which follows this line constitutes a number of small utility subroutines.

```
10 REM *************************
12 REM * JONES ANALYSIS PROGRAM *
14 REM *                        *
16 REM *  written by            *
18 REM *      David A Imrie     *
20 REM *            March 1991  *
22 REM *************************
30 CLS
40 REM SET UP BRACKETS FOR MULTIPLYING OUT
50 DIM B(20)
60 DIM P(20)
70 DIM PD(20)
80 DIM FACT$(100)
90 DIM SQ$(1000)
100 DIM B$(10,15)
```

```
110 DIM MAG(100):DIM S$(100)
120 F$(1)="d":F$(2)="TH":REM DEFINE OSCILLATING TERMS
130 DIM Q$(700)
140 DIM CO(700)
150 DIM T$(500):REM HOLDS TERMS AFTER EXPANDING
160 DIM E$(4,500):REM HOLDS TERMS MULTIPLYING I,i,j,k
170 B(0)=5:B(1)=2:B(2)=6:B(3)=3:B(4)=3:B(5)=3:REM B(0) IS
    NUMBER OF BRACKETS
180 DIM HOLD$(100)
190 NS=9:REM NUMBER OF SMALL TERMS
200 OM=2.1:REM MIN ORDER OF MAGNITUDE THAT WE WILL REJECT
210 FOR I=1 TO B(0)
220 LPRINT "TERM";I:REM DUMP EACH TERM TO PRINTER TO AID CHECKING
230 FOR J=1 TO B(I)
240 READ B$(I,J)
250 LPRINT B$(I,J);" "
260 NEXT J
270 LPRINT
280 NEXT I
290 FOR I=1 TO NS
300 READ S$(I),MAG(I)
310 NEXT I
320 REM MULTIPLY OUT AND PUT TERMS INTO T$
330 PRINT"MULTIPLYING OUT...";TIME$:REM LOG START TIME TO MONITOR
340 TN=0:REM CURRENT TERM NUMBER
350 FOR K=1 TO B(0)
360 LET P(K)=1
370 NEXT K
380 TN=TN+1
390 LET T$(TN)=""
400 FOR I=1 TO B(0)
410 LET T$(TN)=T$(TN)+B$(I,P(I))+" "
420 NEXT I
430 REM UPDATE POSITIONS OF POINTERS
440 REM FIND BRACKET FOR UPDATING
450 UB=B(0):P(0)=999
460 IF P(UB)= B(UB) THEN P(UB)=1:UB=UB-1:GOTO 460
470 IF UB=0 THEN GOTO 520
480 P(UB)=P(UB)+1
490 GOSUB 540
500 IF INSTR(T$(TN),"*")<>0 THEN TN=TN-1
510 GOTO 380
520 REM ALL MULTIPLICATION COMPLETED
530 GOTO 710
540 REM DISCARD ENTRIES WITH TOO SMALL ORDER OF MAGNITUDE
550 F=0
```

```
560 FOR J=1 TO NS
570 N=1
580 LET PO=INSTR(N,T$(TN),S$(J))
590 IF PO=0 THEN 620
600 F=F+MAG(J):N=PO+1
610 GOTO 580
620 NEXT J
630 IF F>=OM THEN T$(TN)=T$(TN)+"*"
640 RETURN
650 DATA "I","j TH"
660 DATA "I 1/r2 cf","- I 1/r2 sf","- i s r2 e cf","- i s r2 e sf",
    "k s 1/r2 cf","k s 1/r2 sf"
670 DATA "I","i C2","k S2"
680 DATA "I","1/2 i d","k d g"
690 DATA "I","i C1","k S1"
700 DATA "A",.5,"e",.5,"C1",.5,"C2",.5,"S1",.5,"S2",.5,"g",.5,
    "d",1,"TH",1
710 REM SIMPLIFY PRODUCTS OF I,i,j,k MATRICES
720 PRINT"      FILTERING QUATERNIANS...";TIME$
730 REM
740 REM filter out i,j,k and - signs
750 FOR I=1 TO TN
760 IF INSTR(T$(I),"*")<>0 THEN GOTO 830
770 FOR J=1 TO LEN(T$(I))
780 IF MID$(T$(I),J,1)="j" THEN Q$(I)=Q$(I)+"j"
790 IF MID$(T$(I),J,1)="k" THEN Q$(I)=Q$(I)+"k"
800 IF MID$(T$(I),J,1)="-" THEN Q$(I)=Q$(I)+"-"
810 IF MID$(T$(I),J,1)="i" AND MID$(T$(I),J+1,1)=" "
    THEN Q$(I)=Q$(I)+"i"
820 NEXT J
830 NEXT I
840 REM SIMPLIFY THESE PRODUCTS
850 PRINT"         SIMPLIFYING QUATERNIAN PRODUCTS...";TIME$
860 FOR I=1 TO TN
870 IF INSTR(T$(I),"*")<>0 THEN GOTO 1260
880 S=1
890 REM FILTER NEGATIVE SIGNS
900 FOR J=1 TO LEN(Q$(I))
910 IF MID$(Q$(I),J,1)="-" THEN S=S*-1
920 NEXT J
930 LET L$=Q$(I):LET RM$="-":GOSUB 3190:LET Q$(I)=L$
940 IF INSTR(Q$(I),"ii")=0 THEN GOTO 970
950 L$=Q$(I):RM$="ii":S=S*-1:GOSUB 3190:Q$(I)=L$
960 GOTO 940
970 IF INSTR(Q$(I),"jj")=0 THEN GOTO 1000
980 L$=Q$(I):RM$="jj":S=S*-1:GOSUB 3190:Q$(I)=L$
```

```
990 GOTO 940
1000 IF INSTR(Q$(I),"kk")=0 THEN GOTO 1030
1010 L$=Q$(I):RM$="kk":S=S*-1:GOSUB 3190:Q$(I)=L$
1020 GOTO 940
1030 IF INSTR(Q$(I),"ij")=0 THEN GOTO 1060
1040 L$=Q$(I):RM$="ij":RP$="k":GOSUB 3240:Q$(I)=L$
1050 GOTO 940
1060 IF INSTR(Q$(I),"jk")=0 THEN GOTO 1090
1070 L$=Q$(I):RM$="jk":RP$="i":GOSUB 3240:Q$(I)=L$
1080 GOTO 940
1090 IF INSTR(Q$(I),"ki")=0 THEN GOTO 1120
1100 L$=Q$(I):RM$="ki":RP$="j":GOSUB 3240:Q$(I)=L$
1110 GOTO 940
1120 IF INSTR(Q$(I),"ji")=0 THEN GOTO 1160
1130 L$=Q$(I):RM$="ji":RP$="k":GOSUB 3240:Q$(I)=L$
1140 S=S*-1
1150 GOTO 940
1160 IF INSTR(Q$(I),"kj")=0 THEN GOTO 1200
1170 L$=Q$(I):RM$="kj":RP$="i":GOSUB 3240:Q$(I)=L$
1180 S=S*-1
1190 GOTO 940
1200 IF INSTR(Q$(I),"ik")=0 THEN GOTO 1240
1210 L$=Q$(I):RM$="ik":RP$="j":GOSUB 3240:Q$(I)=L$
1220 S=S*-1
1230 GOTO 940
1240 REM SIMPLIFICATION COMPLETED
1250 IF S=-1 THEN Q$(I)="-"+Q$(I)
1260 NEXT I
1270 REM CLEAN UP T$
1280 PRINT"            CLEANING UP...";TIME$
1290 FOR I=1 TO TN
1300 IF INSTR(T$(I),"*")<>0 THEN GOTO 1370
1310 L$=T$(I):RM$="i ":GOSUB 3190
1320 RM$="j ":GOSUB 3190
1330 RM$="k ":GOSUB 3190
1340 RM$="-":GOSUB 3190
1350 RM$="I ":GOSUB 3190
1360 T$(I)=L$
1370 NEXT I
1380 REM SEPARATE OUT FOUR ELEMENTS OF MATRIX
1390 REM
1400 A1=1:A2=1
1410 B1=1:B2=1
1420 FOR I=1 TO TN
1430 IF RIGHT$(T$(I),1)="*" THEN GOTO 1580
1440 IF Q$(I)="" THEN S=1:Q=1
```

```
1450 IF Q$(I)="-" THEN S=-1:Q=1
1460 IF Q$(I)="i" THEN S=1:Q=2
1470 IF Q$(I)="-i" THEN S=-1:Q=2
1480 IF Q$(I)="j" THEN S=1:Q=3
1490 IF Q$(I)="-j" THEN S=-1:Q=3
1500 IF Q$(I)="k" THEN S=1:Q=4
1510 IF Q$(I)="-k" THEN S=-1:Q=4
1520 IF S=1 THEN T$(I)="+ "+T$(I)
1530 IF S=-1 THEN T$(I)="- "+T$(I)
1540 IF Q=1 THEN E$(1,A1)=T$(I):A1=A1+1
1550 IF Q=2 THEN E$(2,A2)=T$(I):A2=A2+1
1560 IF Q=3 THEN E$(3,B1)=T$(I):B1=B1+1
1570 IF Q=4 THEN E$(4,B2)=T$(I):B2=B2+1
1580 NEXT I
1590 A1=A1-1:A2=A2-1:B1=B1-1:B2=B2-1
1600 FOR I= 1 TO TN:T$(I)="":NEXT I
1610 FOR I=1 TO A1:LPRINT E$(1,I);" ";:NEXT I
1620 LPRINT:LPRINT:LPRINT
1630 FOR I=1 TO A2:LPRINT E$(2,I);" ";:NEXT I
1640 LPRINT:LPRINT:LPRINT
1650 FOR I=1 TO B1:LPRINT E$(3,I);" ";:NEXT I
1660 LPRINT:LPRINT:LPRINT
1670 FOR I=1 TO B2:LPRINT E$(4,I);" ";:NEXT I
1680 LPRINT:LPRINT:LPRINT
1690 REM
1700 REM
1710 REM WE MUST SQUARE AND ADD THESE TERMS
1720 REM NO. OF ELEMENTS IN E$(2,I) IS A2, IN E$(3,I) IS B1
1730 PRINT"                ANALYSING THE BEAM...";TIME$
1740 REM WE WILL REJECT ALL TERMS INDEPENDENT OF DELTA AND THETA
     OR WHICH ARE QUADRATIC IN THEM
1750 REM SQUARE Im(a) AND PUT RESULT IN SQ$
1760 PT=1
1770 FOR I=1 TO A2
1780 FOR J=1 TO A2
1790 IF INSTR(E$(2,I),F$(1))=0 AND INSTR(E$(2,I),F$(2))=0
     AND INSTR(E$(2,J),F$(1))=0 AND INSTR(E$(2,J),F$(2))=0
     THEN GOTO 1850
1800 IF (INSTR(E$(2,I),F$(1))<>0 OR INSTR(E$(2,I),F$(2))<>0)
     AND (INSTR(E$(2,J),F$(1))<>0 OR INSTR(E$(2,J),F$(2))<>0)
     THEN GOTO 1850
1810 LET SQ$(PT)="   "+E$(2,I)+" "+E$(2,J)+" "
1820 FLG=0:GOSUB 2240
1830 LET PT=PT+1
1840 IF FLG=1 THEN PT=PT-1
1850 NEXT J
```

```
1860 NEXT I
1870 PRINT"A"
1880 REM SQUARE Re(b) AND ADD RESULT TO SQ$
1890 FOR I=1 TO B1
1900 FOR J=1 TO B1
1910 IF INSTR(E$(3,I),F$(1))=0 AND INSTR(E$(3,I),F$(2))=0
     AND INSTR(E$(3,J),F$(1))=0 AND INSTR(E$(3,J),F$(2))=0
     THEN GOTO 1970
1920 IF (INSTR(E$(3,I),F$(1))<>0 OR INSTR(E$(3,I),F$(2))<>0)
     AND (INSTR(E$(3,J),F$(1))<>0 OR INSTR(E$(3,J),F$(2))<>0)
     THEN GOTO 1970
1930 LET SQ$(PT)="  "+E$(3,I)+" "+E$(3,J)
1940 FLG=0:GOSUB 2240
1950 LET PT=PT+1
1960 IF FLG=1 THEN PT=PT-1
1970 NEXT J
1980 NEXT I
1990 PRINT"B"
2000 REM MULTIPLY Re(a) AND Re(b) AND ALPHA AND ADD RESULT TO Q$
2010 FOR I=1 TO A1
2020 FOR J=1 TO B1
2030 IF INSTR(E$(1,I),F$(1))=0 AND INSTR(E$(1,I),F$(2))=0
     AND INSTR(E$(3,J),F$(1))=0 AND INSTR(E$(3,J),F$(2))=0
     THEN GOTO 2090
2040 IF (INSTR(E$(1,I),F$(1))<>0 OR INSTR(E$(1,I),F$(2))<>0)
     AND (INSTR(E$(3,J),F$(1))<>0 OR INSTR(E$(3,J),F$(2))<>0)
     THEN GOTO 2090
2050 LET SQ$(PT)="   "+"2 A "+E$(1,I)+" "+E$(3,J)+" "
2060 FLG=0:GOSUB 2240
2070 LET PT=PT+1
2080 IF FLG=1 THEN PT=PT-1
2090 NEXT J
2100 NEXT I
2110 PRINT"C"
2120 REM MULTIPLY Im(a) AND Im(b) AND ALPHA AND ADD RESULT TO Q$
2130 FOR I=1 TO A2
2140 FOR J=1 TO B2
2150 IF INSTR(E$(2,I),F$(1))=0 AND INSTR(E$(2,I),F$(2))=0
     AND INSTR(E$(4,J),F$(2))=0 AND INSTR(E$(4,J),F$(2))=0
     THEN GOTO 2210
2160 IF (INSTR(E$(2,I),F$(1))<>0 OR INSTR(E$(2,I),F$(2))<>0)
     AND (INSTR(E$(4,J),F$(1))<>0 OR INSTR(E$(4,J),F$(2))<>0)
     THEN GOTO 2210
2170 LET SQ$(PT)="   "+"2 A "+E$(2,I)+" "+E$(4,J)+" "
2180 FLG=0:GOSUB 2240
2190 LET PT=PT+1
```

```
2200 IF FLG=1 THEN PT=PT-1
2210 NEXT J
2220 NEXT I
2230 GOTO 2440
2240 REM DISCARD SMALL ORDER TERMS
2250 F=0
2260 FOR K=1 TO NS
2270 N=1
2280 LET PO=INSTR(N,SQ$(PT),S$(K))
2290 IF PO=0 THEN 2320
2300 F=F+MAG(K):N=PO+1
2310 GOTO 2280
2320 NEXT K
2330 IF F>=OM THEN FLG=1:RETURN
2340 REM CHECK IF TERM IS QUADRATIC IN F$(1) OR F$(2)
2350 F=0
2360 FOR K=1 TO 2
2370 N=1
2380 PO=INSTR(N,SQ$(PT),F$(K))
2390 IF PO=0 THEN GOTO 2410
2400 F=F+1:N=PO+1:GOTO 2380
2410 NEXT K
2420 IF F>1 THEN FLG=1
2430 RETURN
2440 PS=PT-1
2450 REM CLEAN UP TERMS
2460 PRINT"                        CLEANING UP AGAIN...";TIME$
2470 REM BUILD EACH TERM UP IN STANDARD FORMAT
2480 FOR I=1 TO PS
2490 REM BREAK EACH TERM UP INTO ITS FACTORS
2500 LET FG=0
2510 FOR J=2 TO LEN(SQ$(I))
2520 IF MID$(SQ$(I),J-1,1)<>" " OR MID$(SQ$(I),J,1)=" " THEN GOTO 2570
2530 P=J:FG=FG+1:FACT$(FG)=""
2540 FACT$(FG)=FACT$(FG)+MID$(SQ$(I),P,1)
2550 P=P+1
2560 IF MID$(SQ$(I),P,1)<>" " THEN GOTO 2540
2570 NEXT J
2580 REM FACTORIZATION IS COMPLETE
2590 REM DETERMINE SIGN
2600 S=1
2610 FOR K=1 TO FG
2620 IF FACT$(K)="-" THEN S=S*-1
2630 NEXT K
2640 SG$="+":IF S=-1 THEN SG$="-"
2650 REM DETERMINE NUMERIC FACTOR
```

```
2660 REC8=0:TWO=0:RT2=0:RECRT2=0:REC2=0
2670 FOR K=1 TO FG
2680 IF FACT$(K)="r2" THEN RT2=RT2+1
2690 IF FACT$(K)="1/r2" THEN RECRT2=RECRT2+1
2700 IF FACT$(K)="1/2" THEN REC2=REC2+1
2710 IF FACT$(K)="2" THEN TWO=TWO+1
2720 IF FACT$(K)="1/8" THEN REC8=REC8+1
2730 NEXT K
2740 NFACT=(SQR(2))^RT2*(1/SQR(2))^RECRT2*(.5)^REC2*(1/8)^REC8*2^TWO
2750 CO(I)=S*NFACT
2760 SQ$(I)=""
2770 FOR K=1 TO FG
2780 IF FACT$(K)<>"2" AND FACT$(K)<>"1/8" AND FACT$(K)<>"r2"
     AND FACT$(K)<>"1/r2" AND FACT$(K)<>"1/2" AND FACT$(K)<>"-"
     AND FACT$(K)<>"+" THEN SQ$(I)=SQ$(I)+" "+FACT$(K)
2790 NEXT K
2800 L$=SQ$(I):GOSUB 3290:REM ORDER TERMS
2810 RM$="s s ":GOSUB 3190
2820 SQ$(I)=L$
2830 NEXT I
2840 PRINT "                          GROUPING TERMS...";TIME$
2850 FOR I=1 TO PS-1
2860 IF SQ$(I)="COMBINED" THEN GOTO 2920
2870 FOR K=(I+1) TO PS
2880 IF SQ$(I)<>SQ$(K) OR SQ$(K)="COMBINED" THEN GOTO 2910
2890 CO(I)=CINT((CO(I)+CO(K))*1000)/1000
2900 SQ$(K)="COMBINED"
2910 NEXT K
2920 NEXT I
2930 REM DROP ALL THE 'COMBINED' TERMS
2940 TOP=1
2950 FOR I=1 TO PS
2960 IF SQ$(I)<>"COMBINED" THEN SQ$(TOP)=SQ$(I):CO(TOP)=CO(I):TOP=TOP+1
2970 NEXT I
2980 TOP=TOP-1
2990 PS=TOP
3000 REM GROUP TERMS
3010 PPS=PS
3020 PRINT "             FACTORING OUT OSCILLATING FACTORS...";TIME$
3030 REM USE E$(A,B) TO HOLD MULTIPLES OF OSCILLATING FACTORS
3040 FOR K=1 TO 2
3050 RM$=F$(K):PO=0
3060 FOR I=1 TO PPS
3070 IF INSTR(SQ$(I),F$(K))=0 THEN GOTO 3120
3080 IF CO(I)=0 THEN GOTO 3120:REM DROP TERMS WITH ZERO COEFFICIENTS
3090 PO=PO+1
```

```
3100 L$=SQ$(I):GOSUB 3190
3110 E$(K,PO)=STR$(CO(I))+" "+L$
3120 NEXT I
3130 IF K=1 THEN N1=PO
3140 IF K=2 THEN N2=PO
3150 NEXT K
3160 LPRINT F$(1):FOR I=1 TO N1:LPRINT E$(1,I):NEXT I
3170 LPRINT F$(2):FOR I=1 TO N2:LPRINT E$(2,I):NEXT I
3180 END
3190 REM ROUTINE TO REMOVE ALL OCCURENCES OF RM$ IN L$
3200 LET PZ=INSTR(L$,RM$)
3210 IF PZ=0 THEN RETURN
3220 LET L$=LEFT$(L$,PZ-1)+RIGHT$(L$,LEN(L$)-PZ+1-LEN(RM$))
3230 GOTO 3200
3240 REM ROUTINE TO REPLACE FIRST OCCURENCE OF RM$ IN L$ WITH RP$
3250 LET PZ=INSTR(L$,RM$)
3260 IF PZ=0 THEN RETURN
3270 LET L$=LEFT$(L$,PZ-1)+RP$+RIGHT$(L$,LEN(L$)-PZ+1-LEN(RM$))
3280 RETURN
3290 REM ROUTINE TO ORDER THE SPACED ELEMENTS OF L$
3300 LET L$=" "+L$+" "
3310 IND=1
3320 REM BREAK STRING UP AND PUT ELEMENTS IN HOLD$
3330 FOR JJ= 2  TO LEN(L$)
3340 LET HOLD$(IND)=""
3350 IF MID$(L$,JJ-1,1)<>" " OR MID$(L$,JJ,1)=" " THEN GOTO 3410
3360 LET LP=JJ
3370 LET HOLD$(IND)=HOLD$(IND)+MID$(L$,LP,1)
3380 LET LP=LP+1
3390 IF MID$(L$,LP,1)<>" " THEN GOTO 3370
3400 IND=IND+1
3410 NEXT JJ
3420 REM NOW REBUILD L$ IN CORRECT ORDER
3430 NC=0
3440 L$=""
3450 LET TEST$=HOLD$(1)
3460 FOR JJ=1 TO IND-1
3470 IF HOLD$(JJ)<=TEST$ THEN TEST$=HOLD$(JJ):MIN=JJ
3480 NEXT JJ
3490 L$=L$+HOLD$(MIN)+" "
3500 HOLD$(MIN)="}"
3510 NC=NC+1
3520 IF NC=IND-1 THEN RETURN
3530 GOTO 3450
3540 FOR I=1 TO PS:LPRINT CO(I);"  ";SQ$(I): NEXT I
3550 RETURN
```

Appendix E

BOUNDARY CONDITIONS FOR THE LINE-CHARGE MODEL

Mention was made in §4.4.3 of the need to consider how the boundary conditions assumed in the line-charge model presented in Appendix A may be compromised by selecting too small a wire spacing for a given wire thickness. Simply stated, these boundary conditions assume that two line charges may be positioned in the quadrupole cell in such a way that one of the equipotential surfaces to which they give rise will coincide with the inner surface of the cell, and one with each of the wire surfaces.

In order to select a spacing for a given thickness of wire, the equipotentials at the cell and wire surfaces calculated for different separations were plotted on top of a line representing the physical surface. A suitable spacing was then chosen based on a fairly subjective assessment of how well the two surfaces coincided. A sample of these plots is given for 0.5 mm-thick wire in Figures E.1–E.6. After examining these, it was decided to use a separation of 4.0 mm between centres for the 0.5 mm wire. The 0 V equipotential for this configuration may be seen in Figure E.1 to coincide extremely closely with the surface of the cell, drawn in a broken line in this diagram. Only half of the 0 V equipotential has been plotted in order to emphasize the presence of the broken line representing the cell surface. The other nine equipotential lines in Figure E.1 are plotted for equal increments of the potential.

In Figures E.2-E.6, the equipotential at the wire surface is shown for a single wire. The wire separation between centres ranges in these plots from 2.0 mm to 4.0 mm in steps of 0.5 mm. In all cases, the solid line represents the equipotential and the broken line is the surface of the wire.

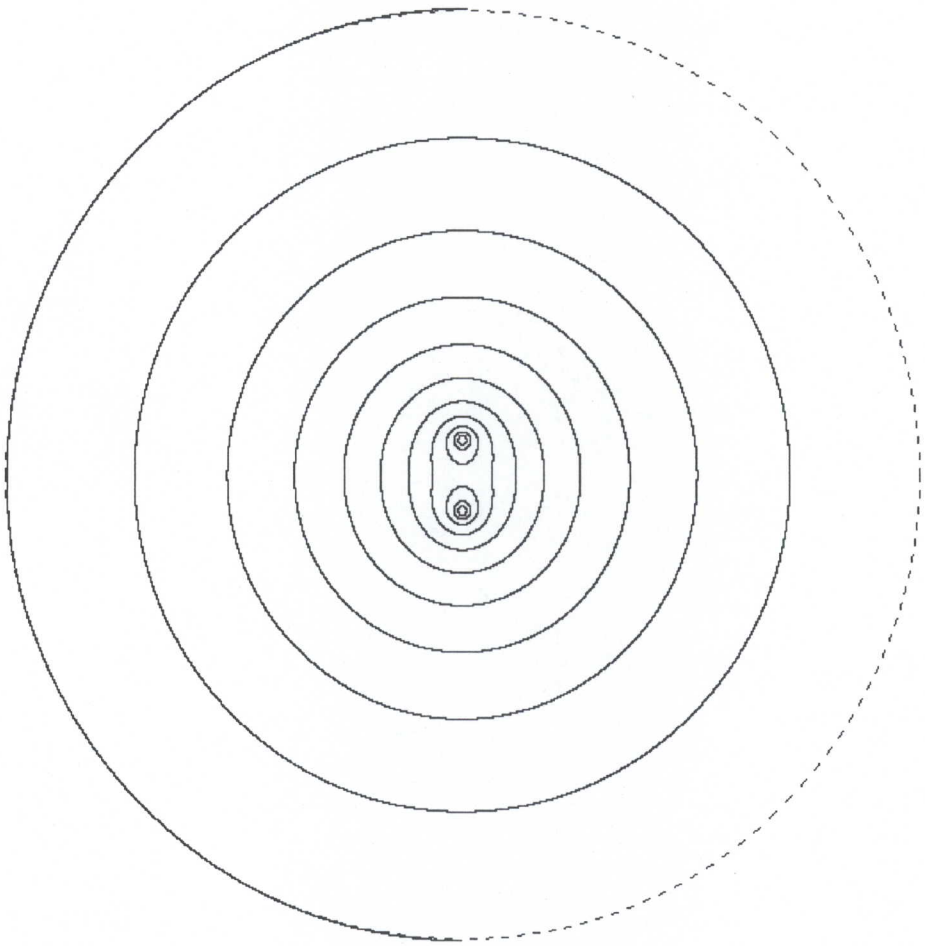

Figure E.1 Calculated equipotential surfaces in the quadrupole cell for 0.5 mm-thick wires spaced 4.0 mm between centres

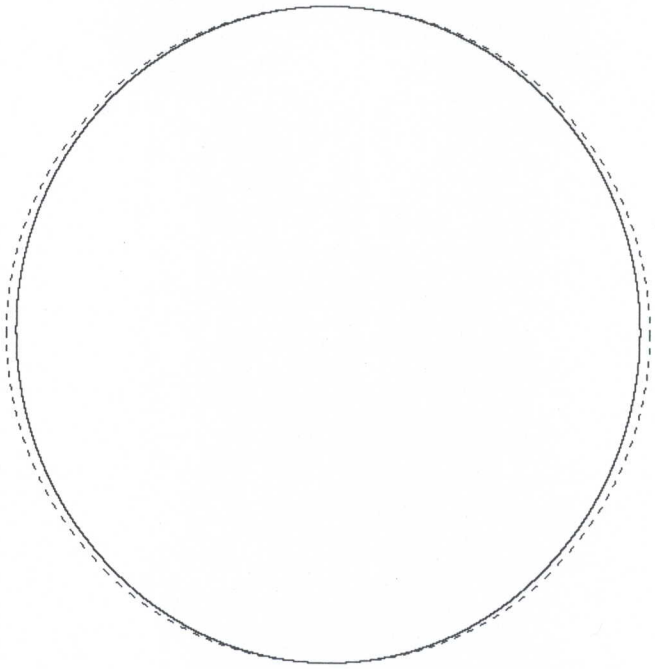

Figure E.2 Calculated equipotential surface (solid line) at the surface of a 0.5 mm-thick wire (broken line) for a spacing of 2.0 mm between centres

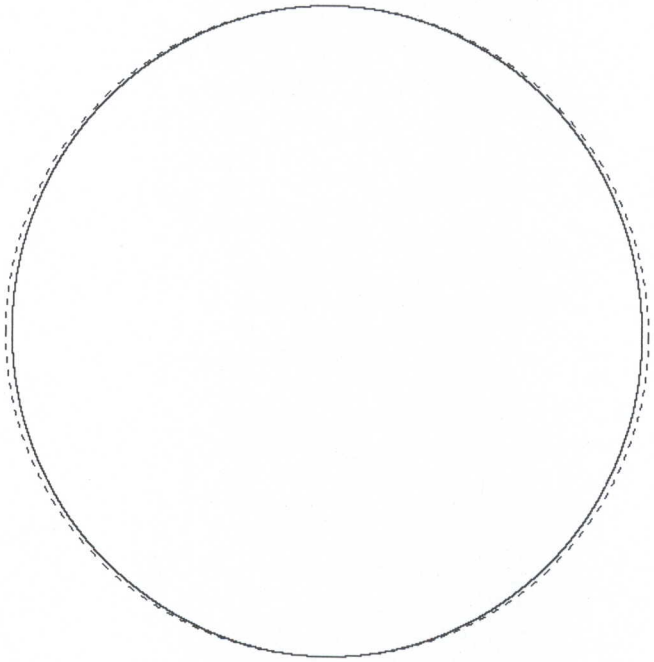

Figure E.3 Calculated equipotential surface (solid line) at the surface of a 0.5 mm-thick wire (broken line) for a spacing of 2.5 mm between centres

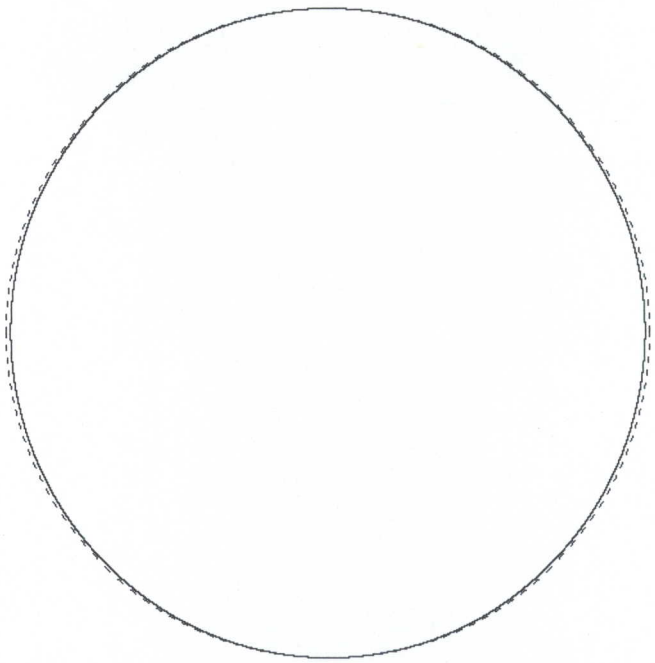

Figure E.4 Calculated equipotential surface (solid line) at the surface of a 0.5 mm-thick wire (broken line) for a spacing of 3.0 mm between centres

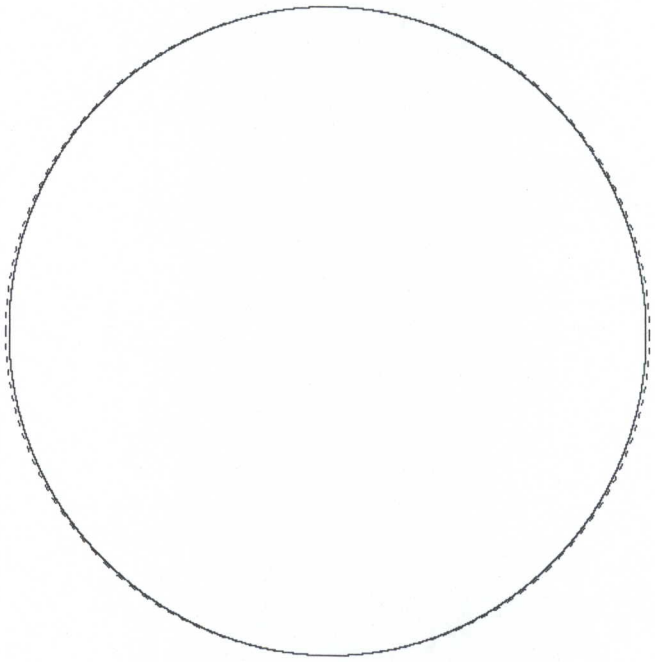

Figure E.5 Calculated equipotential surface (solid line) at the surface of a 0.5 mm-thick wire (broken line) for a spacing of 3.5 mm between centres

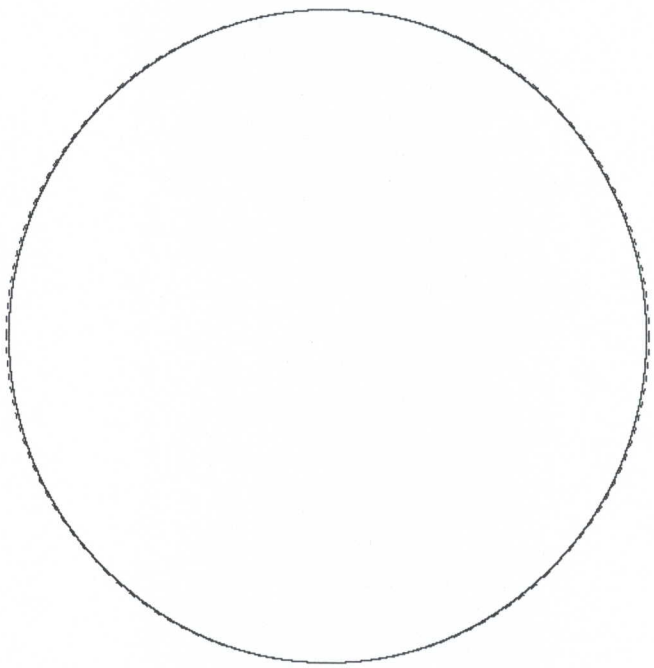

Figure E.6 Calculated equipotential surface (solid line) at the surface of a 0.5 mm-thick wire (broken line) for a spacing of 4.0 mm between centres

Appendix F

HP86 PROGRAM FOR CONTROLLING THE EXPERIMENT

```
10 REM ************************************************************
20 REM * PROGRAM FOR FINDING THE NULL CURRENT IN THE QUADRUPOLE *
30 REM * EXPERIMENT USING A FARADAY NULLING CELL.  THIS PROGRAM *
40 REM * IS STORED UNDER THE NAME "QUADNUL".   THIS VERSION WAS *
50 REM * WRITTEN BY DAVID A IMRIE IN THE PIETERMARITZBURG  DEPT *
60 REM * OF PHYSICS.  JANUARY 1991.                             *
70 REM ************************************************************
80 REM
90 REM
100 REM DEFINE VARIABLES AND ARRAYS
110 NR=50 @ ! NUMBER OF PSD READINGS TO AVERAGE FOR A NULL
120 REM THE FOLLOWING VARIABLES ARE DEFINED AS ARRAYS FOR
    HP86->IBM CONVERSION PURPOSES
130 L$="1466" ! LENGTH OF WIRES IN mm
140 D$="0.499" ! WIRE DIAMETER IN mm
150 SA$="2.914" ! LASER END SEPARATION OF WIRES IN mm
160 SB$="2.896" ! CENTRE SEPARATION OF WIRES IN mm
170 SC$="2.874" ! EXIT END SEPARTATION OF WIRES IN mm
180 FC$="3.260e-06" ! FARADAY CELL CONSTANT IN radians/mA
    AS AT 19/01/93
190 WL$="632.8" ! WAVELENGTH OF RADIATION IN nm
200 R1=950000 ! INPUT IMPEDANCE OF HP3478A VOLTMETER ON AC RANGE
210 REM *** THERMISTOR CALIBRATION COEFFICIENTS ***
220 AA=-.043826 @ CA=22.3283
230 AB=-.043596 @ CB=22.1737
240 AC=-.043363 @ CC=22.0845
250 DI=1 @ COUNTS=0 @ PS$="DUMMY" @ NM=0
260 DIM ZERO$(4)
```

```
270 ZERO$="0000"
280 DIM NAME$[50],NOTE$[80]
290 DIM V$(20)
300 REM SET ORDER OF MEASUREMENTS
310 DIM OM(20)
320 FOR I=1 TO 20
330 READ OM(I)
340 NEXT I
350 DATA 20,10,19,9,18,8,17,7,16,6,15,5,14,4,13,3,12,2,11,1
360 OUTPUT 509 ;"OPN"
370 NM$(0)="[QWP OFFSET]" @ NM$(1)="[ANALYSER OFFSET]"
380 CLEAR
390 DISP @ DISP @ DISP "THROW THE JUNCTION-BOX TOGGLE SWITCH TO THE
    'OHMS' POSITION AND HIT 'CONT'..."
400 BEEP 100,40 @ BEEP 30,80
410 PAUSE
420 BEEP 40,50
430 REM *** TAKE 4-WIRE MEASUREMENT OF THE STANDARD RESISTANCE ***
440 OUTPUT 525 ;"H4"
450 ENTER 525 ; SR
460 DISP SR
470 R=1/(1/R1+1/SR) ! EFFECTIVE STANDARD RESISTANCE
480 REM *** RESET MULTIMETER MODE TO AC VOLTS ***
490 DISP @ DISP "RETURN THE JUNCTION-BOX TOGGLE SWITCH TO THE
    'VOLTS' POSITION AND HIT 'CONT'..."
500 BEEP 100,40 @ BEEP 30,80
510 PAUSE
520 OUTPUT 525 ;"F2R-2RAZ1N4T1"
530 BEEP 40,50
540 PRINTER IS 701
550 OUTPUT 509 ;"OPN0" @ OUTPUT 509 ;"OPN1"
560 OUTPUT 509 ;"OPN3"
570 DISP
580 DISP "ENTER THE PSD TIME CONSTANT IN SECONDS"
590 BEEP 100,40 @ BEEP 30,80
600 INPUT PSDTC
610 BEEP 40,50
620 DISP
630 DISP "ENTER THE PRESENT DATE AND TIME"
640 BEEP 100,40 @ BEEP 30,80
650 INPUT DT$
660 BEEP 40,50
670 DISP @ DISP "ENTER THE NAME OF THE GAS"
680 BEEP 100,40 @ BEEP 30,80
690 INPUT NAME$
700 BEEP 40,50
```

```
710 REM GET ADDITIONAL NOTES FOR LOG FILE
720 DISP @ DISP "ENTER ANY NOTES FOR THIS RUN"
730 BEEP 100,40 @ BEEP 30,80
740 INPUT NOTE$
750 BEEP 40,50
760 DISP
770 DISP "ENTER THE ATMOSPHERIC PRESSURE IN mmHg"
780 BEEP 100,40 @ BEEP 30,80
790 INPUT AP
800 BEEP 40,50
810 DISP
820 DISP "ENTER THE GAUGE GAUGE PRESSURE OF THE GAS IN THE CELL IN MPa"
830 BEEP 100,40 @ BEEP 30,80
840 INPUT GP
850 BEEP 40,50
860 DISP
870 DISP "ENTER A NAME FOR THE DATA FILE"
880 INPUT DF$
890 FOR J=1 TO 10 @ DISP @ NEXT J
900 DISP
910 DISP
920 DISP "                ****************************************"
930 DISP "                *** HIT 'CONT' TO BEGIN THE EXPERIMENT ***"
940 DISP "                ****************************************"
950 FOR J=1 TO 7 @ DISP @ NEXT J
960 BEEP 100,40 @ BEEP 30,80
970 PAUSE
980 FOR I=1 TO 100 STEP 4
990 BEEP I,8*(400-I)/300
1000 NEXT I
1010 FOR I=100 TO 1 STEP -4
1020 BEEP I,8*(400-I)/300
1030 NEXT I
1040 REM *** TAKE INITIAL TEMPERATURE MEASUREMENTS ***
1050 OUTPUT 509 ;"TWO2"
1060 NM=1
1070 ENTER 509 ; DR
1080 IF DR<50000 THEN NM=0  ! DETERMINE MODE OF THE EXPERIMENT
1090 NOTE$=NOTE$&NM$(NM)
1100 GOSUB 1820
1110 TI=TBAR
1120 REM *** PRINT INITIAL DATA ***
1130 PRINT
1140 PRINT "                DATE & TIME:";DT$
1150 PRINT "                       GAS:";NAME$
1160 PRINT "                     NOTES:";NOTE$
```

```
1170 PRINT "ATMOSPHERIC PRESSURE (mmHg):";AP
1180 PRINT "GAUGE PRESSURE OF GAS (MPa):";GP
1190 PRINT "INITIAL GAS TEMPERATURE (C):";TI
1200 PRINT "                    DATA FILE:";DF$
1210 REM *** OPEN DATA FILE AND STORE HEADER INFORMATION ***
1220 AP$=VAL$ (AP) @ GP$=VAL$ (GP) @ TI$=VAL$ (TI)
1230 CREATE DF$,12 ! SEQUENTIAL FILE OF 3k
1240 ASSIGN# 1 TO DF$
1250 PRINT# 1; DT$,NAME$,NOTE$,AP$,GP$,TI$,L$,D$,SA$,SB$,SC$,FC$,WL$
1260 ON KEY# 7,"END EXPT." GOTO 1740
1270 GOSUB 1970 @ REM FIND ANALYSER LIMIT POSITIONS
1280 REM *** ROUTINE FOR FINDING NULL CURRENT ***
1290 BEEP 50,50 @ BEEP 40,40 @ BEEP 30,30 @ BEEP 20,20 @ BEEP 40,70
1300 FOR L=1 TO 2
1310 IF L=1 AND PS$ <> "NEG" THEN PS$="NEG" @ NS=COUNTS @ D=-(1*DI)
     @ GOSUB 2700
1320 IF L=2 AND PS$ <> "POS" THEN PS$="POS" @ NS=COUNTS @ D=DI
     @ GOSUB 2700
1330 GOSUB 1820
1340 T(L)=TBAR
1350 GX,GY,XY,X2,Y2=0
1360 FOR P=1 TO 20
1370 TOTX=0 @ TOTY=0
1380 OUTPUT 510 ;V$(OM(P))
1390 IF OM(P)=20 OR OM(P)=19 THEN WAIT 60000*PSDTC
1400 WAIT 15000*PSDTC
1410 BEEP 10,20 @ BEEP 40,10 @ BEEP 15,30
1420 ENTER 525 ; TOTX
1430 FOR I=1 TO NR
1440 ENTER 523;Y
1450 TOTY=TOTY+Y
1460 NEXT I
1470 ENTER 525 ; X @ TOTX=(TOTX+X)/2
1480 XBAR=TOTX/R*1000
1490 YBAR=TOTY/NR
1500 GX=GX+XBAR
1510 GY=GY+YBAR
1520 XY=XY+XBAR*YBAR
1530 X2=X2+XBAR^2
1540 Y2=Y2+YBAR^2
1550 NEXT P
1560 M(L)=(20*XY-GX*GY)/(20*X2-GX^2)
1570 C(L)=(GY*X2-GX*XY)/(20*X2-GX^2)
1580 R(L)=(20*XY-GX*GY)^2/((20*X2-GX^2)*(20*Y2-GY^2))
1590 OUTPUT 509 ;"DCV3"
1600 ENTER 509 ; HV(L)
```

```
1610 HV(L)=ABS (HV(L))
1620 BEEP 100,50 @ BEEP 50,30 @ BEEP 100,50
1630 NEXT L
1640 I_NULL=ABS ((C(2)-C(1))/(M(1)-M(2)))
1650 HV=(HV(1)+HV(2))/2
1660 T=(T(1)+T(2))/2
1670 I_NULL=INT (1000*I_NULL)/1000 @ HV=INT (1000*HV)/1000
1680 M(1)=INT (1000*M(1))/1000 @ C(1)=INT (1000*C(1))/1000
     @ R(1)=INT (10000*R(1))/10000
1690 M(2)=INT (1000*M(2))/1000 @ C(2)=INT (1000*C(2))/1000
     @ R(2)=INT (10000*R(2))/10000
1700 PRINT I_NULL;HV;T;"  ";M(1);C(1);R(1);"   ";M(2);C(2);R(2)
1710 PRINT
1720 PRINT# 1 ; VAL$ (HV),VAL$ (T),VAL$ (M(1)),VAL$ (C(1)),VAL$ (R(1)),
     VAL$ (M(2)),VAL$ (C(2)),VAL$ (R(2))
1730 GOTO 1280
1740 REM *** EXPERIMENT TERMINATED BY USER ***
1750 OUTPUT 509 ;"OPN0" @ OUTPUT 509 ;"OPN1"
1760 DISP @ DISP @ DISP
1770 BEEP 100,50 @ BEEP 50,30 @ BEEP 100,50
1780 PRINT# 1 ;"END"
1790 ASSIGN# 1 TO  * ! CLOSE DATA FILE
1800 DISP "EXPERIMENT TERMINATED BY USER"
1810 END
1820 REM
1830 REM *  TEMPERATURE MEASUREMENTS SUBROUTINE  *
1840 REM
1850 OUTPUT 509 ;"TWO6"
1860 ENTER 509 ; TRA
1870 OUTPUT 509 ;"TWO7"
1880 ENTER 509 ; TRB
1890 OUTPUT 509 ;"TWO8"
1900 ENTER 509 ; TRC
1910 OUTPUT 509 ;"DCV5" ! DUMMY MEASUREMENT
1920 TA=INT ((LOG (TRA)-CA)/AA*1000)/1000-273.15
1930 TB=INT ((LOG (TRB)-CB)/AB*1000)/1000-273.15
1940 TC=INT ((LOG (TRC)-CC)/AC*1000)/1000-273.15
1950 TBAR=INT ((TA+TB+TC)/3*10)/10
1960 RETURN
1970 REM *** SUBROUTINE TO FIND ANALYSER POSITIONS FOR +-105% FSD ***
1980 REM
1990 IF NM=0 THEN GOTO 2220
2000 REM GET INITIAL PSD READING
2010 GOSUB 2830
2020 PSD1=PSD
2030 REM NOW TAKE 100 STEPS FORWARD
```

```
2040 D=1 @ NS=100 @ GOSUB 2700
2050 REM CHECK WHETHER READING HAS INCREASED OR DECREASED
2060 GOSUB 2830
2070 PSD2=PSD
2080 DI=1
2090 IF PSD1>PSD2 THEN DI=-1 @ REM DI IS DIRECTION OF INCREASE
2100 REM NOW STEP UNTIL POSITION OF +105% FSD IS REACHED
2110 GOSUB 2830
2120 D=DI
2130 IF PSD>11 THEN D=-(1*DI)
2140 DL=ABS (11-PSD)
2150 NS=20
2160 IF DL>1.5 THEN NS=60
2170 IF DL>4 THEN NS=200
2180 IF DL>10 THEN NS=500
2190 GOSUB 2700
2200 GOSUB 2830
2210 IF PSD<10.5 OR PSD>11 THEN GOTO 2120
2220 REM SET AC CURRENT SPAN FOR THIS ANALYSER POSITION
2230 VS1=5
2240 VS1$=ZERO$[1,4-LEN (VAL$ (INT (VS1*100)))]&$VAL$ (INT (VS1*100))
2250 OUTPUT 510 ;VS1$
2260 WAIT 5000*PSDTC
2270 IF VS1=5 THEN WAIT 15000*PSDTC
2280 GOSUB 2380
2290 IF PSD>-10.5 AND VS1<7 THEN VS1=VS1+.2 @ GOTO 4264
2300 OUTPUT 510 ;"0000"
2310 DISP VS1
2320 WAIT 15000*PSDTC
2330 REM NOW STEP TO -105% FSD
2340 IF NM=0 THEN OUTPUT 509 ;"CLS0" @ GOTO 2530
2350 REM STEP LARGE DISTANCE TO -80% FSD FIRST
2360 IF DI=1 THEN OUTPUT 509 ;"CLS1"
2370 OUTPUT 509 ;"CLS0"
2380 OUTPUT 509 ;"TOT4"
2390 ENTER 523 ; V
2400 IF V>-8 THEN GOTO 2390
2410 ENTER 509 ; COUNTS
2420 OUTPUT 509 ;"OPN0" @ OUTPUT 509 ;"OPN1"
2430 COUNTS=COUNTS+3 @ REM COMPENSATE FOR 'OVERWIND'
2440 REM NOW ZERO IN
2450 GOSUB 2830
2460 IF PSD<-10.5 AND PSD>-11 THEN GOTO 2520
2470 IF PSD<-11 THEN D=DI
2480 IF PSD>-10.5 THEN D=-(1*DI)
2490 NS=30 @ GOSUB 2700
```

```
2500 COUNTS=COUNTS+30
2510 GOTO 2450
2520 PS$="NEG"
2530 REM SET SECOND AC CURRENT SPAN
2540 VS2=5
2550 VS2$=ZERO$[1,4-LEN (VAL$ (INT (VS2*199)))]&VAL$ (INT (VS2*100))
2560 OUTPUT 510 ;VS2$
2570 WAIT 5000*PSDTC
2580 IF VS2=5 THEN WAIT 15000*PSDTC
2590 GOSUB 2830
2600 IF PSD<10.5 AND VS2<7 THEN VS2=VS2+.2 @ GOTO 2550
2610 OUTPUT 510 ;"0000"
2620 WAIT 15000*PSDTC
2630 VS=VS1 @ IF VS2<VS1 THEN VS=VS2
2640 DISP VS2 @ DISP VS
2650 FOR I=1 TO 20
2660 V=INT (100*((I-1)/19*VS))
2670 V$(I)=ZERO$[1,4-LEN (VAL$ (V))]&VAL$ (V)
2680 NEXT I
2690 RETURN
2700 REM *** SUBROUTINE FOR STEPPING NS STEPS IN DIRECTION D ***
2710 IF NM=0 AND PS$="NEG" THEN OUTPUT 509 ;"OPN0" @ RETURN
2720 IF NM=0 AND PS$="POS" THEN OUTPUT 509 ;"CLS0" @ RETURN
2730 REM FORWARD: D=1       REVERSE: D=-1
2740 OUTPUT 509 ;"OPN0" @ OUTPUT 509 ;"OPN1"
2750 IF D=-1 THEN OUTPUT 509 ;"CLS1"
2760 OUTPUT 509 ;"CLS0"
2770 OUTPUT 509 ;"TOT4"
2780 ENTER 509 ; ST
2790 IF ST<NS-4 THEN GOTO 2780
2800 OUTPUT 509 ;"OPN0" @ OUTPUT 509 ;"OPN1"
2810 DISP ST
2820 RETURN
2830 REM *** ROUTINE TO OBTAIN TIME-AVERAGED PSD READINGS ***
2840 WAIT 6000*PSDTC @ REM WAIT FOR PSD TO CATCH UP
2850 TOTV=0
2860 FOR I=1 TO 20
2870 ENTER 523 ; V
2880 TOTV=TOTV+V
2890 NEXT I
2900 PSD=TOTV/20
2910 RETURN
```

Bibliography

[1] A D Buckingham, 1959, *Q Rev Chem Soc (Lond)*, **13**, 183.

[2] L D Barron, 1982, *Molecular Light Scattering and Optical Activity*, Cambridge University Press.

[3] R E Raab, 1975, *Mol Phys*, **29**, 1323.

[4] L Rosenfeld, 1951, *Theory of Electrons*, North-Holland.

[5] E B Graham, J Pierrus, and R E Raab, 1992, *J Phys B*, **25**, 4673.

[6] A D Buckingham and M B Dunn, 1971, *J Chem Soc (London) A Inorg Phys Theor*, 1988.

[7] D E Logan, 1982, *Mol Phys*, **46**, 271.

[8] D A Imrie and R E Raab, 1991, *Mol Phys*, **74**, 833.

[9] H J Böhm, 1985, *Mol Phys*, **56**, 375.

[10] J T Brobjer and J N Murrel, 1983, *J Chem Soc Faraday Trans II*, **79**, 1455.

[11] A D Buckingham, 1959, *J Chem Phys*, **30**, 1580.

[12] A D Buckingham and H C Longuet-Higgins, 1968, *Mol Phys*, **14**, 63.

[13] S Gustafson and W Gordy, 1970, *J Chem Phys*, **52**, 579.

[14] V P Krishnaji, 1966, *Rev Mod Phys*, **38**, 690.

[15] T H Spurling and E A Mason, 1967, *J Chem Phys*, **46**, 322.

[16] T K Bose and R H Cole, 1970, *J Chem Phys*, **52**, 140.

[17] T K Bose and R H Cole, 1971, *J Chem Phys*, **54**, 3829.

[18] S Kirouac and T K Bose, 1973, *J Chem Phys*, **59**, 3043.

[19] J M St-Arnaud and T K Bose, 1978, *J Chem Phys*, **68**, 2129.

[20] T K Bose, K Boudjarane, J Huot, and J M St-Arnaud, 1988, *J Chem Phys*, **89**, 7435.

[21] A D Buckingham and J A Pople, 1955, *Trans Farady Soc*, **51**, 1029.

[22] J Huot and T K Bose, 1991, *J Chem Phys*, **94**, 3849.

[23] W Hüttner and W H Flygare, 1967, *J Chem Phys*, **47**, 4137.

[24] W H Flygare, W Hüttner, R L Shoemaker, and P D Foster, 1969, *J Chem Phys*, **50**, 1714.

[25] S L Hartford, W C Allen, C L Norris, E F Pearson, and W H Flygare, 1973, *Chem Phys Lett*, **18**, 153.

[26] W H Flygare and R C Benson, 1971, *Mol Phys*, **20**, 225.

[27] R G Stone, H L Tigelaar, and W H Flygare, 1970, *J Chem Phys*, **53**, 3947.

[28] D H Levy, 1968, *J Chem Phys*, **48**, 5026.

[29] T G Copeland and R H Cole, 1973, *Chem Phys Lett*, **21**, 289.

[30] U Buontempo, S Cunsolo, and G Jacucci, 1973, *J Chem Phys*, **59**, 3750.

[31] F E Budenholzer, E A Gislason, A D Jorgensen, and J Grobe, 1977, *Chem Phys Lett*, **47**, 429.

[32] M Bloom, I Oppenheim, M Lipsicas, C G Wade, and C F Yarnell, 1965, *J Chem Phys*, **43**, 1036.

[33] M Abramowitz and I A Stegun, editors, 1972, *Handbook of Mathematical Functions*, Dover Publications.

[34] A D Buckingham, 1967, Permanent and induced molecular moments and long-range intermolecular forces, In J O Hirschfelder, editor, *Intermolecular Forces*, Interscience.

[35] A L Andrews and A D Buckingham, 1960, *Mol Phys*, **3**, 183.

[36] J H van Vleck, 1932, *The Theory of Electric and Magnetic Susceptibilities*, Clarendon Press.

[37] M R Battaglia, A D Buckingham, D Neumark, R K Pierens, and J H Williams, 1981, *Mol Phys*, **43**, 1015.

[38] A D Buckingham and M Pariseau, 1966, *Trans Farady Soc*, **62**, 1.

[39] J Pierrus, 1989, PhD thesis, University of Natal.

[40] R Piazza, V Degiorgio, and T Bellini, 1986, *Opt Commun*, **58**, 400.

[41] A D Buckingham and R L Disch, 1963, *Proc R Soc London A*, **273**, 275.

[42] I C D Stuckenberg, 1984, MSc thesis, University of Natal.

[43] C Graham, J Pierrus, and R E Raab, 1989, *Mol Phys*, **67**, 939.

[44] R C Weast, editor, 1988, *Handbook of Chemistry and Physics*, CRC Press, Inc., 68th edition.

[45] J H Dymond and E B Smith, 1969, *The Virial Coefficients of Gases — A Critical Compilation*, Oxford University Press.

[46] A A Maryott and F Buckley, 1953, *Circ US Natn Bur Stand*, **537**, 11.

[47] D C Baird, 1964, *Experimentation: An Introduction to Measurement Theory and Design*, Prentice-Hall.

[48] M P Bogaard, A D Buckingham, R K Pierens, and A H White, 1978, *J Chem Soc Faraday Trans I*, **74**, 3008.

[49] N J Bridge and A D Buckingham, 1966, *Proc R Soc London A*, **295**, 334.

[50] J E Harries, 1970, *J Phys B*, **3**, 704.

[51] W Ho, G Birnbaum, and A Rosenberg, 1971, *J Chem Phys*, **55**, 1028.

[52] D R Johnston and R H Cole, *J Chem Phys*, **36**, 318.

[53] E G Butcher and R S Dadson, 1964, *Proc R Soc London A*, **277**, 448.

[54] R D Amos, 1982, *Chem Phys Lett*, **85**, 123.

[55] G Maroulis and A J Thakkar, 1990, *J Chem Phys*, **93**, 4164.

[56] A Michels, J M Lupton, T Wassenaar, and W De Graaf, 1952, *Physica's Grav*, **18**, 121.

[57] A D Buckingham, R L Disch, and D A Dunmur, 1968, *J Amer Chem Soc*, **90**, 3104.

[58] R D Amos, 1982, *Chem Phys Lett*, **87**, 23.

[59] D G Bounds and S Wilson, 1985, *Mol Phys*, **54**, 445.

[60] W A Sokalski and A Sawaryn, 1987, *J Chem Phys*, **87**, 526.

[61] G Maroulis and A J Thakkar, 1990, *J Chem Phys*, **92**, 812.

[62] K Woliński, A J Sadlej, and G Karlström, 1991, *Mol Phys*, **72**, 425.

[63] W L Meerts, F H de Leeuw, and A Dymanus, 1977, *Chem Phys*, **22**, 319.

[64] A Michels, R J Lunbeck, and G J Walters, 1951, *Physica's Grav*, **17**, 801.

[65] D R Johnston, G J Oudemans, and R H Cole, 1960, *J Chem Phys*, **33**, 1310.

[66] A D Buckingham, C Graham, and J H Williams, 1983, *Mol Phys*, **49**, 703.

[67] G Maroulis and A J Thakkar, 1988, *J Chem Phys*, **88**, 7623.

[68] A Rastogi and R P Lowndes, 1977, *J Phys B*, **10**, 495.

[69] P A Morrison, 1972, PhD thesis, California Institute of Technology.

[70] R J Emrich and W Steele, 1980, *Mol Phys*, **40**, 469.

[71] D R Douslin and R H Harrison, 1976, *J Chem Thermodyn*, **8**, 301.

[72] H G David, S D Hamann, and J F Pearce, 1951, *J Chem Phys*, **19**, 1491.

[73] D E Stogryn and A P Stogryn, 1966, *Mol Phys*, **11**, 371.

[74] G Maroulis, 1993, *J Phys B*, **26**, 775.

[75] *Landolt-Börnstein, Zahlenwerte und Funktionen*, Band II, Teil 8, 1962, Springer.

[76] B Schramm and H Schmiedel, 1979, Communicated privately to J H Dymond and E B Smith.

[77] R Shankar, 1984, *Principles of Quantum Mechanics*, Plenum Press.

[78] L D Barron and C G Gray, 1973, *J Phys A*, **6**, 59.